Title
ASYMMETRY PARAMETERS IN E-->ne- 7 AND u+ -> p y

Author
Gershwin, Lawrence Kenneth.

Publication Date
1969-06-02

ASYMMETRY PARAMETERS IN $\Sigma^- \rightarrow ne^- \bar{\nu}$ AND $\Sigma^+ \rightarrow p\gamma$

Lawrence Kenneth Gershwin
(Ph. D. Thesis)

June 2, 1969

AEC Contract No. W-7405-eng-48

LAWRENCE RADIATION LABORATORY
UNIVERSITY of CALIFORNIA BERKELEY

DISCLAIMER

ASYMMETRY PARAMETERS IN $\Sigma^- \rightarrow ne^-\bar{\nu}$ AND $\Sigma^+ \rightarrow p\gamma$

Contents

ASYMMETRY PARAMETERS IN $\Sigma^- \rightarrow ne^-\overline{\nu}$ AND $\Sigma^+ \rightarrow p\gamma$

Lawrence Kenneth Gershwin

Lawrence Radiation Laboratory
University of California
Berkeley, California

June 2, 1969

ABSTRACT

An experiment was performed in the Lawrence Radiation Laboratory 25-inch hydrogen bubble chamber. 1.3×10^6 pictures were taken of the interactions of a K^- beam ranging in momentum from 270 to 470 MeV/c, with most of the pictures taken in the vicinity of 390 MeV/c, where the $Y_0^*(1520)$ resonance is formed. The interference of the resonant amplitude with those of the predominantly S-wave background produces polarized Σ's in the reactions $K^-p \rightarrow \Sigma^-\pi^+$ and $K^-p \rightarrow \Sigma^+\pi^-$. From a sample of 85,000 $\Sigma^- \rightarrow n\pi^-$ decays and 57,000 $\Sigma^+ \rightarrow p\pi^0$ decays we have found 53 examples of $\Sigma^- \rightarrow ne^-\overline{\nu}$, 8 of $\Sigma^- \rightarrow n\mu^-\overline{\nu}$, and 61 of $\Sigma^+ \rightarrow p\gamma$.

The leptonic Σ^- decays were analyzed to measure the correlation between the Σ^- polarization and the direction of the charged lepton, as described by the lepton distribution $(1 + \alpha\, P_\Sigma \cos\theta)$. The asymmetry parameter α for the electron events was found to be $\alpha = -0.26 \pm 0.37$. The asymmetry parameter is related to g_A/g_V, the ratio of the axial-vector to vector weak coupling constants. We found $g_A/g_V = 0.16 {}^{+\,0.19}_{-\,0.18}$ for the electron events. The sign convention is such that $g_A/g_V = -1.2$ for $n \rightarrow pe^-\overline{\nu}$. Assuming μ-e univer-

sality, we found $g_A/g_V = 0.19 {+0.20 \atop -0.17}$ for the combined electron and muon events. A comparison with Cabibbo's theory of semi-leptonic decays showed reasonable agreement with the prediction of the theory when a fit was carried out to presently published data for baryon leptonic decays.

For the 61 $\Sigma^+ \rightarrow p\gamma$ events, we measured the asymmetry parameter expressing the correlation of the Σ^+ polarization with the direction of the proton, obtaining $\alpha = -1.03 {+0.52 \atop -0.42}$. The branching ratio $(\Sigma^+ \rightarrow p\gamma) / (\Sigma^+ \rightarrow p\pi^0) = (2.76 \pm 0.51) \times 10^{-3}$ was measured, using 31 of the $\Sigma^+ \rightarrow p\gamma$ events. We find both the branching ratio and asymmetry parameter to be in agreement with some theoretical calculations, although the asymmetry parameter is two standard deviations from the value $\alpha = 0$ predicted by SU(3) invariance.

I. INTRODUCTION

There has been theoretical interest[1,2] in rare baryon decays, particularly the leptonic decays, for a long time. The leptonic decays offered the possibility of studying the hadronic part of the weak current directly, whereas the more copious non-leptonic decays involved the hadronic part of the current interacting with itself.

The experimental study of rare Σ decays has become possible only in the last five years, as a result of the tremendous increase in the capabilities of bubble chamber experiments. This increase has come about primarily because of the development of high-speed computers and precision measuring machines. The development of rapid precision measuring machines, such as the Spiral Reader in the Alvarez group at the Lawrence Radiation Laboratory, has greatly enhanced the productivity of experiments, as it has become possible to measure several hundred thousand events from a single experiment.

Previously,[3-6] the analysis of rare Σ decays has been confined to experiments in which a K^- beam stopped in the bubble chamber, giving rise to large numbers of Σ's. These experiments, although they provided good information on the rates of the rare decays, were limited in that the Σ's were unpolarized due to their arising from an interaction at rest. Correlations with the Σ polarization are necessary in the study of the detailed nature of the decay.

An earlier experiment[7] indicated that the region about K^- momentum of 400 MeV/c was an excellent place to produce polarized Σ's, in that the K^-p system resonates with the $Y_0^*(1520)$. The interference of this resonant D-wave amplitude with the predominantly S-wave background is responsible for large Σ polarizations.

This experiment was begun in 1965, along with a similar experiment performed at Brookhaven, with the primary intention of producing large numbers of polarized Σ's through the reactions $K^-p \rightarrow \Sigma^-\pi^+$ and $K^-p \rightarrow \Sigma^+\pi^-$ in the vicinity of 390 MeV/c, and studying the polarization correlations for the large number of non-leptonic Σ decays. The analysis of these and other reaction channels was carried out with the aid of the Spiral Reader measuring machine, as well as with a slower Franckenstein measuring machine developed earlier in the group. A number of rare Σ decays were found by this experiment in the course of the measuring process. We have chosen here to analyze the asymmetry parameters for the correlation between the Σ polarization and the charged decay particle direction, for the leptonic decay $\Sigma^- \rightarrow ne^-\bar{\nu}$ and the weak electromagnetic decay $\Sigma^+ \rightarrow p\gamma$. Previous experimental work on both of these decays has been confined to measurements of the branching ratios.

In Section II we briefly discuss the beam and begin the discussion of the scanning and measuring procedure, as it applied to Σ events. The remainder of the thesis is devoted to a study first of the Σ^- leptonic decays and then of the $\Sigma^+ \rightarrow p\gamma$ decays.

In Section III we discuss the experimental analysis of Σ^- leptonic decays. We show the techniques used to isolate the three-body Σ^- decays and the means used to identify the negative decay particle. We find 53 examples of $\Sigma^- \rightarrow ne^-\bar{\nu}$ and 8 of $\Sigma^- \rightarrow n\mu^-\bar{\nu}$. The asymmetry parameter of the electron events is found to be

$\alpha = -0.26 \pm 0.37$.

In Section IV we discuss first the development, both theoretical and experimental, of the understanding of the leptonic decays of baryons, starting with the universal Fermi interaction and the conserved vector current hypotheses proposed before there was any experimental knowledge about hyperon leptonic decays. A discussion of the successive generations of experiments is given. We then present our determination of g_A/g_V, the ratio of the weak coupling constants for the axial-vector and vector weak currents, by means of its relation to α. We find, for our 53 $\Sigma^- \rightarrow n e^- \bar{\nu}$ decays, a best value of $g_A/g_V = 0.16 {+0.19 \atop -0.18}$. Assuming μ-e universality, we find for the 61 Σ^- leptonic decays the value $g_A/g_V = 0.19 {+0.20 \atop -0.17}$. The sign convention is such that g_A/g_V is -1.2 for $n \rightarrow p e^- \bar{\nu}$. Finally, we discuss Cabibbo's[8] theory of semi-leptonic decays and find that our value of g_A/g_V is in reasonable agreement with the predictions of the theory when a fit to all of the currently published data is carried out. In Section V we briefly recapitulate the findings of our experiment on Σ^- leptonic decays.

In Section VI we present the experimental analysis of the $\Sigma^+ \rightarrow p\gamma$ decays. A brief discussion of the previous experimental work is given. We then show the techniques employed in this experiment to isolate 61 $\Sigma^+ \rightarrow p\gamma$ events. The asymmetry parameter is found to be $\alpha = -1.03 {+0.52 \atop -0.42}$. We then give the procedure by which we were able to obtain the branching ratio $(\Sigma^+ \rightarrow p\gamma) \,/\, (\Sigma^+ \rightarrow p\pi^0)$, using 31 $\Sigma^+ \rightarrow p\gamma$ events. We find a branching ratio of $(2.76 \pm 0.51) \times 10^{-3}$.

In Section VII we discuss the various theoretical calculations that have been made which relate to $\Sigma^+ \rightarrow p\gamma$. In particular, we present an SU(3) result that $\alpha = 0$, under the assumptions of SU(3) invariance of the matrix element and a U-spin singlet nature of the γ. We find our measured values of the asymmetry parameter and branching ratio to be in agreement with some of the theoretical values, although our measurement of α differs from the SU(3) result by two standard deviations.

In Section VIII we discuss briefly our findings for these rare Σ decays.

II. GENERAL EXPERIMENTAL METHOD

A. Beam

A separated K^- beam of momentum 400 MeV/c designed by Dr. Joseph J. Murray was used to achieve a K^- : π^- ratio of 3: 1 at the bubble chamber entry window, starting from an unseparated ratio of 1: 50,000. This was achieved in a short beam of length 40 feet by means of a new septum separator. More details are given in Ref. 9.

B. Scanning

1.3×10^6 pictures were taken in the Lawrence Radiation Laboratory 25-inch hydrogen bubble chamber, with K^- momenta from 270 to 470 MeV/c. The film was scanned topologically for all events of interest to the entire experiment. About 375,000 two-vertex events and 185,000 one-vertex events were found in the scan. A two-vertex event is the production and decay of a strange particle.

The two topologies of interest to this part of the experiment are shown in Fig. 1. The reactions are

(1) $K^-p \to \Sigma^-\pi^+$, Σ^- decays, and

(2) $K^-p \to \Sigma^+\pi^-$, $\Sigma^+ \to p$ + neutral.

An example of $K^-p \to \Sigma^-\pi^+$, $\Sigma^- \to ne^-\bar{\nu}$ with a low momentum e^- is shown in Fig. 2, and an example of $K^-p \to \Sigma^+\pi^-$, $\Sigma^+ \to p\gamma$ with a converting γ is shown in Fig. 3. The image of dark tracks on a light background is the same as that viewed by the scanners on the scanning table.

The scanners were required to record all Σ^- or Σ^+ events if

1) the event was within a defined fiducial volume

2) the Σ decay vertex was recognizable in at least two views

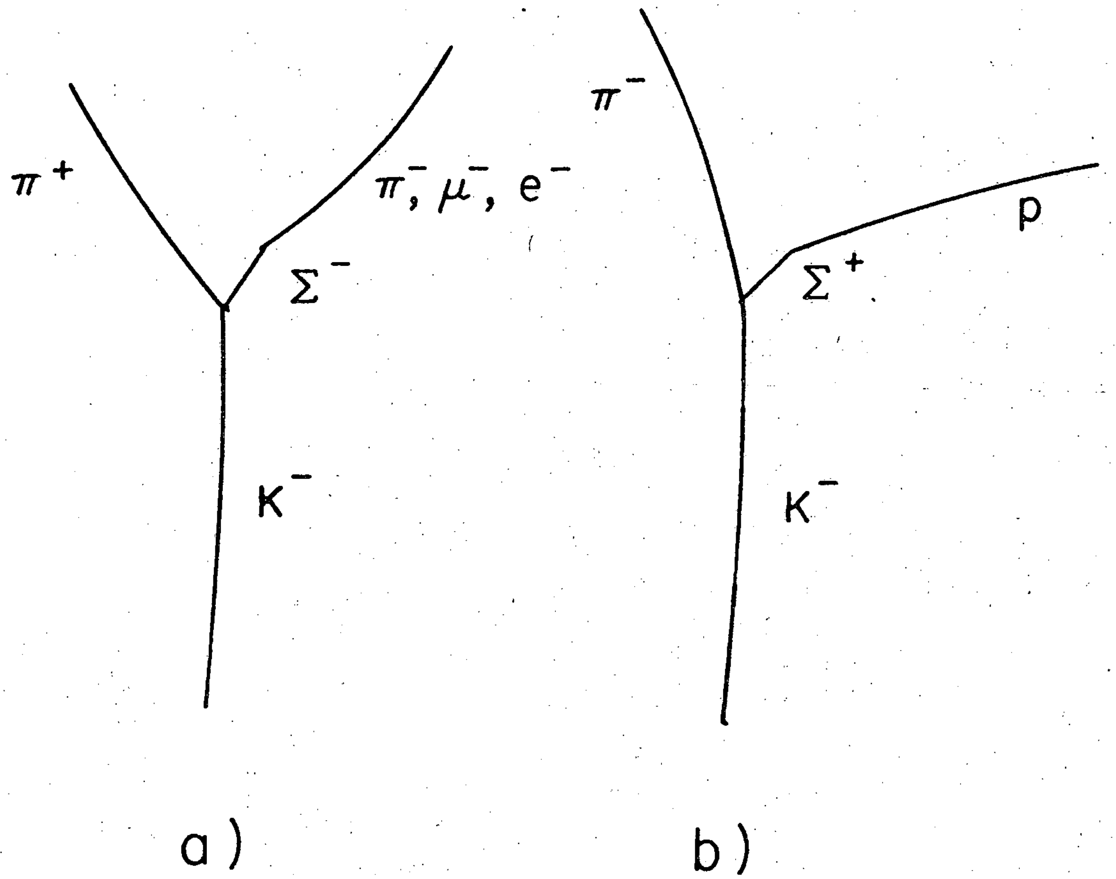

XBL 696-778

Fig. 1. The topologies for a) Σ^- decay and b) $\Sigma^+ \to p$ decay.

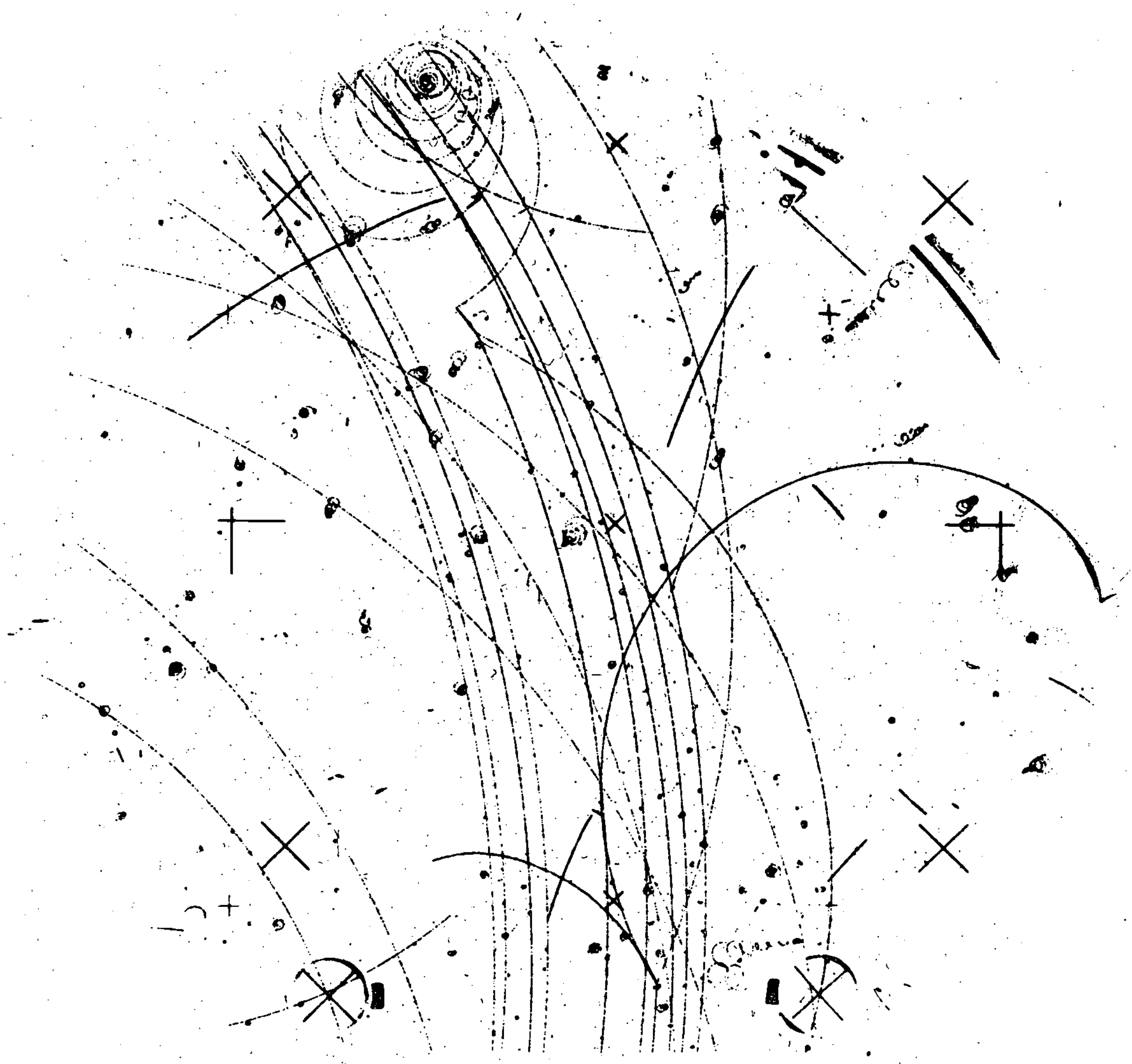

Fig. 2. An example of the decay $\Sigma^- \rightarrow ne^- \bar{\nu}$.

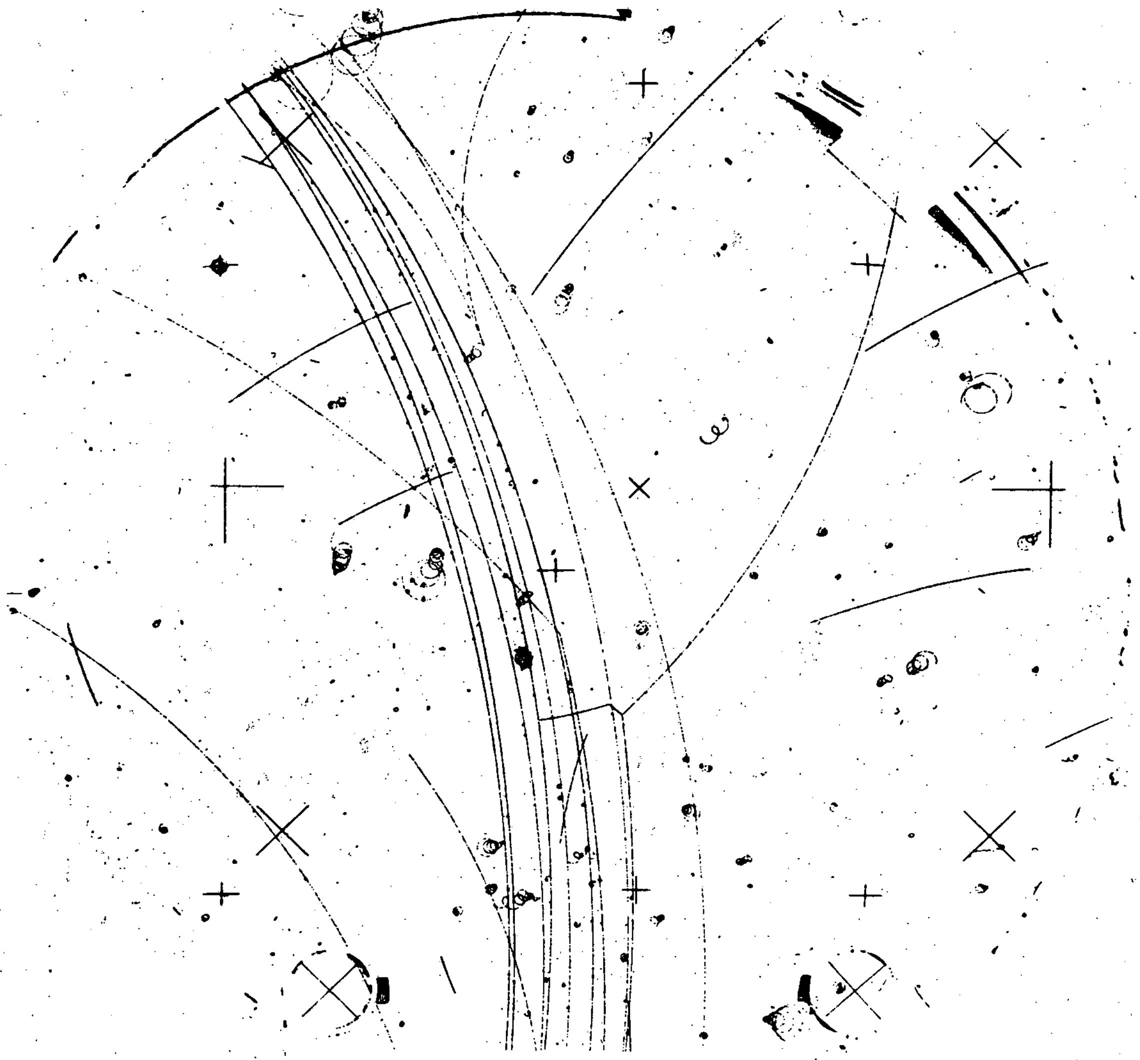

Fig. 3. An example of the decay $\Sigma^+ \rightarrow p\gamma$, where the γ converts.

3) the Σ was greater than 0.5 mm. in projection in at least two views (corresponding to 0.75 mm. in space)

Since both the Σ^+ and p in $\Sigma^+ \rightarrow p$ + neutral are heavily ionizing due to the low momentum of the tracks, and since the p tends to be in the same direction as the Σ^+ because of the Lorentz transformation, it is more difficult to distinguish a decay vertex than for Σ^- decay or $\Sigma^+ \rightarrow \pi^+$ + neutral.

In principle one could have special scanning criteria to identify $\Sigma^- \rightarrow ne^-\bar{\nu}$ decays in which the electron could be identified because of its light ionization. These criteria were not imposed, because they would have slowed the scanning considerably. The scanners were requested to flag such events if they recognized the electron by its low momentum and minimum ionization, but the efficiency for this was rather poor because of the low stress placed upon this instruction. Of the 53 electron events, only 8 were flagged as such by the scanners.

Scanners were required to distinguish between the decays $\Sigma^+ \rightarrow p$ + neutral and $\Sigma^+ \rightarrow \pi^+$ + neutral. If the positive decay particle stopped in the chamber, it was identifiable, because π^+ decays via $\pi^+ \rightarrow \mu^+ \rightarrow e^+$, while p does nothing. If the particle left the chamber, the scanners were supposed to distinguish between π^+ and p on the basis of ionization, since the proton is heavily ionizing while the π^+ is considerably lighter. This distinction could be made with good efficiency for tracks that were flat in the chamber, but with decreasing efficiency as the dip angle increased. Even so, misidentification for large dip angles was only about 10%.

No attempt was made in the scanning to differentiate $\Sigma^+ \rightarrow p\gamma$

from $\Sigma^+ \to p\pi^0$. The procedure for identifying events of both of the rare decay modes, $\Sigma^- \to ne^-\bar{\nu}$ and $\Sigma^+ \to p\gamma$, was to measure all of the Σ^- and Σ^+ events within a defined fiducial volume and to separate the rare decays on the basis of kinematics. This procedure fit in well with our general measuring scheme, since it was necessary to measure all the Σ events in order to determine the Σ polarizations accurately.

C. Measuring

The events were measured either on a Franckenstein measuring machine or on a Spiral Reader. Over 400,000 events of all types were measured in this experiment, with about 60% on the Spiral Reader. The number of measurements was even greater, since a considerable number of remeasurements were made of failing events. The scanning and measuring totals for our event types are given below.

Event Type	Scanned	Measured	Passed the measuring
Σ^-	85,589	79,646	78,013
$\Sigma^+ \to p$	57,116	48,247	47,343

D. Computer Analysis

The measurements were processed through the filter program POOH[10] for the Spiral Reader and PANAL or MOTIF for the Franckenstein. POOH filters the points taken by the Spiral Reader, constructing matching tracks in the three views. PANAL and MOTIF simply put the points recorded on the Franckenstein into a form useable by the geometry program. All measurements were then processed by the program SIOUX, consisting of two parts: TVGP[11], which performs three-dimensional track reconstruction for the measured tracks according to their various mass hypotheses, and SQUAW[12], which does a χ^2 fit to the specific reaction hypotheses, using conservation of energy and momentum.

III. EXPERIMENTAL ANALYSIS OF Σ^- LEPTONIC DECAYS

A. Kinematic Reconstruction

Σ^- events which were passed by the geometric reconstruction program TVGP were submitted to SQUAW for kinematical fitting. All events were fitted to the hypotheses

$$\text{(1)}\quad K^-p \to \Sigma^-\pi^+,\ \Sigma^- \to n\pi^- \text{ and}$$

$$\text{(2)}\quad K^-p \to \Sigma^-\pi^+\pi^0,\ \Sigma^- \to n\pi^-.$$

Reaction 2 occurs only about 1% of the time, since the center of mass energy is barely above threshold for the reaction. No attempt was made later to identify leptonic decays from Σ's produced in this three-body production state. Events which failed to fit either of these hypotheses with a confidence level greater than 10^{-5} were fitted to

$$\text{(3)}\quad K^-p \to K^-p,\ K^- \text{ decays.}$$

This reaction is topologically equivalent to the Σ^- reaction, but the ionization of the positive production particle generally differentiates the two. The scanners were supposed to distinguish events of reaction 3 by ionization, and thus not identify them as Σ^- decays, but this was not always possible, especially if the positive particle had a large dip angle. 872 events originally called Σ^- decays fit only reaction 3.

Events failing to fit reactions 1 or 2 were also fit to the production hypothesis alone,

$$\text{(4)}\quad K^-p \to \Sigma^-\pi^+.$$

An event which fit this hypothesis was considered to be a three-body candidate and was fitted to

$$K^- p \rightarrow \Sigma^- \pi^+$$
$$\begin{array}{ll} (5) & \\ (6) & \Sigma^- \rightarrow \left\{ \begin{array}{c} e^- \\ \mu^- \\ \pi^- \end{array} \right\} + \text{missing mass.} \\ (7) & \end{array}$$

These hypotheses will almost always fit if reaction 4 was successful, since they are essentially a calculation of the missing mass recoiling against the negative decay particle. It is possible to get a fit to only one or two of the missing mass hypotheses if the negative track cannot be successfully reconstructed to the specific mass required, because of a mismatch between the curvature as measured and that expected from the range-momentum relation.

A substantial number of remeasurements were made in order to achieve the high passing rate that we desired. All events which failed to fit the ordinary two- or three-body Σ^- production hypotheses 1 or 2 were remeasured at least once. Events which fit reactions 1 or 2, but with a confidence level < .01 were remeasured on the Franckenstein after most events had been successfully measured. At the end of the experiment, all events which had not yet passed were remeasured on the Franckenstein. In addition to measuring the Σ^- events within the measuring fiducial volume, we measured once many of the events which lay outside the volume. Six electron events were found as a result of measuring outside the volume. The remeasuring procedure was quite fruitful in finding Σ^- leptonic decays, since several events with low energy electrons (< 100 MeV/c) were found which had previously failed on the Spiral Reader because the electron track was light in ionization and too highly curved for proper digitization. In all, about half of the electron events were successfully identified as a result of their Spiral Reader measurement, although more than half the Σ^- events were measured on the Spiral Reader.

B. Procurement of Three-Body Candidates

There were 1100 missing mass fits. The missing mass distribution for the π^- fit, reaction 7, is shown in Fig. 4. Many of those events with very low missing mass (< 850 MeV/c^2) were Spiral Reader measurements where a nearby beam track was improperly filtered as if it were the negative decay track, while the real negative decay track was lost. The 450 events for which the missing mass is greater than the mass of the neutron were initially considered candidates for three-body decays. Since only those events failing the usual decay hypothesis were fitted to the missing mass hypothesis, there is an enormous depletion of events in the region of the neutron mass, 940 MeV/c^2.

The three-body decays of the Σ^- are listed below, along with the compiled world averages[13] for the branching ratios to the two-body decay and the maximum Σ^- rest frame (RF) momenta for the negative decay particles.

Decay	Branching ratio	q_{max} (MeV/c)
$\Sigma^- \to ne^-\bar{\nu}$	$(1.08 \pm 0.05) \times 10^{-3}$	230
$\Sigma^- \to n\mu^-\bar{\nu}$	$(0.48 \pm 0.06) \times 10^{-3}$	210
$\Sigma^- \to n\pi^-\gamma$	$\approx (1.1 \pm 0.2) \times 10^{-3}$ for $q_\pi < 166$ MeV/c	193

The negative decay particles have laboratory momenta that are

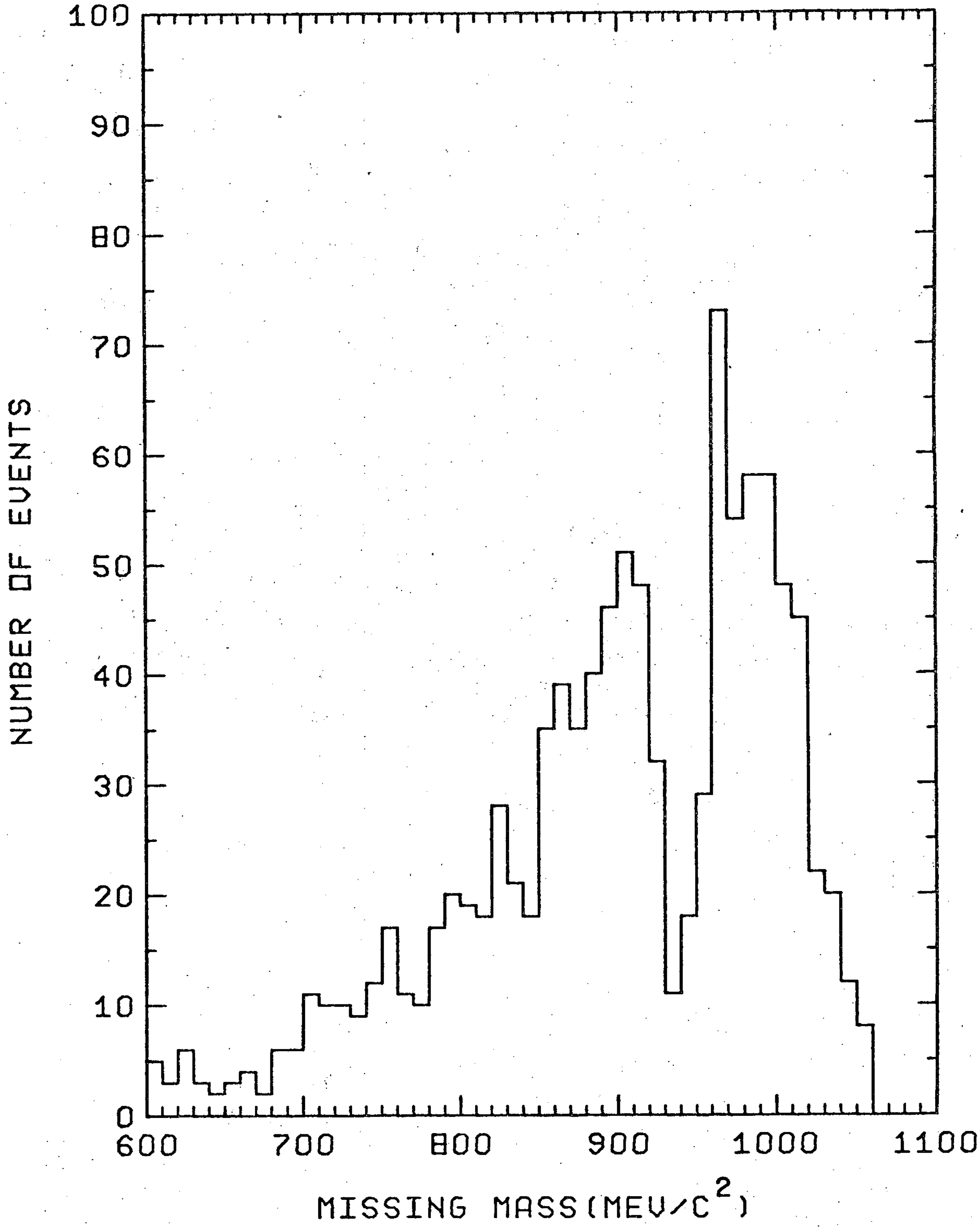

XBL 696-665

Fig. 4. Missing mass distribution for those events with a $\Sigma^- \to \pi^-$ + missing mass fit.

quite low (< 300 MeV/c), and the Σ^-'s travel quite slowly (maximum $\beta=0.5$), so that the calculation of the rest frame momentum from the laboratory momentum of the negative decay particle does not depend very heavily on whether the particle is a π^-, μ^-, or e^-. The variation in rest frame momentum is always less than 25 MeV/c, and usually much less. Thus it is apparent that electron events with rest frame momentum from 170 to 230 MeV/c will often fit the two-body decay. The phase space for the decay is low in this region, and the laboratory momentum is generally too high to distinguish the electron by ionization. Thus, we did not consider events with RF momentum above 170 MeV/c as leptonic candidates.

A set of criteria was developed to apply to the events which successfully fit the two-body decay in order to procure additional three-body candidates. 68 events were found which satisfied the following criteria:

1) two-body decay fit with $10^{-5} <$ confidence level $< .05$

2) measured momentum of the decay track corresponded to a π^- RF momentum < 170 MeV/c

3) measured momentum of the decay track was greater than two standard deviations from the fitted momentum for the two-body decay

4) measured length of decay track > 10 cm.

5) dip angle of decay track $< 60°$ unless measured momentum was less than 100 MeV/c

Two of these events eventually proved to be electron events, both with low momentum electrons with dip angles between 60° and 70°. 23 remained as three-body, non-electron decays after remeasurement, while the rest were bad measurements.

C. Examination and Remeasuring of Three-Body Candidates

The three-body candidates were all examined on the scanning table to determine whether the event was measured properly and to make a preliminary identification of the mass of the negative decay particle by ionization. There were several sources of bad measurement:

1) Most commonly, there was a small angle scattering or decay of the negative decay particle which was overlooked by the measurer. If the direction of the scattering or decay was such as to make the measured track more curved, the consequent lower measured momentum corresponded to a missing mass greater than the mass of the neutron. The event might then have appeared among the three-body candidates if the change in momentum was severe enough.

2) If the Spiral Reader was not calibrated properly, there may have been bad digitization of points, or the filter program POOH may not have reconstructed the tracks properly.

3) If the fiducial marks were measured badly, the tracks did not have the correct momentum after reconstruction by TVGP.

4) Some events were difficult to measure because of overlying beam tracks or other obscurities.

Those events which appeared, on first inspection, to have been measured properly, or which, even though badly measured, might still have been three-body decays, were remeasured on the Franckenstein at least once with instructions to measure carefully and to watch for small-angle scatterings or decays. About 720 remeasurements were made in all, some being several measurements of the same event with different instructions. Remeasuring removed some events which had been measured badly previously and fit the two-body decay well upon remeasurement. The remaining candidates were re-examined on the scanning table to look for kinks in the tracks and to make sure that the remeasurement was satisfactory.

D. Three-Body Decay Criteria

Several cuts were applied to the sample of remaining three-body candidates to remove possible sources of contamination. The number of two-body decays removed by successive application of the cuts is indicated by the numbers in parentheses, if the cut was applicable. Events were eliminated if:

1) the Σ^- length was less than 1 mm. This was done to insure that the event was well measurable and was in fact a Σ^- decay and not a decay of a very short K^0 or Σ^+, or a two-prong event. (1993 events)

2) the fitted Σ^- momentum at the decay vertex was less than 80 MeV/c, corresponding to a residual range of less than 0.7 mm. This was done because a Σ^- which comes to rest usually interacts with a proton, producing either a Σ^0 or a Λ. If a Σ^0 produced in this way decays via $\Sigma^0 \rightarrow \Lambda e^+ e^-$ with a subsequent neutral decay of the Λ and an invisible e^+, the event completely simulates a Σ^- leptonic decay. Also, contributions to the radiative decay sample would come from Σ^- capture in which the resultant Λ goes less than 1 mm., decays via $\Lambda \rightarrow \pi^- p$, and the proton is too short to be visible. (763 events)

3) the dip angle of the negative decay particle was greater than 60°, unless the measured momentum was less than 100 MeV/c and the track was clearly an electron by ionization, in which case the limit was set at 70°. This was done for several reasons: such tracks

cannot be identified well by ionization criteria, they can be difficult to measure if they are faint, and they can be difficult to measure properly because small-angle scatterings or decays are harder to detect. Five events were retained as electron events where the dip angle was between 60° and 70° with a measured momentum less than 100 MeV/c. (8881 events)

4) the RF momentum of the negative decay particle as a π^- was greater than 170 MeV/c. This cut was applied to define a sample of events which had a reasonable efficiency for being found as three-body events.

After imposition of these cuts, 172 three-body events and 64,935 two-body events remained.

E. Identification of Electron Events

A program was written which calculated the bubble density relative to that of minimum ionization for the beginning and end of each track in each view, according to its particular mass hypothesis. This program took into account the positions of the cameras and the angles of the tracks, as well as their momenta. This procedure provided three different sets of ionizations for the negative decay particle, corresponding to its being a π^-, μ^-, or e^-. From visual inspection on the scanning table, and utilizing the predicted bubble densities for the negative decay particle in comparison with those for the K^- and π^+, a tentative mass identification could be made for most three-body events. For events with negative decay particle laboratory momentum less than 140 MeV/c, we considered this method to be sufficient to identify electrons with a high degree of confidence, since, relative to minimum ionizing, the e^- is 1.0, the μ^- is 1.6, and the π^- is 2.0. Also, both the μ^- and π^- are increasing in ionization as they traverse the chamber.

For negative decay particles of momentum > 140 MeV/c, a method of bubble-gap measuring was employed if the track seemed to be sufficiently lightly ionizing to be an electron. The mean gap length is inversely proportional to the bubble density.[14] Thus, measuring the lengths of the bubble gaps for both the electron candidate and the π^+ or K^- leads to a determination of the candidate's bubble density. β^2, the square of the velocity, is inversely proportional to the bubble density, so β^2, and consequently the mass, is thereby determined. 13 events were gap measured on the Franckenstein measuring machine, with resultant β^2's shown in Fig. 5. The events are plotted for the average laboratory momentum. The statistical error is the combined error for the two tracks measured. The events plotted with squares are considered to be electron events, while the others are either undetermined or are μ^- or π^- events. The event at 143 MeV/c has a large error because the π^+ was short and had few gaps; it was considered to be an electron event because the electron track was unusually long and did not darken at all in its traversal of the chamber. The solid curves represent the β^2 curves for π^-, μ^-, and e^- as a function of momentum. As is evident, the resolution by this method is not very good, but it is helpful in providing a quantitative estimate of the ionization for events which appear to have minimum-ionizing decay particles from visual inspection. The visual inspection

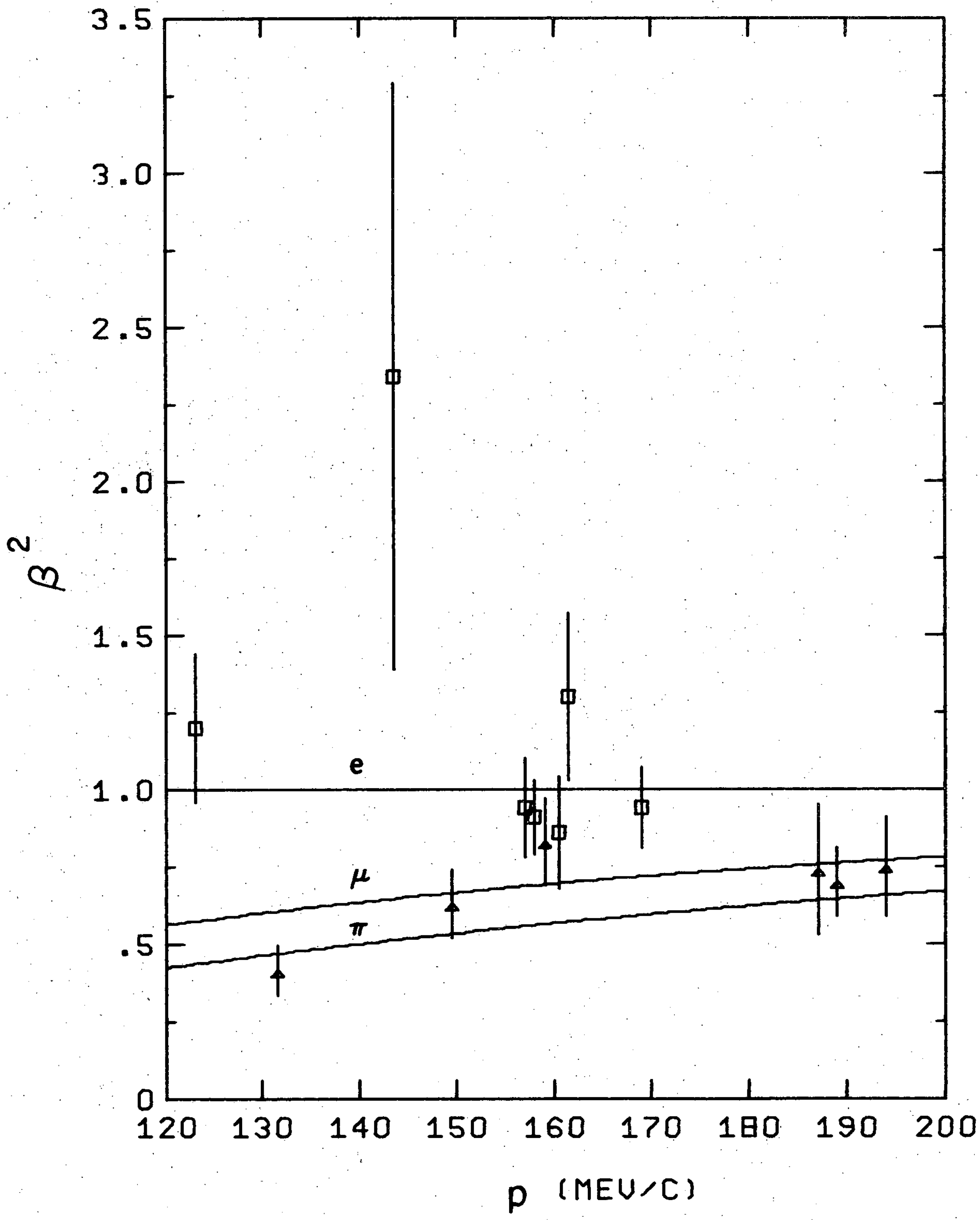

XBL 696-666

Fig. 5. The experimental values of β^2 of the negative decay particle determined for 13 events by means of gap-length measuring. The 7 events with squares were considered to be electron events.

is valuable in that one can estimate the relative darkness of the bubbles and can see whether the ionization appears to be increasing as the particle traverses the chamber. Other authors[5,15] have found the gap-measuring technique to be more successful. The number of measurable gaps per track in this experiment was quite small, from 50-100 on a minimum-ionizing track and considerably fewer on a non-minimum track such as the π^+ or K^-. This occurred because the film was taken with a high bubble density and fairly large bubbles in order to facilitate its measurement on the Spiral Reader. The sensitivity was also high, but there still remained a considerable difference in the darkness of tracks.

Two restrictions were placed on events ultimately included in the electron sample:

1) No event with a negative decay particle with laboratory momentum > 180 MeV/c was included because of the difficulty in separating such an event from a radiative decay by ionization. With optimum film conditions it is possible to extend identification past this momentum, but our conditions were not optimum.

2) Events for which the electron RF momentum was greater than 150 MeV/c were eliminated from the electron sample, since the efficiency for detecting and identifying such events is low. The laboratory momentum is often too high to identify the particle by ionization. Also, the a priori probability of such an event being a radiative decay becomes increasingly greater than that for it to be an electron decay, as the RF momentum increases. This can be seen in Fig. 6, where the momentum distribution of π^-, μ^-, and e^- are

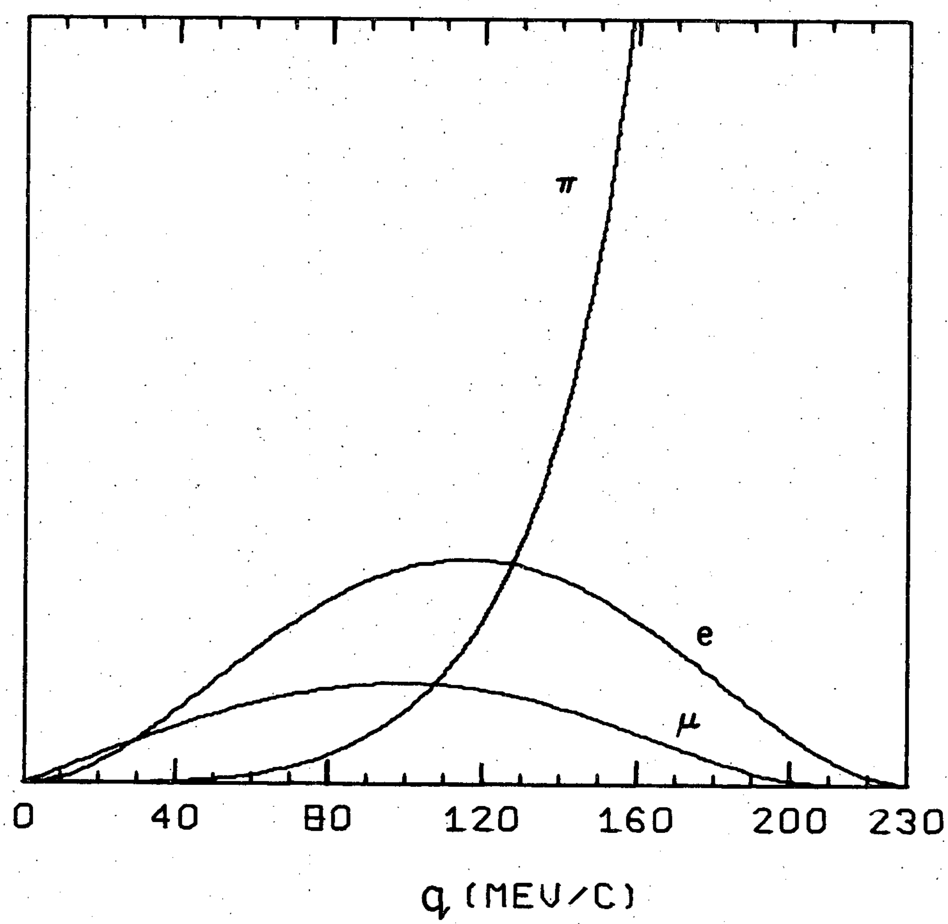

Fig. 6. The phase space curves for the rest frame momentum of the negative decay particle, for $\Sigma^- \rightarrow ne^-\bar{\nu}$, $n\mu^-\bar{\nu}$, and $n\pi^-\gamma$, based upon the branching ratios of Sec. IIIB.

shown on the basis of the phase space and the branching ratios of Sec. IIIB. The cutoff of 150 MeV/c was arrived at by assuming that the ionization determination of the particle by gap measuring and visual examination carried a weight of at least 3: 1 as a conservative estimate, whereas the a priori probability of e^-: π^- at 150 MeV/c is about 1: 3.

The laboratory momentum spectrum of the 53 identified electron events is displayed in Fig. 7. The RF momentum spectrum is displayed in Fig. 8. The curve is the phase space distribution based upon a branching ratio of 1.08×10^{-3} to the 64,935 two-body decays which satisfy the criteria of Sec. IIID. There are five events in the histograms with large electron dip angle which did not satisfy these criteria. The electrons seem to have been identified with good efficiency up to 120 MeV/c.

F. Identification of Muon Events

The RF momentum spectrum of the 8 identified muon events is displayed in Fig. 9. Five of the muons were identifiable because they decayed to electrons. The other three are considered to be muons because they had at least five times the a priori probability of being muons rather than pions (RF momentum < 70 MeV/c). Furthermore, they appeared to be muons rather than pions from ionization, since they had laboratory momenta in a fairly sensitive region for distinguishing μ^- from π^- by ionization. It was necessary to restrict the RF momentum to be less than 100 MeV/c to avoid including muons resulting from the collinear decay of pions from two-body Σ^- decays.

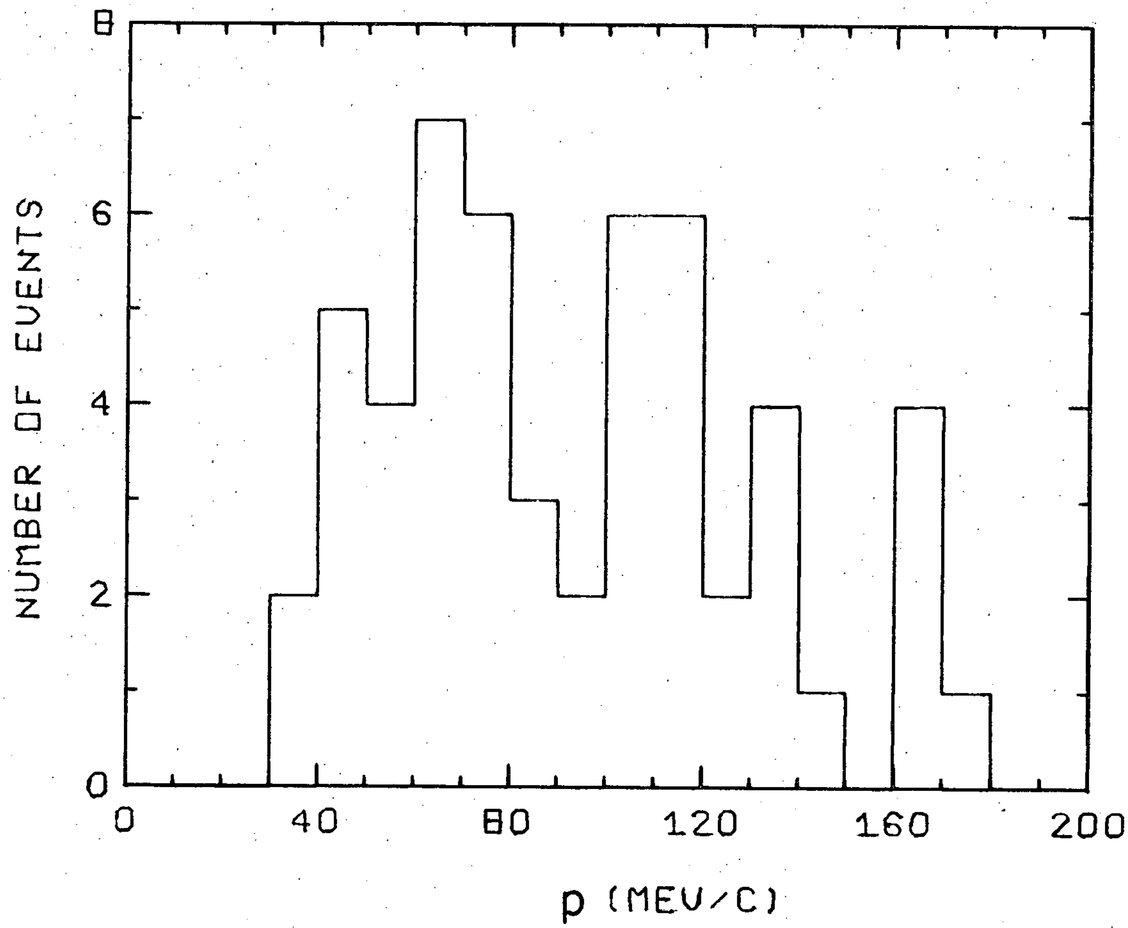

XBL 696-667

Fig. 7. The electron laboratory momentum distribution for the 53 $\Sigma^- \rightarrow ne^-\bar{\nu}$ events.

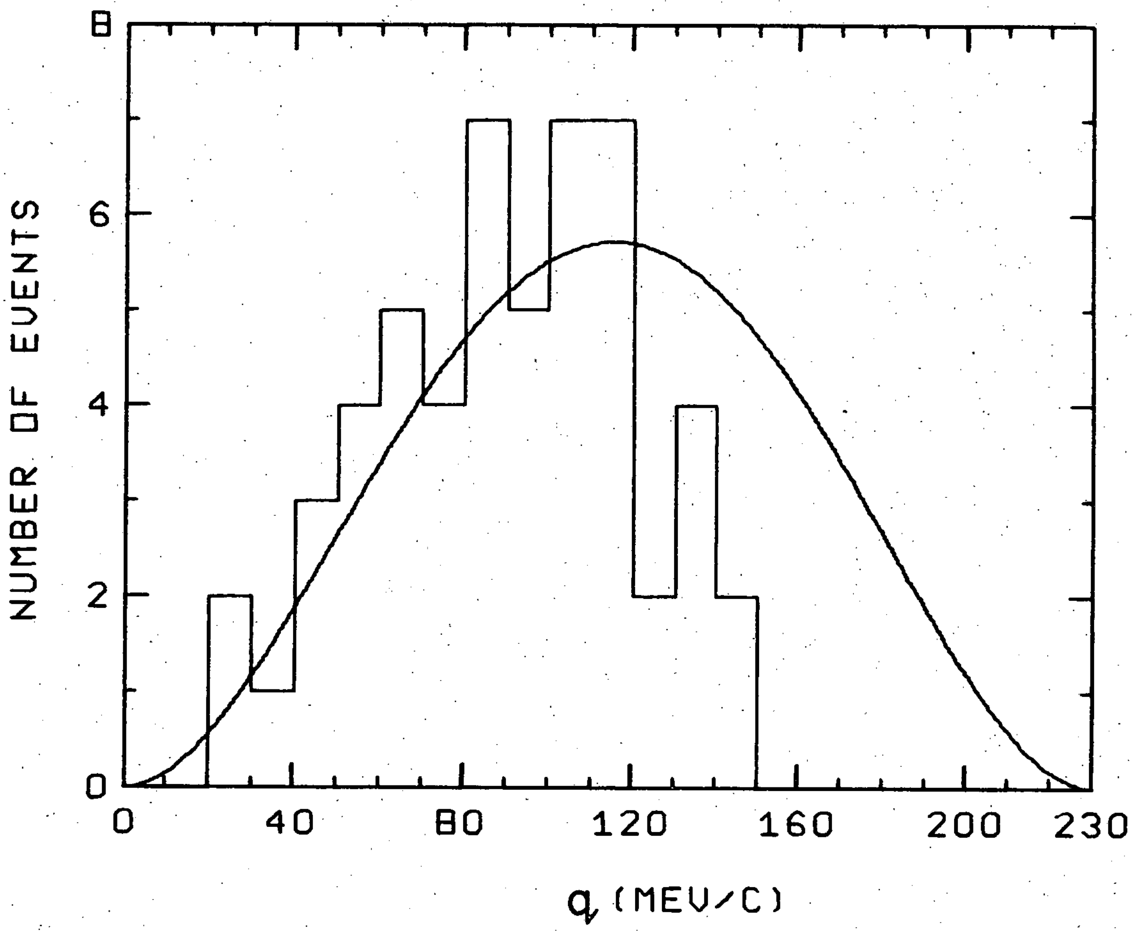

XBL 696-669

Fig. 8. The rest frame momentum distribution of the electron for the 53 $\Sigma^- \to ne^-\bar{\nu}$ events. The curve is the phase space curve based upon a branching ratio of 1.08×10^{-3} and the 64,935 events of $\Sigma^- \to n\pi^-$ which satisfied the same cuts imposed on the leptonic events.

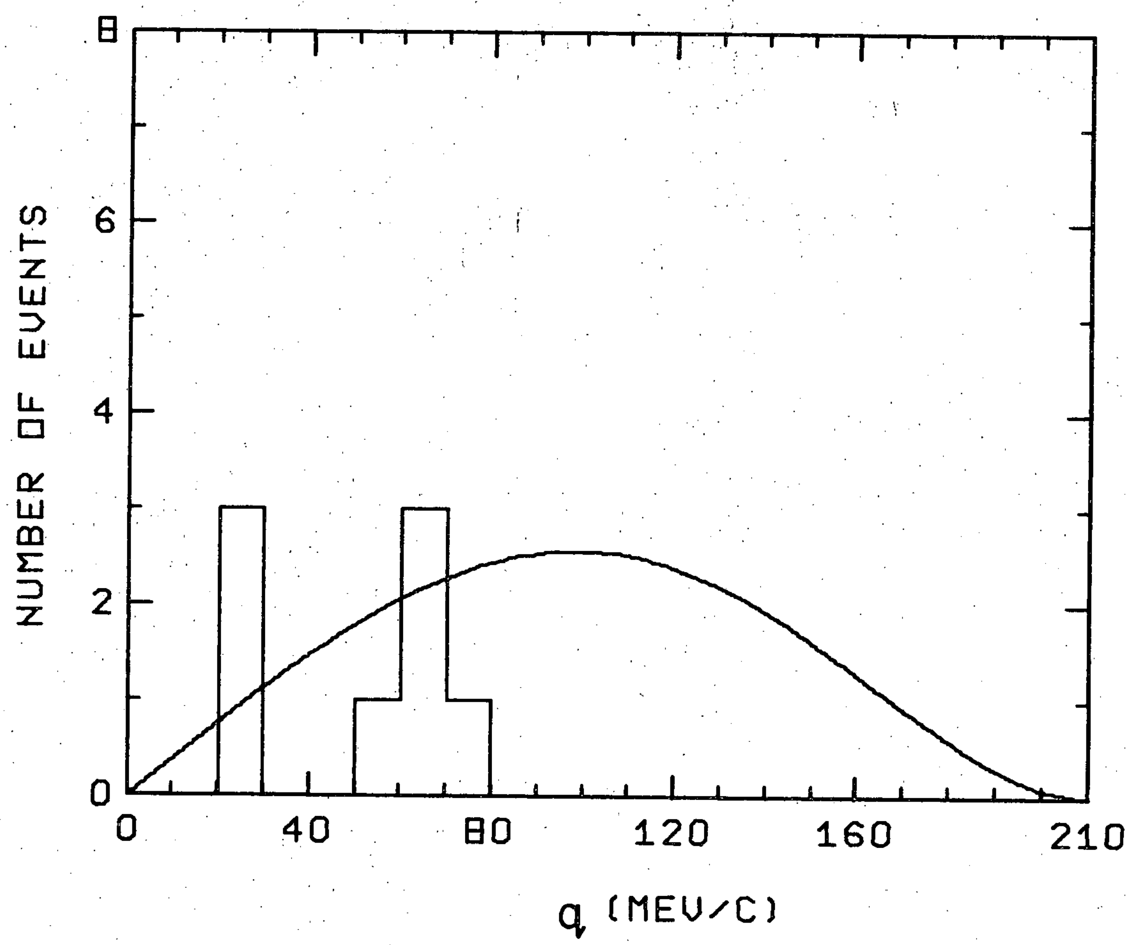

XBL 696-670

Fig. 9. The rest frame momentum distribution of the muon for the 8 $\Sigma^- \to n\mu^-\bar{\nu}$ events. The curve is the phase space curve based upon a branching ratio of 0.48×10^{-3} and the 64,935 events of $\Sigma^- \to n\pi^-$ which satisfied the same cuts imposed on the leptonic events.

G. Remaining Three-Body Events

Several cuts in addition to those of Sec. IIID were applied to the remaining three-body events and the two-body events in order to define a sample of events for the purpose of comparing the spectrum of remaining three-body events to that expected from the radiative-decay phase space. The numbers in parentheses are the number of two-body events removed by successive application of these cuts.

1) A restricted fiducial volume was defined which was approximately the same as the standard measuring volume. Since Σ^- events which were not in the standard measuring volume were measured in order to obtain additional electron events, this cut removed a considerable number of events. (10,054 events)

2) The beam track dip angle was required to be $-.064$ radians $<$ dip angle $< .052$ radians. Some events with a large measured beam track dip were bad measurements in which part of a different beam track was measured in one view, while others arose from K^-'s which scattered before entering the chamber and consequently had momenta differing somewhat from the beam-averaged momenta derived from the measurements of $K^- \to \pi^-\pi^-\pi^+$ (τ) decays. The two electron events with large beam track dip angle were both inspected to make sure that the fitted, measured, and beam-averaged momenta all were in good agreement. (2326 events)

3) The negative decay track was required to be greater than 10 cm. in length in order to provide a reasonable momentum measurement, unless it came to rest in less than 10 cm. (2332 events)

87 of the remaining three-body decays and 50,223 of the two-body decays survived these cuts.

These cuts, including a strict 60° dip angle cut for the electron tracks, when applied to the electron sample gave 40 events, whose RF momentum distribution is shown in Fig. 10. The solid curve is the phase space distribution based upon the 50,223 two-body decays. The agreement is quite good up to 140 MeV/c.

The RF momentum spectrum for the 87 three-body events not identified as either electrons or muons is shown in Fig. 11. The radiative decay spectrum is indicated by the curve, and is based upon the branching ratio of 1.1×10^{-3} for $q_\pi < 166$ MeV/c. There are several sources of events contributing to the remaining three-body decays, with the number, if known, indicated in parentheses:

1) π^- events which were identified because the π^- annihilated in flight or at rest (8 events)

2) events which were definitely non-electron events by ionization but which had negative decay particle RF momentum too great to be included in the muon sample (53 events)

3) events where the negative decay particle had laboratory momentum > 180 MeV/c and thus were not determinable by ionization (22 events)

4) events which appeared to be electron events by ionization, but where the negative decay particle had RF momentum > 150 MeV/c (1 event)

5) events which could not be identified by ionization, but where the negative decay particle had laboratory momentum < 180 MeV/c (3 events)

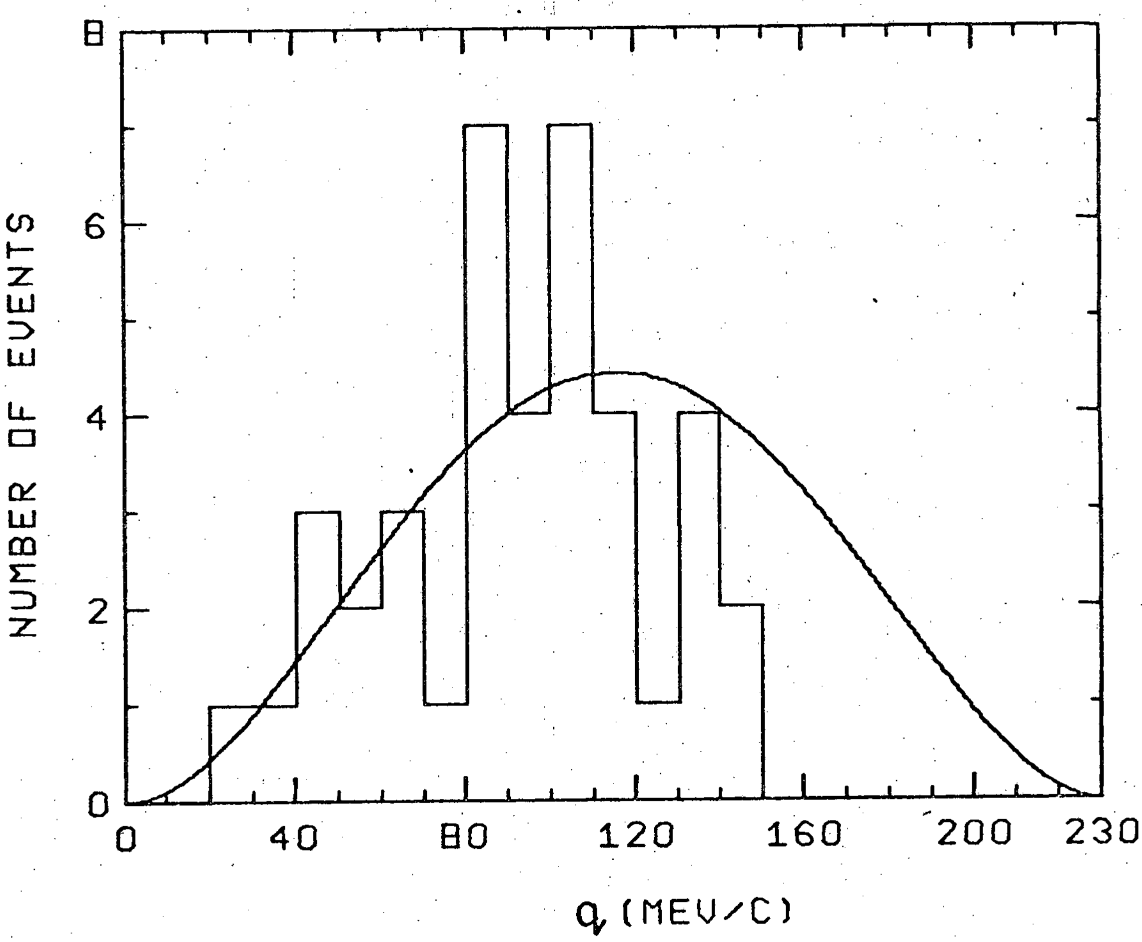

XBL 696-671

Fig. 10. The rest frame momentum distribution of the electron for the 40 $\Sigma^- \to ne^-\bar{\nu}$ events satisfying the restrictive three-body criteria of Sec. IIIG. The curve is the phase space curve based upon a branching ratio of 1.08×10^{-3} and the 50,223 events of $\Sigma^- \to n\pi^-$ which satisfied these criteria.

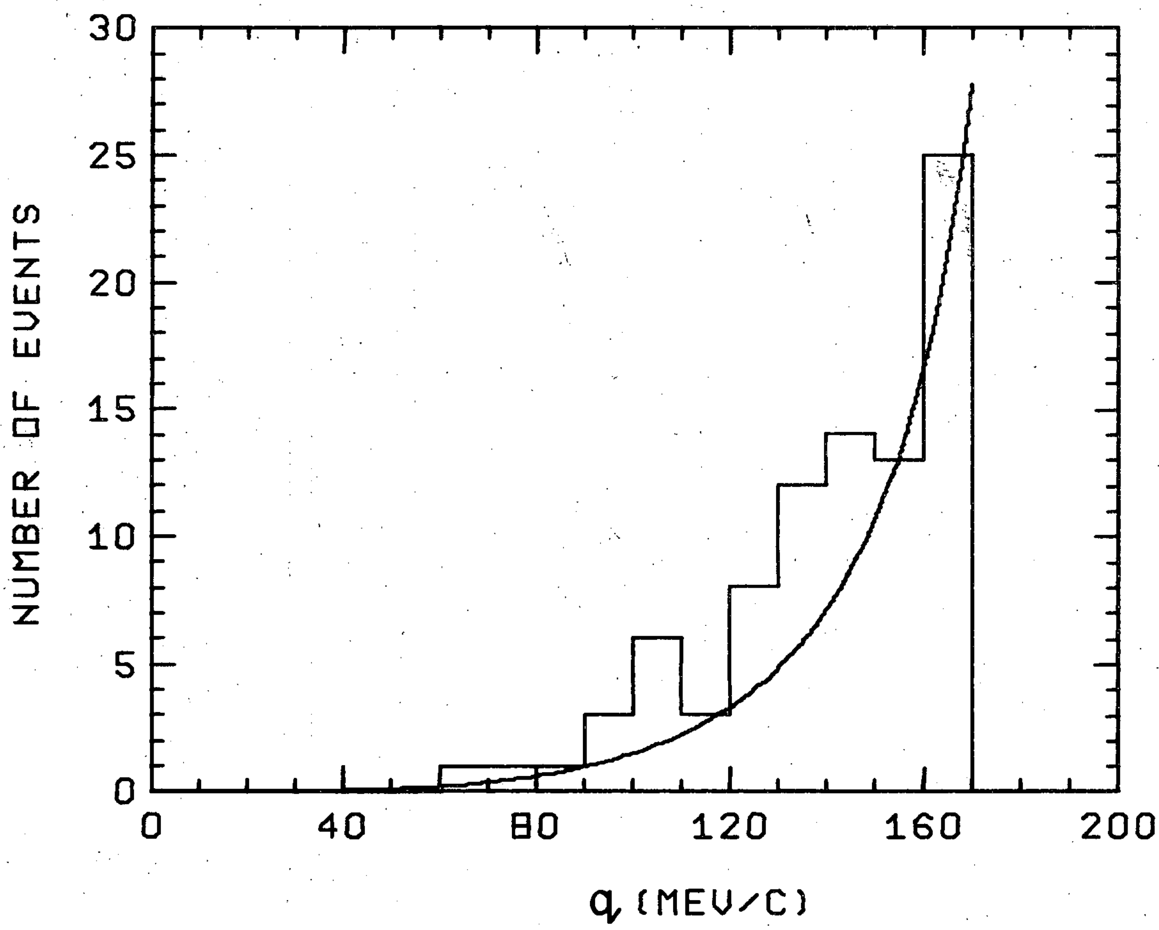

XBL 696-672

Fig. 11. The rest frame momentum distribution of the pion for the three-body Σ^- decays which were non-leptonic or non-identifiable. The curve is the phase space curve for $\Sigma^-_3 \rightarrow n\pi^-\gamma$ from Ref. 16, based upon a branching ratio of 1.1×10^{-3} for $q_\pi < 166$ MeV/c and the 50,223 events of $\Sigma^- \rightarrow n\pi^-$ which satisfied the criteria of Sec. IIIG.

6) events which may have been two-body decays where the negative decay particle had an unidentified scattering or decay, or excessive multiple Coulomb scattering

There seems to be some excess of events above the radiative decay curve. Some of these are undoubtedly muon events, since we identified only muons below RF momentum 80 MeV/c. It appears that we had good success in finding three-body events for RF momentum < 170 MeV/c with the techniques that we employed.

H. Electron Asymmetry Parameter

The electron asymmetry distribution is

$$I(\hat{q}) = 1 + \alpha \vec{P}_{\Sigma} \cdot \hat{q} , \qquad (3.1)$$

where $\vec{P}_{\Sigma}$ is the Σ^- polarization vector and $\hat{q}$ is the unit vector of the electron RF momentum. Such a correlation involving a pseudoscalar quantity may be expected to be non-zero because the decay is weak and thus does not necessarily conserve parity.

The polarization of the Σ^- arises from the interference between the amplitudes of the D-wave, $Y_0^*(1520)$ resonance occurring near 390 MeV/c K^- momentum and the predominantly S-wave background. Preliminary polarization data and asymmetry parameters for Σ non-leptonic decays from this experiment were presented in Ref. 17. Most of the events occurred quite near the resonant momentum, since we were intent on producing the highest possible Σ polarizations. The Σ^- polarizations cannot be determined well directly in the non-leptonic decay $\Sigma^- \to n\pi^-$, because the decay asymmetry parameter α for this decay is nearly zero,

$\alpha = -0.071 \pm 0.012$.[9] A fit to the data for all reaction channels in the experiment, involving essentially all the measured events, determined the magnitude and phase of all the partial wave amplitudes contributing to the reactions. These partial waves were particularly well determined for the reactions $K^-p \rightarrow \Sigma^-\pi^+$ and $K^-p \rightarrow \Sigma^+\pi^-$, since approximately 140,000 events were used to determine angular distributions, and the Σ^+ polarizations were well determined through the large asymmetry parameter, $\alpha = -0.999 \pm 0.022$, for the decay $\Sigma^+ \rightarrow p\pi^0$. Since the partial wave amplitudes fit the angular distributions for both Σ^- and Σ^+ and the polarizations in $\Sigma^+ \rightarrow p\pi^0$ quite well, the predicted polarizations for Σ^- should be quite reliable.

A maximum likelihood fit of the 53 electron events to the distribution in Eq. 3.1 was carried out, using the polarizations calculated from the multi-channel partial wave analysis. The likelihood function is defined by

$$\mathcal{L}(\alpha) = \prod_{i=1}^{53} (1 + \alpha\, P_{\Sigma_i} \cos\theta_i) , \qquad (3.2)$$

where P_Σ is the Σ^- polarization along the normal direction $\hat{n} = \vec{K}^- \times \vec{\pi}^+ / |\vec{K}^- \times \vec{\pi}^+|$, and $\cos\theta = \hat{n} \cdot \hat{q}$.

The logarithm of $\mathcal{L}$ is plotted in Fig. 12 as a function of the asymmetry parameter α. We find

$$\alpha = -0.26 \pm 0.37 ,$$

where the standard deviation points are determined by the values of α for which $\ln \mathcal{L}$ decreases by 0.5.

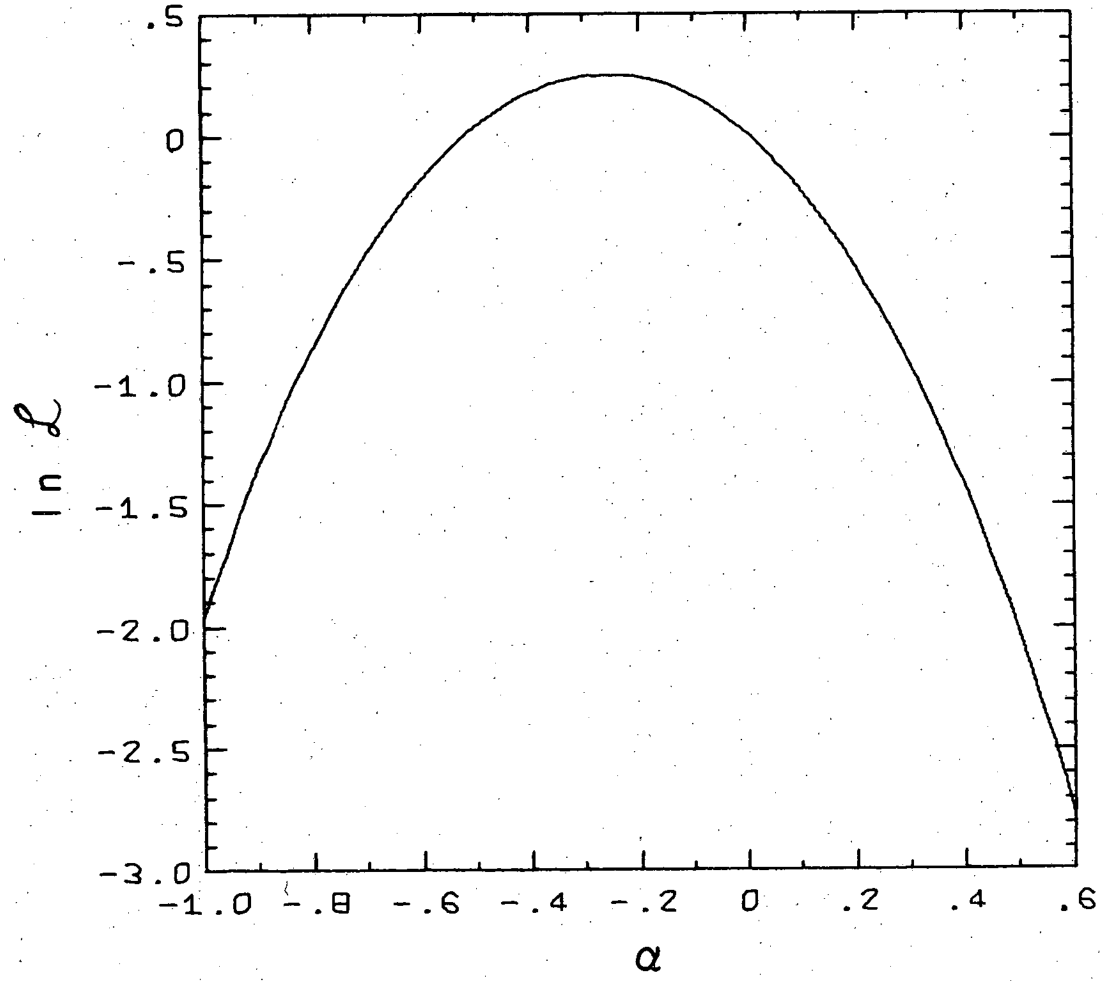

XBL 696-783

Fig. 12. The logarithm of the likelihood function, as a function of α, for the 53 $\Sigma^- \to ne^-\bar{\nu}$ decays. $\alpha = -0.26 \pm 0.37$.

All relevant data for each of the 53 electron events is listed in Table Ia, and for each of the 8 muon events, in Table Ib. The average polarization for the electron events was 0.58.

We estimate that there are 1.4 events of the type $K^- p \to \Sigma^- \pi^+$, $\Sigma^- \to \Lambda e^- \overline{\nu}$, $\Lambda \to \pi^0 n$ which are present in the electron sample. We do not feel that these represent any serious source of error in our determination of α.

There are three experimental biases occurring in the distribution defined by Eq. 3.1. Because of poorer scanning efficiency, we may be missing events where the e^- is emitted along the direction of the Σ^-, because the decay vertex may not have been distinguishable. Because we have not been able to identify as electron events those events for which the laboratory electron momentum was greater than 180 MeV/c, we have a bias against detecting events for which the e^- was emitted in a forward direction. Also, we are missing all events with electron dip angles $> 70°$, and some with angles $> 60°$. None of these biases should have any effect on our determination of α by a maximum likelihood technique. This is because these effects are functions of $\cos^2 \theta$, and not of $\cos \theta$, and consequently contribute terms independent of α when $\ln \mathcal{L}$ is evaluated for different values of α. The first effect is also negligible, since it occurs for values of $\cos \theta \approx 0$, so that such events carry no weight when the logarithm is evaluated.

The value of α that we have measured does not depend sensitively on the fact that we have cut the RF momentum spectrum of the electron at 150 MeV/c. α is, in fact, somewhat dependent on the RF momentum,

Table I. Data for the Σ^- leptonic decays.

ID is the identification number, K is the K^- laboratory momentum, $K^- \cdot \pi^+$ is the center of mass production cosine, e lab and e RF are the electron laboratory and rest frame momenta, e dip is the electron dip angle, P_Σ and cos Θ are the Σ^- polarization and the correlation angle as defined in Eq. 3.2.

ID	K	$K^- \cdot \pi^+$	e lab	e RF	e dip	P_Σ	cos Θ
			a) Electrons				
40120737	391.8	.536	73.0	82.3	57.5	-.978	.790
40170283	376.7	-.473	162.4	132.9	24.5	.534	-.341
40210916	387.7	.417	79.2	69.5	14.6	-.771	.593
40651039	372.7	.432	115.8	131.3	29.3	-.356	-.769
40711156	394.0	-.250	137.6	107.6	57.1	.593	.797
40810153	380.8	.685	51.8	46.7	59.2	-.922	-.439
40911350	374.4	.790	136.9	139.8	12.0	-.875	-.837
40971200	391.0	-.125	45.8	53.1	9.0	.305	-.831
41221306	369.6	.448	172.3	142.3	17.1	-.298	-.631
41490691	374.5	-.783	95.4	75.2	26.7	.769	.394
41950109	378.1	-.376	62.6	84.3	27.7	.472	.435
42020532	387.5	.212	136.0	121.6	28.2	-.398	.835
42230062	393.0	.305	46.1	45.8	43.3	-.722	.497
42461465	390.1	-.013	76.0	94.7	53.3	.053	.650
42551730	365.9	.133	101.0	101.9	25.3	.012	-.132
42580012	388.8	.613	81.0	80.8	10.6	-.988	.872
42601533	377.7	-.055	112.1	119.4	53.3	.131	-.677
42891728	392.2	.310	164.4	129.3	25.9	-.711	.372
42900779	383.6	-.219	69.5	97.5	10.0	.379	.011
43410775	326.7	-.650	102.6	113.7	28.7	.122	.518
43810285	347.5	-.922	103.4	84.2	54.4	.233	-.065
44160477	358.8	-.396	73.7	67.2	42.3	.247	-.955
44170177	379.6	-.005	76.4	71.7	69.9	.069	.770

Table I. (continued)

ID	K	$K^- \cdot \pi^+$	e lab	e RF	e dip	P_Σ	cos Θ
44340496	357.5	.806	113.5	110.4	31.4	-.312	-.927
44350476	389.7	-.738	161.8	138.6	35.5	.887	-.892
44411187	391.9	-.765	115.1	103.0	55.1	.871	-.637
44471266	385.5	-.113	57.3	43.0	28.0	.238	-.514
44490228	370.6	.179	64.2	60.0	65.9	-.063	.020
44880392	419.7	-.801	145.5	119.6	13.8	.661	.688
45050817	397.3	-.946	136.9	107.7	25.5	.475	.374
45380087	392.4	.731	108.1	95.0	52.3	-.942	.523
45420117	409.7	.242	129.4	112.0	39.3	-.780	-.603
45421481	401.5	.439	105.4	100.8	5.6	-.974	-.518
45440728	409.7	-.629	67.9	99.3	12.3	.919	.221
45500815	382.2	.700	93.3	78.9	63.1	-.962	.086
45521425	414.5	.924	100.5	105.8	28.1	-.290	.494
45580594	398.5	.851	161.2	145.0	43.0	-.640	.418
45600342	392.6	-.676	34.7	29.0	33.2	.908	.111
45651171	401.7	-.366	111.5	102.3	16.8	.893	.480
45871351	396.0	-.283	53.6	62.3	23.4	.688	.210
45921354	383.1	.678	39.4	35.9	20.2	-.958	.729
45960211	409.4	.581	126.9	118.6	29.4	-.817	.698
46380029	403.0	-.636	65.2	86.7	48.9	.932	-.581
46470434	424.2	-.814	56.4	63.7	68.3	.620	.612
46501660	389.7	-.812	47.7	56.3	2.7	.844	.425
46680132	385.7	.453	63.8	73.4	37.7	-.767	.590
46740557	416.6	-.837	46.9	29.4	20.4	.615	.011
46770888	392.4	.394	75.2	83.1	37.4	-.853	-.498
46960072	408.3	.839	67.8	66.4	60.1	-.505	.969
47350374	333.4	-.376	83.2	95.6	46.9	.145	.819
47691373	439.5	.930	118.5	112.0	10.2	-.176	-.433
48160664	392.4	-.721	42.0	58.2	27.6	.894	.309
48200679	387.7	-.062	88.5	88.3	23.7	.156	-.310

Table I. (continued)

ID	K	$K^- \cdot \pi^+$	μ lab	μ RF	μ dip	P_Σ	cos θ
			b) Muons				
41170304	374.9	.034	52.5	29.1	6.6	.041	.117
43690418	367.7	-.601	67.8	24.6	6.0	.461	-.066
44830950	365.5	-.630	88.6	51.3	40.1	.439	.799
45161349	400.4	-.590	73.9	29.3	3.7	.951	.426
45460851	407.3	-.306	109.0	63.9	39.6	.888	-.667
46310583	405.0	-.776	75.9	79.4	35.7	.783	-.708
47511430	437.5	-.987	78.3	61.2	22.8	.152	.328
48270821	398.4	.465	101.1	69.9	7.3	-.983	.287

as will be discussed in Sec. IVB. Since we have detected more than 2/3 of the spectrum, and since the momentum dependence of α is not very great, we believe that our measured value of α closely approximates that which would be measured if we had detected the entire electron spectrum.

The determination of α is dependent on a good knowledge of the Σ^- polarizations. The great amount of data so constrains the amplitudes that, even when we parameterize the amplitudes in a different way, the average polarization of 0.58 changes by only 1% and α changes by 0.01. The greatest difference in the polarization for an individual event for the two parameterizations was 0.08, but most of the differences were considerably smaller. Even an overall 10% change in the polarization would change α by an insignificant amount in comparison with the statistical error.

IV. BARYON LEPTONIC DECAYS AND g_A/g_V

A. Theoretical Description and Experimental History

1. Neutron Beta Decay

Neutron beta decay $n \rightarrow pe^-\bar{\nu}$ is well known to be described by the Hamiltonian

$$H = G_n/\sqrt{2}\; J_\mu\, \ell^\mu \;, \tag{4.1}$$

where

$$J_\mu = \bar{\psi}_p\, \gamma_\mu\, (g_V - g_A\gamma_5)\, \psi_n \tag{4.2}$$

and

$$\ell^\mu = \bar{\psi}_e\, \gamma^\mu\, (1 + \gamma_5)\, \psi_\nu \;. \tag{4.3}$$

The product $G_n g_V$ has been measured by looking at the decay rate for the pure Fermi (vector) decay of a nucleus. The ratio g_A/g_V has been determined by looking at the rate for neutron decay and also by looking at the asymmetry of the electron with respect to the neutron polarization, as we have done in correlating the electron with the Σ^- polarization. The angular distribution of electrons from polarized neutrons is given by

$$I(\hat{q}) = 1 + \alpha\, \vec{P}_n \cdot \beta\hat{q} \;, \tag{4.4}$$

where $\vec{P}_n$ is the neutron polarization vector, $\beta\hat{q}$ is the electron velocity, and α is given by[18]

$$\alpha = -2\; \frac{|g_A|^2 + \mathrm{Re}(g_V g_A{}^*)}{|g_V|^2 + 3\;|g_A|^2} \;. \tag{4.5}$$

The measurements are consistent with time-reversal invariance, implying that g_A and g_V are real. The measurement[19] of $\alpha = -0.111 \pm 0.018$, which gives the solution $g_A/g_V = -1.25 \pm 0.05$, is consistent with previous information on $|g_A/g_V|$ from the rate. A recent experiment[20] measuring the neutron lifetime is in statistical disagreement with the original determination of the lifetime, and more in accord with the measurement of g_A/g_V from the asymmetry parameter.

2. Universal Fermi Interaction and Conserved Vector Current

It was noticed by Feynman and Gell-Mann[1] in 1958 that the coupling constants for muon beta decay and nuclear beta decay were very similar. Muon decay was found to be represented by a Hamiltonian

$$H = G_\mu/\sqrt{2}\, \bar{\psi}_\nu \gamma_\lambda (1 + \gamma_5) \psi_\mu \bar{\psi}_e \gamma^\lambda (1 + \gamma_5) \psi_\nu , \qquad (4.6)$$

while neutron beta decay had the Hamiltonian described by Eqs. 4.1-4.3, with $g_V = 1$ and $g_A = -1.15$ at that time. G_μ and G_n were nearly equal. They proposed that the near equality of G_μ and G_n and the equality of the coefficients of γ_μ arose from two hypotheses: a universal Fermi interaction (UFI), which made the G's the same and the bare couplings identical, and a conserved vector current (CVC), which made the coefficients of the γ_μ terms equal to 1.

UFI implied that any beta decay could be described by a Hamiltonian similar to that of the muon, with factors of $(1 + \gamma_5)$ appearing before every annihilation operator. The remarkable fact that, after renormalization by the strong interactions, the vector current still had coefficient equal to one, was explained by CVC. A parallel was drawn with electromagnetism, where the electric charge is not renormalized by the strong interactions. The vector current for beta decay, which behaves like the isospin-raising operator τ^+, was identified as a member of the same isospin multiplet as the electromagnetic current, which behaves like τ^3. The vector current for beta decay with emission of a positron is associated with the third member of the isospin triplet. With this identification of the weak vector current with the electromagnetic current, the conservation of the electromagnetic current implies the conservation of the weak vector current for nuclear beta decay.

CVC had considerable success in its predictions for weak leptonic decays. It predicted successfully the rate for $\pi^\pm \to \pi^o e^\pm \nu$ from the presence of the meson field terms in the electromagnetic current. A weak magnetism term was predicted, in analogy with the anomalous magnetic moment term for the electromagnetic current. The weak magnetism term was found in nuclear beta decay and was in agreement with the prediction.

UFI implied that Λ and Σ^- leptonic decays existed, with the same coupling as neutron beta decay. This assumption implied that Λ leptonic decay should occur in 1.6% of the Λ decays, and Σ^- leptonic decay, in 5.6% of the Σ^- decays.

These predictions were not borne out by experiment. The first Λ leptonic decays were found in 1958 [21], while three experiments[22] each found a single event of $\Sigma^- \to ne^-\bar{\nu}$ in 1961. The rates appeared to be an order of magnitude lower than the UFI prediction.

3. Leptonic Decay Experiments and Cabibbo's Theory

The next generation of experiments was completed between 1963 and 1965, before this experiment was begun. These experiments succeeded in measuring the rates for $\Lambda \to pe^-\bar{\nu}$, $\Sigma^- \to ne^-\bar{\nu}$, $\Sigma^- \to \Lambda e^-\bar{\nu}$, and $\Sigma^+ \to \Lambda e^+\nu$, and g_A/g_V for $\Lambda \to pe^-\bar{\nu}$. The latter was determined by angular correlations among the decay particles and by measurement of α and application of Eq. 4.5. The results are summarized in Table II, where only the major experiments are listed. The idea of an UFI for leptonic decays had failed, since the decay rates for the strangeness-changing decays were too low.

A great step in understanding the leptonic decays was made by Cabibbo[8] in 1963, when he suggested that the various baryon leptonic decays can be related to each other through SU(3) symmetry. He made the following assumptions:

1) The weak current of the hadrons, J_μ, transforms as an octet representation of the group SU(3). This assumption limits the theory from considering $\Delta S = -\Delta Q$ decays, such as $\Sigma^+ \to ne^+\nu$, and $\Delta S = 2$ decays, such as $\Xi^- \to ne^-\bar{\nu}$.

2) The vector current, V_μ, is in the same octet representation as the electromagnetic current. This assumption is analogous to the conserved vector current theory, in that in the presence of SU(3) symmetry, the conservation of the electromagnetic current implies the conservation of all members of the vector current octet.

3) $$J_\mu = \cos\theta\,(V_\mu^{(0)} + A_\mu^{(0)}) + \sin\theta\,(V_\mu^{(1)} + A_\mu^{(1)}) , \quad (4.7)$$

where $V_\mu^{(i)}$ ($A_\mu^{(i)}$) is the vector (axial-vector) current for decays

Table II. Second generation of leptonic decay experiments.

Decay	Events	Year	Branching Ratio	Reference
$\Lambda \to p e^- \bar{\nu}$	150	1963	$(8.2 \pm 1.2) \times 10^{-4}$	23
	20	1964	(15.5 ± 3.4)	24
	102	1965	(7.8 ± 1.2)	25
$\Sigma^- \to n e^- \bar{\nu}$	9	1964	$(1.0 {+0.4 \atop -0.3}) \times 10^{-3}$	4
	16	1964	(1.4 ± 0.3)	5
	16	1964	(1.2 ± 0.4)	26
	31	1964	(1.4 ± 0.3)	3
$\Sigma^- \to \Lambda e^- \bar{\nu}$	11	1964	$(7.5 \pm 2.8) \times 10^{-5}$	3
$\Sigma^+ \to \Lambda e^+ \nu$	4	1964	$(3.3 \pm 1.7) \times 10^{-5}$	3

Decay	Events	Year	g_A/g_V	Reference
$\Lambda \to p e^- \bar{\nu}$	22	1964	$-1.03 {+0.34 \atop -0.70}$	24
	59	1965	$\lvert g_A/g_V \rvert > 0.7$	27
	102	1965	$\lvert g_A/g_V \rvert > 0.6$	25
		1965	$-1.1 < g_A/g_V < 0$	28

of ΔS = i.

The assumption of different strengths cos θ and sin θ for the strangeness-conserving and strangeness-changing decays is a departure from UFI, but UFI is almost preserved for $\Delta S = 0$ decays by the theory. The angle θ is expected to be small, since the rates for $\Delta S = 1$ decays are small compared to the UFI rates. The use of an angle is suggestive, in that were there not a rotation by θ in SU(3) space, the current J_μ would have the same strength for strangeness-conserving decays as the coupling for muon decay. The factor of cos θ for $\Delta S = 0$ decays explained the small lack of equality for the vector couplings for neutron beta decay and muon beta decay- a fact which had been disturbing, in light of the success of CVC.

The application of the theory to baryon leptonic decays in Cabibbo's original paper led to a successful fit to the data available at the time, with $\theta = 0.26$, assuming the same angle for both vector and axial-vector currents. The data included preliminary results from some of the experiments listed in Table II. Cabibbo also included some information on K and π leptonic decays, which should also be related by the theory.

Willis et al.[3], with the completion of their experiment on Σ leptonic decays in 1964, made a new, somewhat more sophisticated fit to the data for leptonic decays. They found two fits to the data, because of the relatively large experimental errors at that time. The two fits predicted $|g_A/g_V| \sim 0.3$ for $\Sigma^- \rightarrow ne\bar{\nu}$, with a positive sign for one fit and a negative sign for the other. The determination of this number was thus considered an important step in testing the validity of the theory and in choosing the correct solution.

Subsequent to the beginning of this experiment, several new experiments have measured the branching ratios and g_A/g_V for various decays. These results are summarized in Table III, along with the value of g_A/g_V for $\Sigma^- \rightarrow ne^-\bar{\nu}$ that we published in 1968.[39] The measurement of the $\Sigma^- \rightarrow \Lambda e^-\bar{\nu}$ branching ratio by Barash et al.[33] succeeded in establishing that only one possible solution to the fit was consistent with the data, the one predicting the positive sign for g_A/g_V for $\Sigma^- \rightarrow ne^-\bar{\nu}$.

B. Determination of g_A/g_V for Σ^- Leptonic Decay

One can obtain an expression for the asymmetry parameter in terms of g_A/g_V for a baryon leptonic decay $B' \rightarrow Be^-\bar{\nu}$ by the procedure of multiplying the square of the matrix element by the phase space factors, integrating over all variables except the electron direction, and summing over the final spins. In this way one obtains the expression given in Eq. 4.5, if one uses the forms for the Hamiltonian and the currents given by Eqs. 4.1-4.3, and if one neglects recoil effects associated with the finite momentum of the electron. This procedure, while good to a high degree of accuracy for neutron beta decay because of the small mass difference between the neutron and the proton, is not so accurate for the case of hyperon leptonic decay.

Harrington[42] and, more recently, Bender et al.[43] and Linke[43] have performed the calculations to obtain the electron distribution for polarized hyperon leptonic decay. The expression for J_μ is gen-

Table III. Third generation of leptonic decay experiments.

Decay	Events	Year	Branching Ratio	Reference
$\Lambda \rightarrow pe^-\bar{\nu}$	99	1969	$(8.4 \pm 1.0) \times 10^{-4}$	29
$\Sigma^- \rightarrow ne^-\bar{\nu}$	180	1968	$(1.11 \pm 0.09) \times 10^{-3}$	30
		1968	(1.11 ± 0.11)	31
		1968	(1.11 ± 0.15)	32
	331	1969	(1.02 ± 0.08)	15
$\Sigma^- \rightarrow \Lambda e^-\bar{\nu}$	35	1967	$(6.4 \pm 1.2) \times 10^{-5}$	33
	31	1969	(5.2 ± 0.9)	34
	31	1969	(6.9 ± 1.2)	35
$\Sigma^+ \rightarrow \Lambda e^+\nu$	6	1967	$(2.0 \pm 0.8) \times 10^{-5}$	33
	5	1969	(1.6 ± 0.7)	34
	10	1969	(2.9 ± 1.0)	35
$\Xi^- \rightarrow \Lambda e^-\bar{\nu}$	4	1968	$(1.15 {}^{+0.90}_{-0.55}) \times 10^{-3}$	36
	14	1968	$(0.61 {}^{+0.18}_{-0.29})$	37

Decay	Events	Year	g_A/g_V	Reference
$\Lambda \rightarrow pe^-\bar{\nu}$	30	1968	$-0.23 {}^{+0.20}_{-0.33}$	38
	139	1969	$\lvert g_A/g_V \rvert = 0.68 {}^{+0.18}_{-0.12}$	29
$\Sigma^- \rightarrow ne^-\bar{\nu}$	57	1968	$0.05 {}^{+0.23}_{-0.32}$	39
	40	1969	$\lvert g_A/g_V \rvert = 0.3 \pm 0.3$	40
	33	1969	$\lvert g_A/g_V \rvert = 0.37 {}^{+0.26}_{-0.19}$	41
$\Sigma^\pm \rightarrow \Lambda e^\pm\nu$	45	1967	$\lvert g_V/g_A \rvert = 0.31 \pm 0.30$	33
	52	1969	$g_V/g_A = 0.7 \pm 0.4$	34
	81	1969	$g_V/g_A = 0.22 \pm 0.28$	35

eralized to account for the momentum of the leptons:

$$J_\mu = \bar{\Psi}_B \left\{ f_1 \gamma_\mu + (f_2/m_B{}') \sigma_{\mu\nu} q^\nu + (f_3/m_B{}') q_\mu + \right. \\ \left. + g_1 \gamma_\mu \gamma_5 + (g_2/m_B{}') \sigma_{\mu\nu} \gamma_5 q^\nu + (g_3/m_B{}') \gamma_5 q_\mu \right\} \psi_B{}' , \qquad (4.8)$$

where, in our notation, $g_V = f_1$ and $g_A = -g_1$, $m_B{}'$ is the mass of the parent baryon, and q_μ is the sum of the lepton momenta. The f_2 term is the weak magnetism term, f_3 is induced scalar, g_2 is axial weak magnetism, and g_3 is induced pseudoscalar.

After performing the requisite integrations and sums over final spins, the authors obtain identical expressions for the electron momentum distribution (valid also for baryon muonic decay if muon quantities are used instead of electron quantities):

$$I(x,\cos\theta) \propto \frac{\beta x^2 (1 - x)^2}{(1 + \epsilon - 2Rx)^3} (a(x) + b(x) \beta P_B{}' \cos\theta) , \qquad (4.9)$$

where

$x = E_\ell/E_\ell^{max}$, E_ℓ is the electron energy, E_ℓ^{max}, the maximum energy;

$P_B{}'$ is the polarization of the parent baryon;

θ is the angle between the polarization and the electron momentum;

$\epsilon = (m_\ell/m_B{}')^2$, m_ℓ is the mass of the electron;

$R = E_\ell^{max}/m_B{}'$; and

$a(x)$ and $b(x)$ are energy-dependent sums of terms in $Re(f_i f_j^*)$, $Re(f_i g_j^*)$, and $Re(g_i g_j^*)$, with $i,j = 1,2,3$.

The asymmetry parameter is thus given by

$$\alpha = \beta\, b(x) / a(x) , \qquad (4.10)$$

so that α is dependent on the electron energy as well as on the values of the f_i and g_i. $\beta = 1$ for essentially the entire spectrum for electrons, although it is relevant for muonic decay.

If one assumes time reversal invariance, which seems to hold in neutron decay, then the f_i and g_i are real. The terms involving f_3 and g_3 are assumed to be zero, since they are of order ϵ with respect to the other terms. In a classification due to Weinberg,[44] f_1, f_2, g_1, and g_3 are first-class currents and f_3 and g_2 are second-class currents. The assumption is generally made on theoretical grounds that the second-class currents are absent. Because of the statistical limitations of our data, we shall take $g_2 = 0$, rather than leaving it as a free parameter. The resulting expressions for a(x) and b(x) are tabulated in Appendix A. The quantity R_p in the appendix is defined by $R_p = m_B/m_B{}'$. A similar number of terms of order ϵ exist which have not been listed in the appendix, since their value is completely negligible for electronic decay and is about 1% for muonic decays. We have assumed that the f_i and g_i have no momentum dependence. The terms tabulated are exact to the extent that terms of order ϵ can be neglected.

In Fig. 13 we have drawn two curves: the relation between α and g_A/g_V in Eq. 4.5 for neutron decay is denoted by the dotted curve, and α as given by b(x)/a(x) for an electron of RF momentum 90 MeV/c, our average momentum, is denoted by the solid curve. A value of $f_2/g_V = -1.02$ was assumed and is explained in the next paragraph. The two curves are very similar, so that Eq. 4.5, the neutron relation, is a very good approximation to Σ^- decay as well.

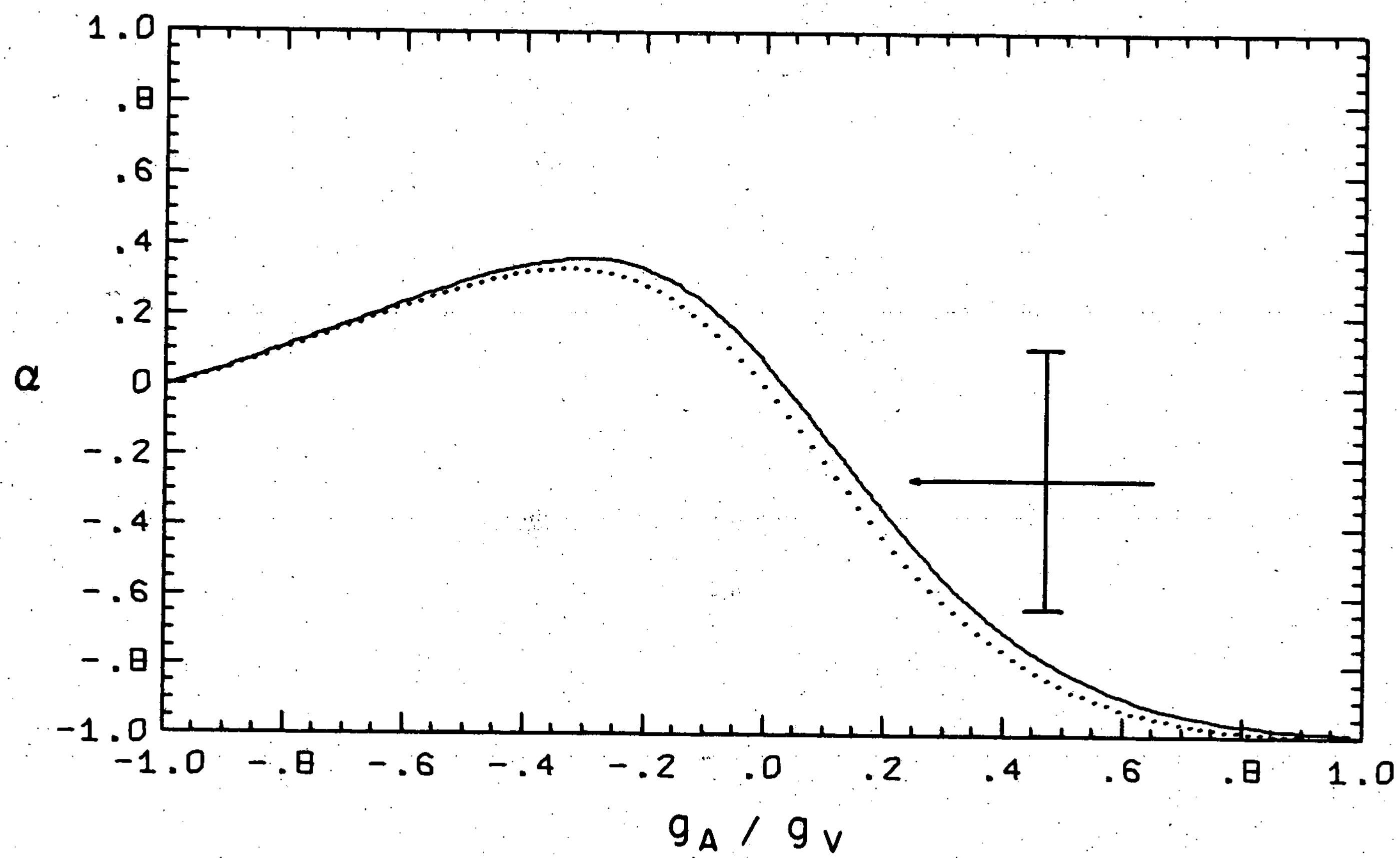

XBL 696-782

Fig. 13. α as a function of g_A/g_V. The solid curve is that obtained for q_e = 90 MeV/c, our average momentum, using Eq. 4.10 with f_2/g_V = -1.02; the dotted curve is Eq. 4.5, the neutron relation. The measured value of $\alpha = -0.26 \pm 0.37$ is indicated.

With $f_2 = 0$, the solid curve would come below the dotted curve, and there would be a greater absolute difference than is the case here. Our measured value $\alpha = -0.26 \pm 0.37$ is indicated by the data point.

A maximum likelihood fit to the electron distribution was carried out for our 53 electron events, with

$$\mathcal{L}(g_A/g_V) = \prod_{i=1}^{53} (1 + \beta_i (b(x_i)/\ a(x_i)) P_{\Sigma_i} \cos\theta_i. \quad (4.11)$$

The likelihood function was much less sensitive to the value of f_2/g_V than to g_A/g_V, but the two quantities were correlated. We thus decided to fix f_2 by its value as predicted by CVC and SU(3), at $f_2/g_V = -1.02$. Other authors, in trying to account for the SU(3) breaking, have calculated values of -1.14[43] and -1.30.[45]

The logarithm of the likelihood function is shown in Fig. 14, for $-1 < g_A/g_V < 1$. We find, for the 53 electron events, the values

$$g_A/g_V = 0.16 \begin{smallmatrix} +\ 0.19 \\ -\ 0.18 \end{smallmatrix}$$

and $\quad g_A/g_V = -1.7$, with large errors.

Changing f_2/g_V by ±1 resulted in a change of ± 0.08 in g_A/g_V.

The likelihood function was also evaluated for the 8 muon events, using the expressions given in Appendix A. These expressions are good to about 1% for muons. We find that the likelihood function is too broad to make a determination of g_A/g_V. Note that the muons are poorer than the electrons in determining g_A/g_V from α because of the factor of β in the asymmetry, which is 1 for electrons but averages 0.35 for the 8 muons.

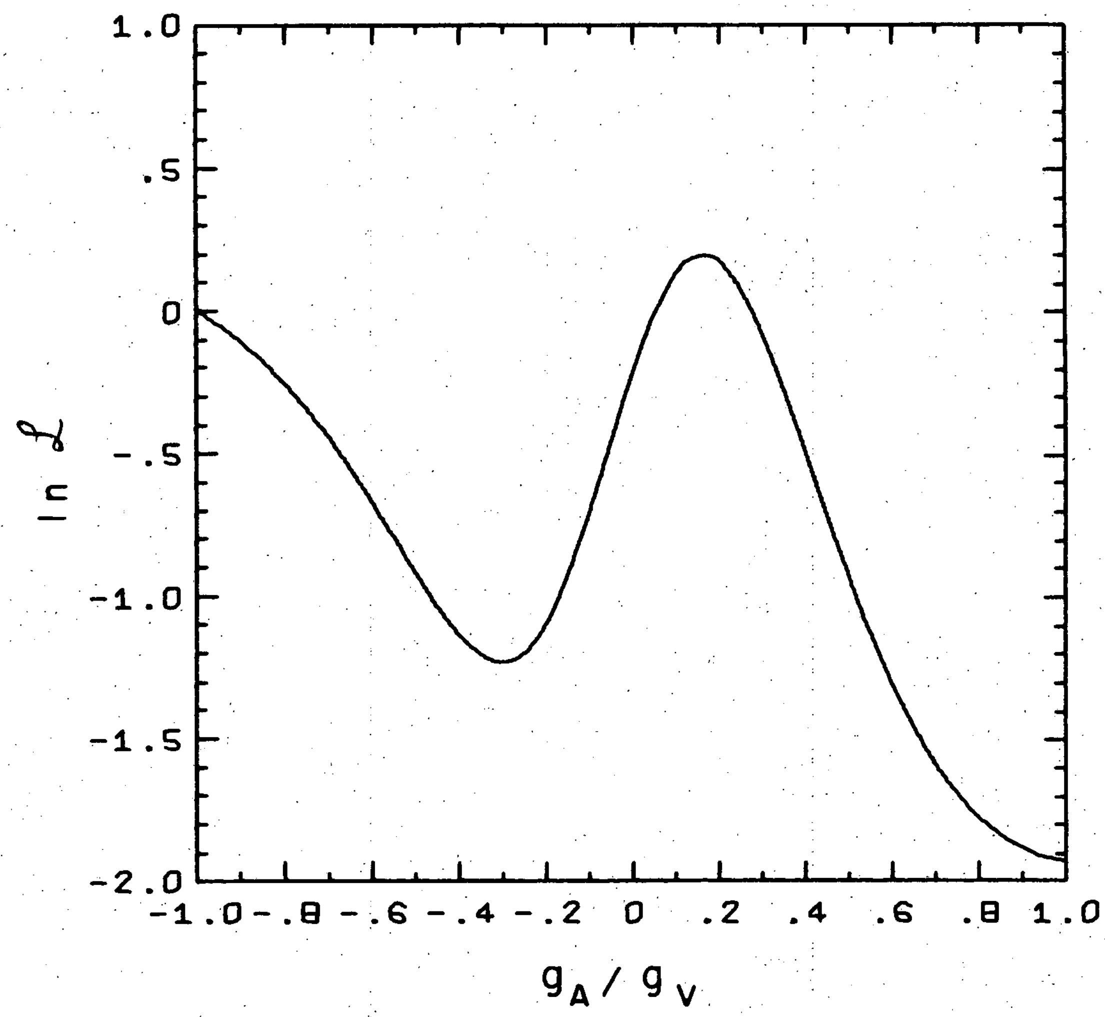

XBL 696-784

Fig. 14. The logarithm of the likelihood function, as a function of g_A/g_V, for the 53 $\Sigma^- \rightarrow ne\bar{\nu}$ decays. $g_A/g_V = 0.16 \begin{smallmatrix} +\ 0.19 \\ -\ 0.18 \end{smallmatrix}$ is the primary solution.

If we assume μ-e universality, we can combine the 53 electrons and 8 muons to determine an overall g_A/g_V for Σ^- leptonic decay. The logarithm of the likelihood function is shown in Fig. 15 for $-1 < g_A/g_V < 1$. We find

$$g_A/g_V = 0.19 \begin{array}{l} + 0.20 \\ - 0.17 \end{array}$$

and $$g_A/g_V = -2.0, \text{ with large errors.}$$

We have chosen the first value as our primary value, since the fits to Cabibbo's theory predict $g_A/g_V \sim 0.3$. In addition, there are two preliminary measurements of $|g_A/g_V|$ of 0.3 ± 0.3[40] and $0.37 \begin{array}{l} + 0.26 \\ - 0.19 \end{array}$[41] obtained by observing the momentum of the neutron through its interaction with a proton in the bubble chamber. These experiments were performed with unpolarized Σ^-'s, so that they are unable to measure the sign of g_A/g_V.

Assuming that $|g_A/g_V| = 0.3$, we have succeeded in measuring the sign to be positive rather than negative to nearly two standard deviations, as given by the likelihood function.

C. Fit to Cabibbo's Theory

Several authors have fit the available data for leptonic decays to Cabibbo's theory.[3,45-48] We shall present here our fit to the currently published data, including this experiment.

The hadronic matrix element for a baryon leptonic decay $B' \to Be^-\bar{\nu}$, $\langle B \mid \gamma_\mu (g_V - g_A\gamma_5) \mid B' \rangle$, is represented in terms of SU(3) symmetry by the coupling of the baryon octet to itself by means of a vector octet of currents and an axial-vector octet of

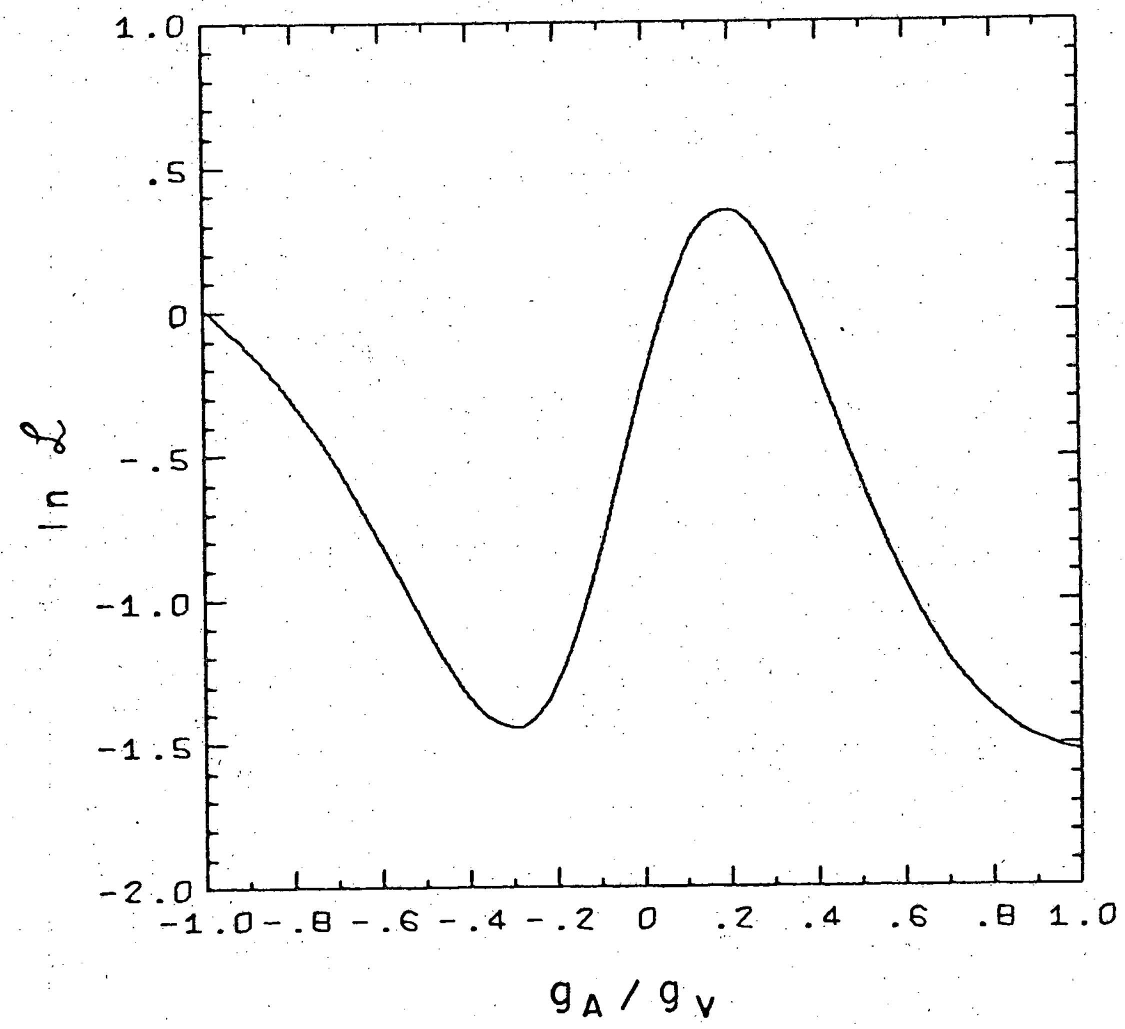

XBL 696-780

Fig. 15. The logarithm of the likelihood function, as a function of g_A/g_V, for the 61 Σ^- leptonic decays. $g_A/g_V = 0.19 {+0.20 \atop -0.17}$ is the primary solution.

currents. The expression for the current J_μ was given in Eq. 4.7. Cabibbo assumed the angle θ to be the same for both vector and axial-vector currents, which it would have to be in order to satisfy the current commutation relations exactly. Some of the authors who fit the data do not impose this condition, because the strong interactions are expected to renormalize θ for the axial-vector current. Nevertheless, the value obtained for θ_A is approximately equal to that of θ_V, so that we will assume throughout that there is but one angle θ.

It is possible to couple three octets to form an SU(3) invariant in two ways: a symmetric (D) coupling, and an antisymmetric (F) coupling. In terms of the D and F couplings one can write the product of the couplings, K, as

$$K = D\ \mathrm{tr}(\overline{B}\ \{J,B\}\ ) + F\ \mathrm{tr}(\overline{B}\ [J,B]\ )\ , \tag{4.12}$$

where D and F are constants, tr stands for the trace of the enclosed expression, and $\overline{B}$, J, and B are the 3x3 matrices representing the anti-baryon octet, weak current octet, and baryon octet, respectively. We have suppressed spatial indices. It is convenient as a mnemonic device to represent J by the meson octet, since the strangeness and isospin quantum numbers are the same. In Appendix B we give the matrices $\overline{B}$, B, and J.

The SU(3) coefficient, either K cos θ or K sin θ, is listed below for the leptonic decays which have been observed.

Decay	SU(3) Coefficient
$n \to pe^-\bar{\nu}$	$(F + D) \cos \theta$
$\Lambda \to pe^-\bar{\nu}$	$-1/\sqrt{6}\,(3F + D) \sin \theta$
$\Sigma^- \to ne^-\bar{\nu}$	$(-F + D) \sin \theta$
$\Sigma^- \to \Lambda e^-\bar{\nu}$	$\sqrt{2/3}\, D \cos \theta$
$\Sigma^+ \to \Lambda e^+\nu$	$\sqrt{2/3}\, D \cos \theta$
$\Xi^- \to \Lambda e^-\bar{\nu}$	$1/\sqrt{6}\,(3F - D) \sin \theta$

The values of D and F for the coupling of the vector current are different from those for the axial-vector current; however, the expressions for the SU(3) coefficients are the same. In our notation, g_V equals the vector SU(3) coefficient while g_A equals the negative of the axial-vector SU(3) coefficient. We would have, in general, five independent parameters in the theory: θ, D_V, F_V, D_A, and F_A. CVC says, however, that $F_V = 1$ and $D_V = 0$, since the coupling K is also responsible for electromagnetism under the assumptions of the Cabibbo theory. If D_V were not zero, the electric charges of the proton and neutron would come out wrong. Another way of seeing that $D_V = 0$ is that only D coupling connects $\Sigma^{\pm}$ to Λ, but the vector current does not contribute to this decay except in the weak magnetism term[49]. We shall henceforth use the notation $D = D_A$ and $F = F_A$; these and θ are the parameters that we wish to determine.

The decay rates are evaluated by integrating the square of the matrix element over the phase space and performing the appropriate spin summations. Bender et al.[43] have performed these integrations for all baryon leptonic decays, for all the f_i and g_i couplings. The weak magnetism (f_2) and axial weak magnetism (g_2) terms are not entirely negligible, but we shall nevertheless neglect them in the expressions used to fit the data, since the experimental errors are still larger than these terms. The f_2 terms increase the calculated Λ rate by about 1% and decrease the calculated $\Sigma^- \rightarrow n$ rate by about 2%, whereas the experimental errors are 11% and 6%, respectively. The contributions to neutron decay and $\Sigma^{\pm} \rightarrow \Lambda$ decay are much smaller. The g_2 terms have not been determined, but they are expected to be small because g_2 is a second-class current term.

The branching ratio for a leptonic decay is the product of its decay rate and the lifetime of the parent baryon. The ratio g_A/g_V is the negative of the ratio of the respective SU(3) coefficients. The expressions for the decay rates calculated by Bender et al. and the experimental lifetimes used are listed in Table IV. The Λ and Ξ^- lifetimes are the compiled values from Ref. 13, while the Σ^- and Σ^+ lifetimes are the preliminary values determined by this experiment.[9] The Σ^- lifetime differs from the compiled value of Ref. 13, but it is in agreement with several recently measured values.[50] The errors on the lifetimes are not used in the fit.

A χ^2 minimization was performed for the best values of the parameters Θ, D, and F, using the expressions in Table Va fitted to the data in Table Vb. The data was compiled only from published experiments. Using the first 8 data points, we obtain a fit which

Table IV. Calculated rates and experimental lifetimes for decays used in the fit to the Cabibbo theory of semi-leptonic decays.

Decay	Rate (sec^{-1})
$n \rightarrow pe^- \bar{\nu}$	$1.89 \times 10^{-4}\ (g_V^2 + 3.00\ g_A^2)$
$\Lambda \rightarrow pe^- \bar{\nu}$	$1.514 \times 10^{7}\ (g_V^2 + 2.98\ g_A^2)$
$\Sigma^- \rightarrow ne^- \bar{\nu}$	$9.00 \times 10^{7}\ (g_V^2 + 2.95\ g_A^2)$
$\Sigma^- \rightarrow \Lambda e^- \bar{\nu}$	$3.66 \times 10^{5}\ (3.00\ g_A^2)$
$\Sigma^+ \rightarrow \Lambda e^+ \nu$	$2.21 \times 10^{5}\ (3.00\ g_A^2)$
$\Xi^- \rightarrow \Lambda e^- \bar{\nu}$	$3.19 \times 10^{7}\ (g_V^2 + 2.98\ g_A^2)$

Particle	Lifetime $\times 10^{-10}$ (sec)
Λ	2.51 ± 0.03
Σ^-	1.46 ± 0.03
Σ^+	0.771 ± 0.014
Ξ^-	1.66 ± 0.04

Table Va. Expressions used in the fit to the Cabibbo theory.

Decay	Branching Ratio
$\Lambda \to pe^- \bar{\nu}$	$5.70 \times 10^{-3} \sin^2 \theta \, (1 + 2.98 \, (F + D/3)^2)$
$\Sigma^- \to ne^- \bar{\nu}$	$1.313 \times 10^{-2} \sin^2 \theta \, (1 + 2.95 \, (F - D)^2)$
$\Sigma^- \to \Lambda e^- \bar{\nu}$	$1.068 \times 10^{-4} \cos^2 \theta \, (D^2)$
$\Sigma^+ \to \Lambda e^+ \nu$	$3.408 \times 10^{-5} \cos^2 \theta \, (D^2)$
$\Xi^- \to \Lambda e^- \bar{\nu}$	$7.94 \times 10^{-3} \sin^2 \theta \, (1 + 2.98 \, (F - D/3)^2)$

Decay	Rate (sec^{-1})
$n \to pe^- \bar{\nu}$	$1.89 \times 10^{-4} \cos^2 \theta \, (1 + 3.00 \, (F + D)^2)$

Decay	g_A/g_V
$n \to pe^- \bar{\nu}$	$-(F + D)$
$\Lambda \to pe^- \bar{\nu}$	$-(F + D/3)$
$\Sigma^- \to ne^- \bar{\nu}$	$D - F$

Table Vb. Data used in the fit to the Cabibbo theory.

Decay	Branching Ratio	Reference
$\Lambda \to pe^-\bar{\nu}$	$(0.80 \pm 0.09) \times 10^{-3}$	51
$\Sigma^- \to ne^-\bar{\nu}$	$(1.08 \pm 0.06) \times 10^{-3}$	52
$\Sigma^- \to \Lambda e^-\bar{\nu}$	$(6.04 \pm 0.60) \times 10^{-5}$	53
$\Sigma^+ \to \Lambda e^+\nu$	$(2.11 \pm 0.45) \times 10^{-5}$	53
$\Xi^- \to \Lambda e^-\bar{\nu}$	$(1.15 {}^{+0.90}_{-0.55}) \times 10^{-3}$	36

Decay	Lifetime (sec)	Reference
$n \to pe^-\bar{\nu}$	$(0.932 \pm 0.014) \times 10^3$	20

Decay	g_A/g_V	Reference
$n \to pe^-\bar{\nu}$	-1.25 ± 0.04	54
$\Lambda \to pe^-\bar{\nu}$	$-1.14 {}^{+0.23}_{-0.33}$	55
$\Sigma^- \to ne^-\bar{\nu}$	$0.19 {}^{+0.20}_{-0.17}$	This work

predicts $g_A/g_V = 0.35$ for $\Sigma^- \rightarrow ne^-\bar{\nu}$. Our value of $0.19 {+0.20 \atop -0.17}$ is in reasonable agreement with the prediction. The best-fit values for all 9 data points are $\theta = .246$, $D = .815$, and $F = .475$. The χ^2 was 8.65, giving a confidence level of 20%.

In Fig. 16 we have plotted the data in D-F space, for $\theta = .246$, using the expressions and data of Table V. The data are represented by straight lines with error bars. The data are numbered in the order in which they appear in Table V. The best-fit point is indicated. The data should all intersect at a single point if the experimental values were perfectly determined and the theory were exactly correct. Recent unpublished data for g_A/g_V for $\Lambda \rightarrow pe^-\bar{\nu}$ [29] and for the branching ratio of $\Xi^- \rightarrow \Lambda e^-\bar{\nu}$ [37] would make the fit considerably better if included, while another unpublished result for g_A/g_V for $\Lambda \rightarrow pe^-\bar{\nu}$ [38] is in disagreement with the other measured values and with the best-fit value. Note that the measurement of the neutron lifetime[20] determines a value of g_A/g_V for $n \rightarrow pe^-\bar{\nu}$ of -1.29, whereas the authors claim a value of -1.23 ± 0.01 when they combine their data with nuclear physics data on O^{14}. The fit by Eisele et al.[48] to the leptonic decay data predicts a value for the neutron lifetime many standard deviations too high, so that the situation with regard to the data for neutron decay is not very satisfactory. However, as seen by the results of our fit, if one ignores the nuclear physics results for g_A/g_V, there is a consistent solution to all of the baryon leptonic decay data.

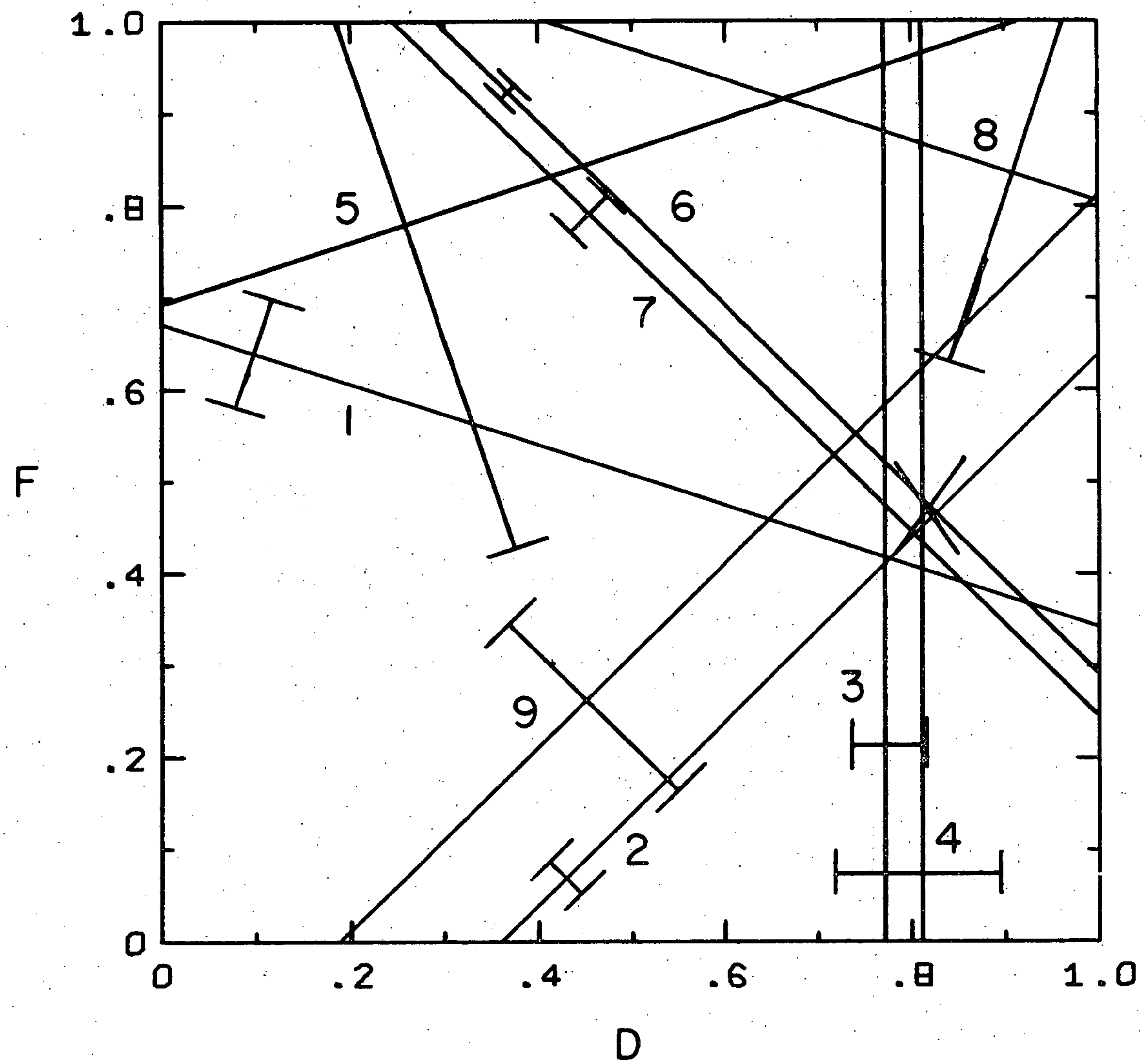

XBL 696-781

Fig. 16. The leptonic decay data of Table Vb, plotted in D-F space, for $\theta = 0.246$. The best-fit point $D = 0.815$, $F = 0.475$ is indicated. The data are numbered in the order in which they appear in Table Vb.

V. CONCLUSIONS

We have determined values of $\alpha = -0.26 \pm 0.37$ and $g_A/g_V = 0.16 {+0.19 \atop -0.18}$ for the decay $\Sigma^- \rightarrow ne\bar{\nu}$. Including the muon events, we found $g_A/g_V = 0.19 {+0.20 \atop -0.17}$. A fit to the published data with Cabibbo's theory indicated that our measurement was in reasonable agreement with the value predicted from the fit. We have made a determination of the sign for g_A/g_V to be positive by nearly two standard deviations.

It will be worthwhile to perform further experiments on baryon leptonic decays in the future in order to determine the ways in which Cabibbo's theory may have to be modified to account for decuplet and 27-plet currents. $\Delta S = -\Delta Q$ decays and $\Delta S = 2$ decays, if they are found, will have to be incorporated into the theory as well. In the meantime, Cabibbo's theory continues to provide an excellent understanding of baryon leptonic decays.

VI. EXPERIMENTAL ANALYSIS OF $\Sigma^+ \to p\gamma$

A. Previous Experimental Results

The first examples of the decay $\Sigma^+ \to p\gamma$ were found in 1959 in an emulsion experiment[56], and a handful of others were reported in the six following years.[57] These early examples indicated a branching ratio to the decay $\Sigma^+ \to p\pi^o$ of less than 1%. In 1965 Bazin et al.[6] succeeded in obtaining 24 $\Sigma^+ \to p\gamma$ events from a large stopping K^- experiment in a hydrogen bubble chamber, using only those $\Sigma^+ \to p$ decays with a stopping proton. They found a branching ratio $(\Sigma^+ \to p\gamma) \;/\; (\Sigma^+ \to p\pi^o) = (3.7 \pm 0.8) \times 10^{-3}$.

B. Experimental Technique

The experimental problems in trying to detect events of such a rare decay mode as $\Sigma^+ \to p\gamma$ are considerable. The proton momentum in the rest frame of the Σ^+ is 189 MeV/c for $\Sigma^+ \to p\pi^o$ and 224.6 MeV/c for $\Sigma^+ \to p\gamma$, so that unless the proton kinematical variables are very well determined, it is difficult to separate the $\Sigma^+ \to p\gamma$ decay from the more copious $\Sigma^+ \to p\pi^o$ decays. Bazin et al. used only events with stopping protons in determining the branching ratio. For such events, the proton momentum is determined from range and is thus very accurately known, so that the two decay modes are completely separable in all but a small fraction of the events. Of the 47,605 $\Sigma^+ \to p$ + neutral fits that we considered, 15,610 had stopping protons.

We discovered that we could use some events with protons which left the chamber as well. Generally such events present considerable resolution difficulty because the proton momentum is determined from the curvature measurement, and the associated error in momentum is determined by the multiple Coulomb scattering, which is rather large for low momentum protons. (Our maximum proton laboratory momentum is about 700 MeV/c.) The $\Sigma^+ \to p\gamma$ decay, however, releases more momentum to the proton than does the $\Sigma^+ \to p\pi^0$ decay, so that it is possible for the laboratory angle between the proton and the Σ^+ in a $\Sigma^+ \to p\gamma$ decay to exceed the maximum possible angle for a $\Sigma^+ \to p\pi^0$ decay. This situation occurs for some of those events with negative decay cosines, where a partial cancellation occurs in the longitudinal momentum between the backward proton momentum along the Σ^+ direction and the forward momentum obtained from the Lorentz transformation from the Σ^+ rest frame to the laboratory. The transverse proton momentum can be greater for the γ decay, and the resultant longitudinal momentum after the Lorentz transformation can be smaller, so that greater laboratory decay angles can be attained. Events with such a characteristic angle are said to lie in the Jacobian peak. Since the laboratory angles are very well determined, in general, such $\Sigma^+ \to p\gamma$ events are completely resolvable when the laboratory decay angle exceeds the maximum possible angle in the $\Sigma^+ \to p\pi^0$ decay by more than a degree or so, in spite of the fact that the multiple Coulomb scattering may have been considerable.

A smaller contribution to the $\Sigma^+ \to p\gamma$ sample came from events with a leaving or scattering proton in which the proton length was too great for the proton to be coming from a $\Sigma^+ \to p\pi^0$ decay.

We found, in measuring the $\Sigma^+ \to p\gamma$ decay asymmetry parameter, that we were able to use 61 events which satisfied one of these three criteria, none of which fit the $\Sigma^+ \to p\pi^0$ decay with a confidence level $> 10^{-5}$. 31 had stopping protons, 24 had decay angles too great for π^0 decay, and 6 had leaving or scattering protons whose length was too great for π^0 decay. In determining the branching ratio $(\Sigma^+ \to p\gamma) / (\Sigma^+ \to p\pi^0)$, we used a more restricted sample of 31 events, in order to make the analysis straightforward and to obtain a cleanly separated γ peak in the missing mass distribution for a $\Sigma^+ \to p$ + missing mass fit.

C. Kinematic Reconstruction

The general scanning and measuring procedure for Σ events has already been discussed in Sec. II. The scanners differentiated between the $\Sigma^+ \to p$ and the $\Sigma^+ \to \pi^+$ decays, so that we had only a small number of misidentified events to contend with in analyzing the $\Sigma^+ \to p$ decays. $\Sigma^+ \to p$ decays were kinematically reconstructed under two separate procedures: the first, to study the ordinary decay $\Sigma^+ \to p\pi^0$, and the second, to study $\Sigma^+ \to p\gamma$.

Under the first reconstruction procedure, events which passed TVGP, the geometrical reconstruction program, were fitted by SQUAW to several hypotheses. All events were fitted to

(1) $K^-p \to \Sigma^+\pi^-$, $\Sigma^+ \to n\pi^+$,

(2) $K^-p \to \Sigma^+\pi^-\pi^0$, $\Sigma^+ \to n\pi^+$,

(3) $K^-p \to \Sigma^+\pi^-$, $\Sigma^+ \to p\pi^0$, and

(4) $K^-p \to \Sigma^+\pi^-\pi^0$, $\Sigma^+ \to p\pi^0$.

Reactions 2 and 4 occur only about 1% of the time, since the center of mass energy is barely above threshold for the reaction. No attempt was made later to identify $\Sigma^+ \rightarrow p\gamma$ decays from three-body production events. If an event failed to fit any of reactions 1-4 with a confidence level $> 10^{-5}$, it was fitted to

(5) $K^-p \rightarrow K^-p$, $pp \rightarrow pp$,

where the p-p scattering resulted in a very short (invisible) proton, and to

(6) $K^-p \rightarrow \Sigma^+\pi^-$.

Events fitting reaction 6 and events failing all of reactions 1-6 were remeasured at least once in the course of the general experiment remeasuring procedures. At a late stage in the experiment, a remeasuring on the Franckenstein was carried out for events which had been successfully fit previously, but for which the measurement was deemed unsuitable. There were four classes of events in this category:

a) If the event fit reaction 5, but not reaction 6, it was looked at by a scanner to determine by ionization of the negative production particle if it was really a K^-p scatter which had been misidentified as a Σ^+ event; it was remeasured if it actually was a Σ^+ event.

b) An event called $\Sigma^+ \rightarrow p$ which fit either reaction 1 or 2, but failed both reactions 3 and 4, was remeasured if the decay particle's dip angle was less than 50° and a scanner concluded that it had been identified properly as $\Sigma^+ \rightarrow p$ but for some reason failed to fit a $\Sigma^+ \rightarrow p\pi^0$ decay. Events fitting the π^0 hypothesis with a confidence level greater than three times that of the p hypothesis were also looked at and remeasured.

c) All events which fit a $\Sigma^+ \rightarrow p\pi^o$ hypothesis with confidence level < .01 were remeasured. Many of these had a low confidence level because of a poor measurement.

d) It was discovered that some events with stopping protons had not been flagged as such when measured on the Spiral Reader because of an error on the part of the measurer. Consequently the proton momentum was derived from curvature instead of range, resulting in a poorer determination of the momentum. Such events were remeasured.

At the end of the experiment, all events which had not yet had a successful fit were remeasured on the Franckenstein.

These procedures determined how many times, and under what conditions, events identified as $\Sigma^+ \rightarrow p$ decays by a scanner were measured. The second reconstruction procedure was performed to analyze the $\Sigma^+ \rightarrow p\gamma$ events. All the measurements as obtained from PANAL and POOH were used to refit all $\Sigma^+ \rightarrow p$ events. After being processed by TVGP, the events were fitted to the three hypotheses

(7) $K^-p \rightarrow \Sigma^+\pi^-$, $\Sigma^+ \rightarrow p\pi^o$,

(8) $K^-p \rightarrow \Sigma^+\pi^-$, $\Sigma^+ \rightarrow p\gamma$, and

(9) $K^-p \rightarrow \Sigma^+\pi^-$, $\Sigma^+ \rightarrow p$ + missing mass.

Of the 47,605 events which fit some hypothesis with a confidence level > 10^{-5}, 45,984 fit reaction 7, 27,787 fit reaction 8, and 46,941 fit reaction 9. Most of the events should fit reaction 7, since almost all of them are in fact $\Sigma^+ \rightarrow p\pi^o$ decays. They should also fit reaction 9, since there is no constraint on the mass of the neutral decay particle. Those events not fitting reaction 9 were almost all events for which no momentum measurement of the proton was made because the proton scattered near the decay vertex. Reaction 9 is underconstrained in such a case. Almost all of the events fitting reaction 8 are $\Sigma^+ \to p\pi^0$ events with leaving protons. The multiple Coulomb scattering of the proton is large enough so that the event can fit $\Sigma^+ \to p\gamma$ as well as $\Sigma^+ \to p\pi^0$, although the confidence level for the π^0 fit is usually much greater than that for the γ fit.

The missing mass fit is essentially a fit to the production vertex and a calculation of the mass recoiling against the measured proton. The distribution of the (missing mass)^2 (MMSQ) for the events fitting the missing mass hypothesis is shown in Fig. 17. The histogram is made in units of MMSQ because it is this quantity which is linearly related to the measured momentum of the proton. The scale is such that $m^2_{\pi^o} = 1$ and $m^2_\gamma = 0$. The events in the tail regions, as indicated by the dashed lines, have been multiplied by 10 in order to display them better. Clearly there is no recognizable signal of γ events above the large number of π^0 events in the region of MMSQ = 0.

In order to determine the branching ratio with a relatively simple analysis, we imposed a fairly strict set of cuts on the data in order to produce a cleanly separated γ peak. However, the events used to determine the asymmetry parameter α correlating the proton direction to the Σ^+ polarization were obtained from a less strict set of conditions, since we were able to use those events which unambiguously fit $\Sigma^+ \to p\gamma$, with characteristics described

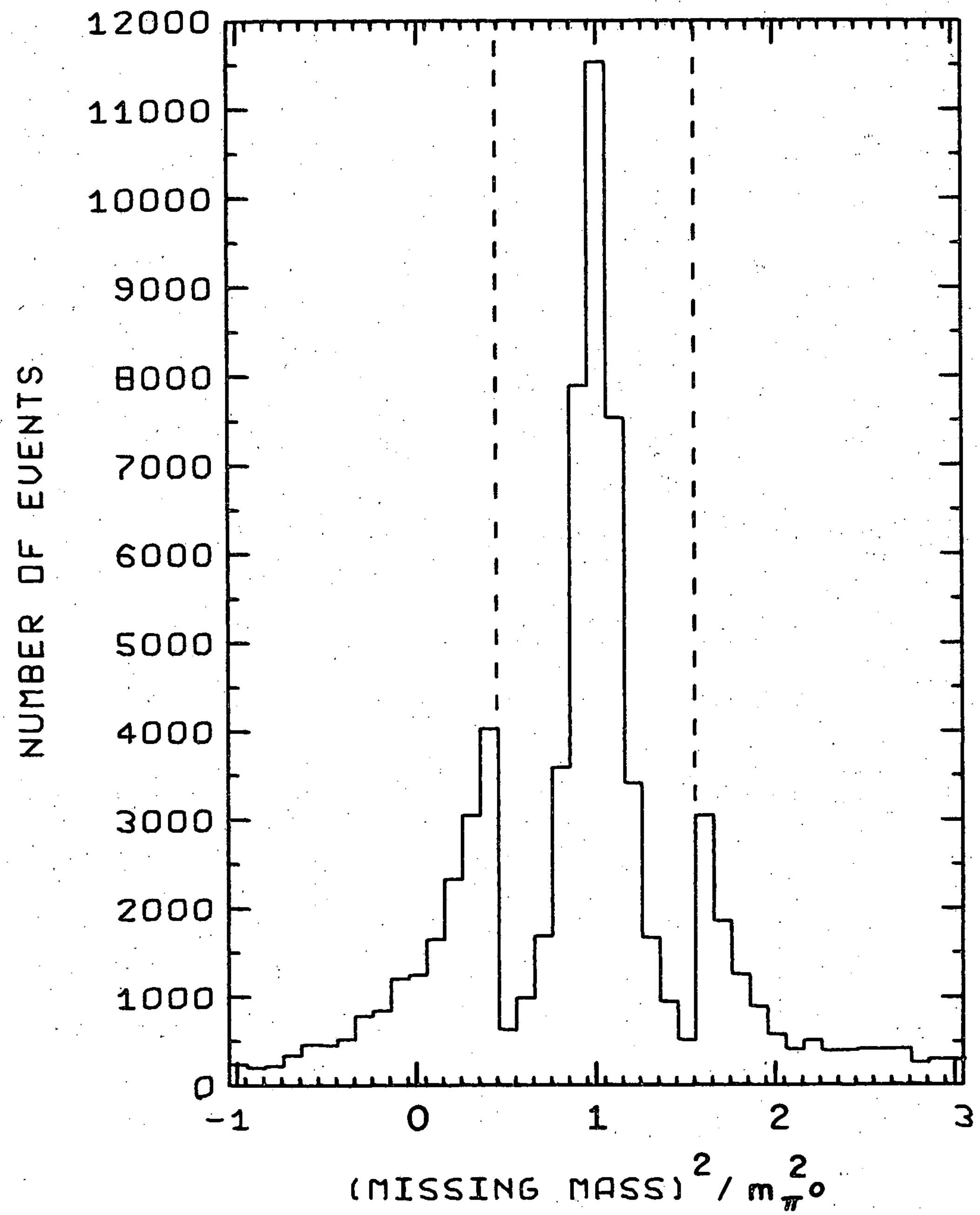

XBL 696-673

Fig. 17. The MMSQ distribution for 46,941 $\Sigma^+ \rightarrow p$ + missing mass events. The number of events in the tail regions indicated by the dashed lines has been multiplied by 10.

in Sec. VIB, while neglecting both γ and π^0 events which had ambiguous fits. There were 253 events which fit $\Sigma^+ \to p\gamma$, but not $\Sigma^+ \to p\pi^0$. Initially, before the remeasuring procedure described above, there were somewhat more, which were also considered.

D. $\Sigma^+ \to p\gamma$ Asymmetry Parameter

1. Examination and Remeasuring of Candidates

All events fitting only the γ hypothesis, as well as all other events with MMSQ $< 0.5\, m^2_{\pi^0}$, were originally considered as candidates. The error in the missing mass squared, DMMSQ, was calculated by SQUAW by propagating the measurement errors for all of the tracks. Those events which fit the π^0 decay were retained as candidates only if their MMSQ was more than three standard deviations from $m^2_{\pi^0}$, although no events fitting the π^0 decay with a confidence level $> 10^{-5}$ after remeasurement were retained as γ decays.

Those events which seemed to be candidates for the decay $\Sigma^+ \to p\gamma$ were carefully examined on the scanning table in order to eliminate those events which had been poorly measured and those which were not, in fact, $\Sigma^+ \to p$ decays. Most sources of bad measurements are the same as those mentioned in Sec. IIIC for Σ^- leptonic decays. In addition there were some others:

1) Due to the heavy ionization of both Σ^+ and p, the decay vertex was sometimes measured poorly because of difficulty in locating the vertex.

2) Events for which the dip angle of the beam track was greater than $\sim 3°$ were often events for which the beam track was mismeasured.

MMSQ was rather sensitive to this problem, and events which seemed to be good γ candidates unambiguously fit π^o when the beam track was measured properly in a remeasurement.

3) Some events had no visible Σ^+, while others had a Σ^+ which scattered.

Events which were not $\Sigma^+ \rightarrow p$ decays were most often $\Sigma^+ \rightarrow \pi^+$ decays which had been misidentified either by mistake or because of difficulty in determining the ionization of the decay particle. Some K^-p elastic scatters were also found, although most of these which fit $\Sigma^+ \rightarrow p$ decays had a high missing mass.

Those events which still seemed to be γ candidates after examination on the scanning table were remeasured at least once on the Franckenstein, with considerable attention given to possible kinks in the proton from a small angle scattering. About 750 remeasurements were made in all, some representing the same event measured several times. This number also included events not γ candidates which were remeasured for the branching ratio part of the experiment. Those events still remaining as candidates were re-examined on the scanning table and perhaps remeasured with different criteria.

A set of criteria was developed in deciding whether to retain an event as a γ decay. An event was considered a $\Sigma^+ \rightarrow p\gamma$ decay if:

1) it was resolvable from $\Sigma^+ \rightarrow p\pi^o$ by either the range or decay angle of the proton. If the proton stopped, the two decay modes were completely resolvable because the proton momentum was so well determined from the measurement of the range, except in a few cases in which the proton was so short or had such a large dip angle that the

range was not very well known. For leaving or scattering protons, we required that either the laboratory decay angle or the length of the proton be greater than that possible for $\Sigma^+ \rightarrow p\pi^o$ decay. The events with stopping protons or with leaving protons for which the laboratory decay angle was too large had MMSQ more than 3.5 standard deviations from $m^2_{\pi^o}$. However, the error is skewed, in the sense that the error more properly applies to lowering MMSQ than to raising it in the case of the leaving protons. The error for leaving and scattering protons is dominated by the uncertainty in the proton's measured momentum, although γ events with too great a laboratory decay angle are separated from the π^o events by the angle, which has a small error, and not the momentum. Similarly, events with too great a proton length are many standard deviations in the measured length from being π^o events, whereas DMMSQ, the missing mass squared error, could be comparable to $m^2_{\pi^o}$.

2) the event was well measured, in the sense that the measured quantities were reproduceable upon remeasurement. This requirement has previously been discussed. The main problem was to make certain that there was not a small scatter in the proton track that was being overlooked in the measurement. The tracks were carefully examined for such scatters and, in some cases, the track was measured several times with different lengths in an attempt to see if the measured quantities were consistent.

3) the fitted beam momentum without beam averaging agreed with that obtained from beam averaging. There were 5 events which did not have a π^o fit when beam averaging was used which had good π^o

fits, with a lower beam momentum, without beam averaging. These events had rather short beam tracks and may have resulted from a K^- which scattered and thereby lost momentum before entering the chamber. If the beam track was short, and consequently the measured momentum had a large error, the beam-averaged momentum determined the fitted momentum almost completely. These 5 events were not considered as γ events because of the possibility that they were really non-beam events.

4) the confidence level for the γ fit was greater than .01.

5) the proton was distinguishable from a π^+ either by its stopping in the chamber or by its greater ionization. The only difficulty in identification by ionization arose from steeply dipping tracks. If the track left the chamber, it was considered unidentifiable if the dip angle was greater than 60°.

6) the Σ^+ length was greater than 0.5 mm. and the production and decay vertices were clearly distinguishable.

7) the event was inconsistent with a stopping Σ^+ decaying via $\Sigma^+ \rightarrow p\pi^o$. When the fitted Σ^+ momentum at decay was less than 80 MeV/c, there were many events which appeared to be γ events which in reality were π^o events with a stopping Σ^+. These events generally did not fit $\Sigma^+ \rightarrow p\pi^o$ unless the Σ^+ was specifically required to be stopping when the fitting was done by SQUAW. There were, in fact, two events which we determined to be $\Sigma^+ \rightarrow p\gamma$ decays with a stopping Σ^+.

There were 61 events which satisfied these requirements, all of which fit only $\Sigma^+ \rightarrow p\gamma$. The MMSQ distribution of 59 of these events is shown in Fig. 18. The other two did not have missing mass fits, but were still considered to be γ events. One of them had a short,

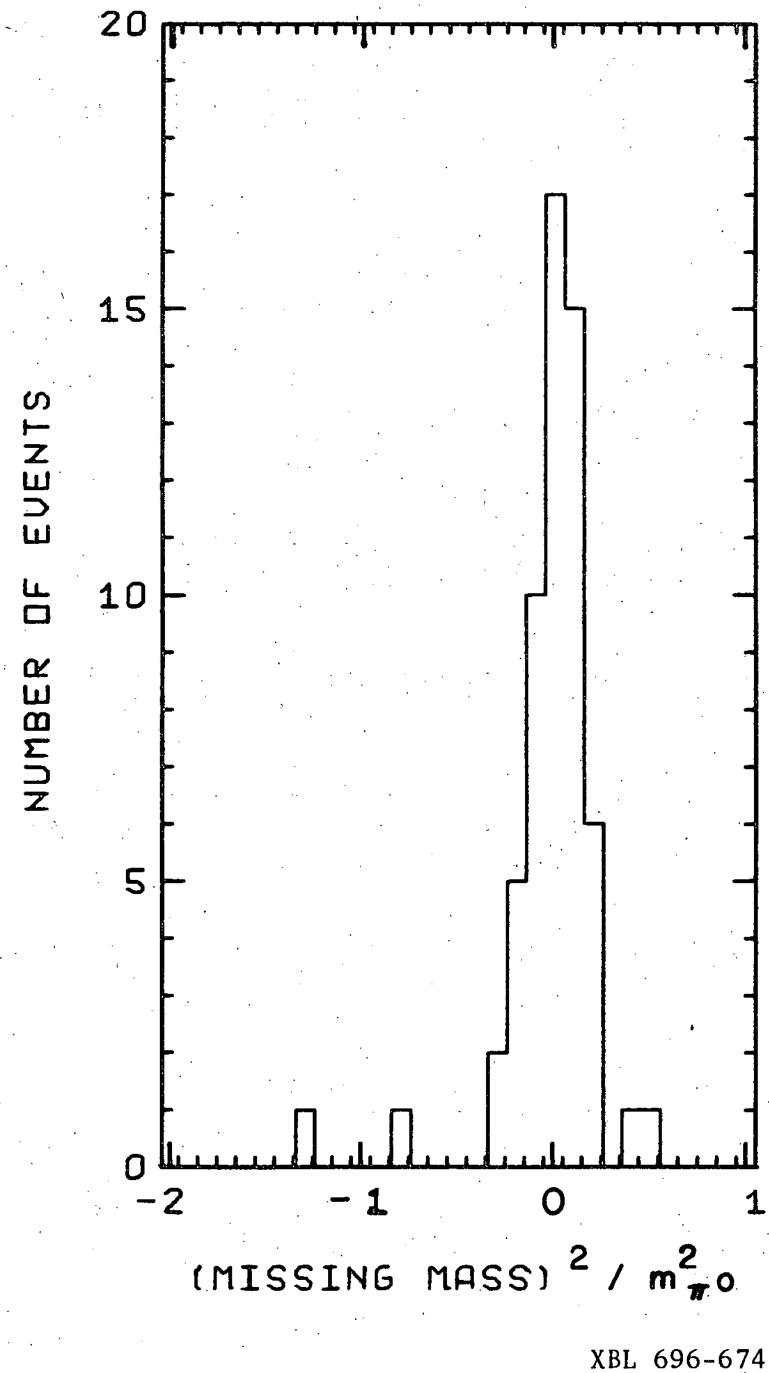

Fig. 18. The MMSQ distribution for 59 of the 61 $\Sigma^+ \rightarrow p\gamma$ events used in determining α. The other two did not have missing mass fits.

scattering proton with no measured momentum possible, but whose length was still too great to be from a π^o event. The other had an almost stopping Σ^+ which the fitting program apparently could not handle properly in doing the missing mass fit, but which had a good γ fit, with a stopping proton.

2. Measurement of the Asymmetry Parameter

The proton asymmetry distribution is

$$I(\hat{q}) = 1 + \alpha \vec{P}_\Sigma \cdot \hat{q} , \qquad (6.1)$$

where $\vec{P}_\Sigma$ is the Σ^+ polarization and $\hat{q}$ is the unit vector of the proton momentum in the rest frame of the Σ^+.

The Σ^+ polarization was obtained by the same multi-channel partial wave analysis discussed in Sec. IIIH for Σ^- leptonic decays. The polarization of the Σ^+ can actually be measured quite well by observing the decay asymmetry in $\Sigma^+ \to p\pi^o$, since the asymmetry parameter is $\alpha = -0.999 \pm 0.022$.[9] The values of the polarization obtained from the multi-channel analysis agree with the measured values.

A maximum likelihood fit for α was performed for the 61 $\Sigma^+ \to p\gamma$ events with the likelihood function

$$\mathcal{L}(\alpha) = \prod_{i=1}^{61} (1 + \alpha P_{\Sigma_i} \cos \theta_i) , \qquad (6.2)$$

where P_Σ is the Σ^+ polarization along the production normal $\hat{n}$ defined by $\hat{n} = \vec{K}^- \times \vec{\pi}^- / |\vec{K}^- \times \vec{\pi}^-|$, and $\cos \theta = \hat{n} \cdot \hat{q}$.

The logarithm of $\mathcal{L}$ is plotted in Fig. 19 as a function of the parameter α. We find

$$\alpha = -1.03 \begin{smallmatrix} + 0.52 \\ - 0.42 \end{smallmatrix} .$$

The standard deviation is the change in α necessary to decrease $\ln \mathcal{L}$ by 0.5 from its maximum value. The physical limit on α is $|\alpha| \leq 1$, so that the most likely physical value is $\alpha = -1$.

Data for each of the 61 $\Sigma^+ \to p\gamma$ events are listed in Table VI, along with the characteristic of each event which enabled it to be identified as $\Sigma^+ \to p\gamma$. 31 events had stopping protons, 24 had laboratory decay angles too large for $\Sigma^+ \to p\pi^o$, and 6 had leaving or scattering protons for which the proton length was too great for $\Sigma^+ \to p\pi^o$. The average polarization was 0.37.

Because of the criteria that we used in obtaining the $\Sigma^+ \to p\gamma$ events, we estimate there to be less than one event of $\Sigma^+ \to p\pi^o$ as contamination. $\Sigma^+ \to p\pi^o$ has $\alpha = -0.999 \pm 0.022$, which is nearly equal to our measured value for $\Sigma^+ \to p\gamma$. If there were a small contamination of $\Sigma^+ \to p\pi^o$ decays in the $\Sigma^+ \to p\gamma$ sample, the central value of α thus determined would be proportional to the amount of contamination of $\Sigma^+ \to p\pi^o$, if $\alpha = 0$ for $\Sigma^+ \to p\gamma$, and would be unaffected if $\alpha = -1$ for $\Sigma^+ \to p\gamma$. Since the statistical error is inversely proportional to the square root of the number of events, it would be relatively unaffected by a small contamination. We emphasize, however, that we believe that we have a pure sample of $\Sigma^+ \to p\gamma$ decays.

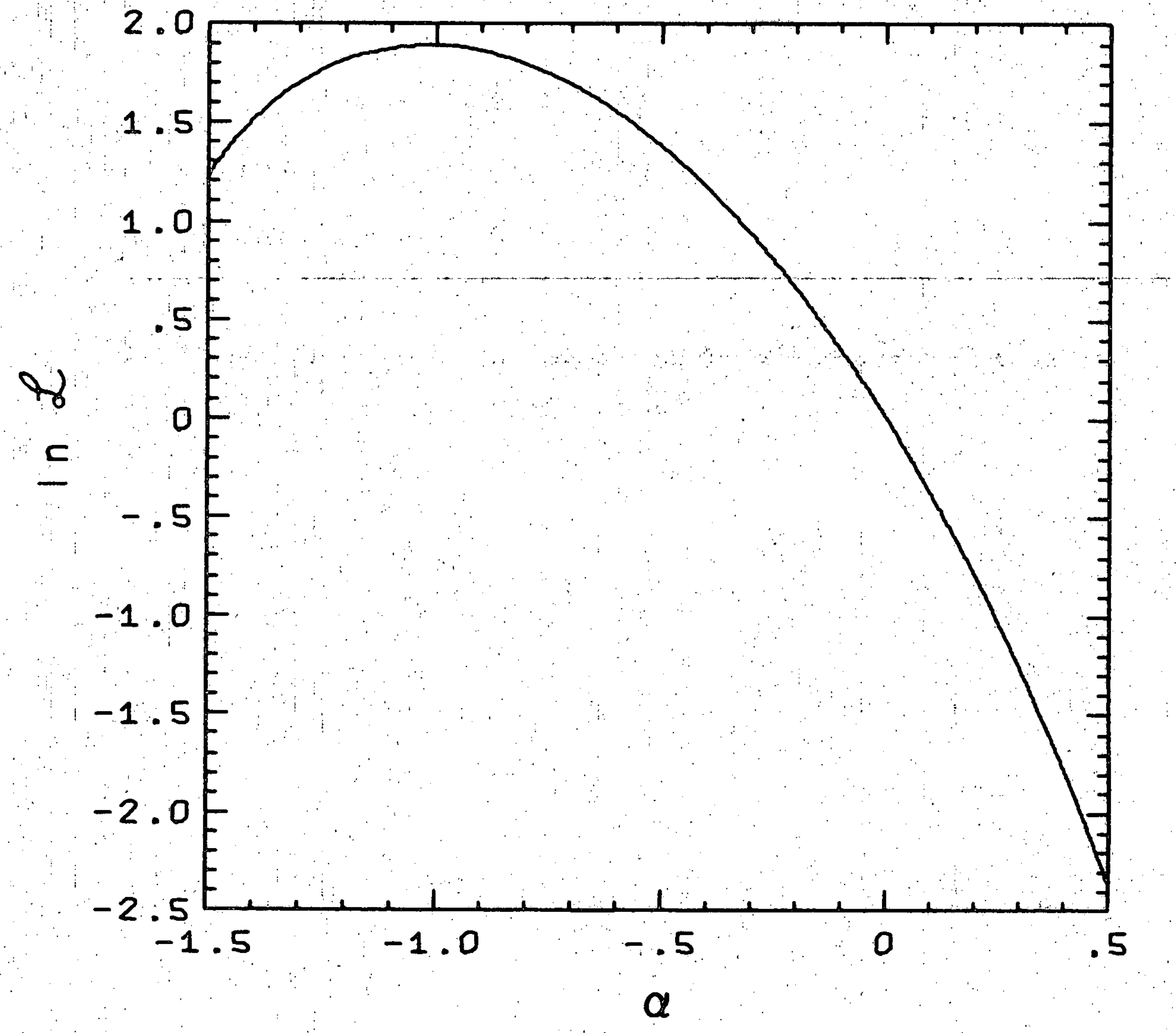

XBL 696-779

Fig. 19. The logarithm of the likelihood function, as a function of α, for the 61 $\Sigma^+ \to p\gamma$ events. $\alpha = -1.03 \begin{smallmatrix} +\ 0.52 \\ -\ 0.42 \end{smallmatrix}$.

Table VI. Data for the $\Sigma^+ \rightarrow p\gamma$ events.

ID is the identification number, K is the K^- laboratory momentum, $K^- \cdot \pi^-$ is the center of mass production cosine, MMSQ and DMMSQ are the missing mass squared and the error in the missing mass squared, in units of $m_{\pi^o}^2$, P_Σ and cos Θ are the Σ^+ polarization and the correlation angle as defined in Eq. 6.2, and the comments, which are listed at the end of the table, relate the special property of the event that enabled it to be identified as $\Sigma^+ \rightarrow p\gamma$.

ID	K	$K^- \cdot \pi^-$	MMSQ	DMMSQ	P_Σ	cos Θ	Comment
40130401	393.2	-.923	.081	.191	.174	.354	a
40550267	359.8	-.232	-.042	.123	.810	.323	b
40551131	387.3	-.911	-.080	.206	.273	.486	a
40840465	384.4	.966	.025	.030	.083	.388	c
40990670	379.5	.822	.104	.077	.052	-.788	b
41041690	384.3	.776	-.806	1.690	.149	.127	d
41061689	393.1	-.375	.149	.205	.510	.607	a
41101201	398.4	.788	.059	.480	.478	-.164	e
41220849	359.6	.463	.152	.106	-.067	-.671	b
41380855	394.8	.686			.467	-.659	f
41390178	382.6	-.557	-.131	.115	.746	.286	b
41400521	367.9	.898	.508	1.188	-.055	.909	d
41500157	367.4	.347	.042	.109	-.043	-.413	b
42021056	376.3	.735	.097	.086	-.043	-.493	b
42251618	372.7	-.969	-.211	.133	.294	-.473	b
42261208	389.1	-.252	-.184	.120	.817	-.169	b
42270122	373.0	-.622	-.005	.277	.850	-.983	a
42310335	383.9	.926			.109	.829	g
42350261	398.4	-.718	.097	.153	.192	-.081	a
42360318	366.1	-.921	-1.331	2.580	.504	-.887	h
42440334	376.6	-.288	.105	.120	.969	-.482	b

Table VI. (continued)

ID	K	$K^- \cdot \pi^-$	MMSQ	DMMSQ	P_Σ	cos Θ	Comment
42580478	390.5	-.736	.221	.128	.379	-.357	b
42660545	365.7	-.895	-.088	.118	.572	-.305	b
43081293	360.7	.214	-.188	2.080	.273	-.667	h
43330201	293.0	-.793	.175	.151	.427	-.882	a
43460989	322.4	-.730	.093	.200	.593	-.763	a
43490838	320.3	-.234	-.295	.129	.601	-.589	b
43671571	333.7	.531	.036	.132	.167	.725	b
44250199	384.2	-.765	.153	.115	.514	-.076	b
44430847	365.7	.875	.083	.061	-.080	.651	b
44531302	368.1	.905	-.024	.070	-.050	-.508	b
44561564	383.4	-.680	-.044	.206	.617	-.411	a
44600491	387.3	-.952	-.064	.116	.202	-.158	b
44721284	371.8	-.614	-.003	.222	.865	.647	a
44850904	409.7	-.961	-.306	.215	.024	.553	b
44880200	388.0	.928	-.046	.060	.160	-.517	b
44921401	414.2	.730	.016	.078	.778	.179	b
45140848	405.9	-.431	-.039	.201	.030	.445	a
45270102	385.9	-.817	-.009	.157	.419	-.750	a
45370595	390.4	.867	-.010	.080	.248	-.551	b
45410089	404.6	-.996	.024	.131	.016	-.027	a
45451568	389.4	-.686	-.067	.182	.447	.086	a
45690521	403.9	-.574	-.080	.233	.075	.832	a
45881000	407.2	-.605	-.144	.169	.020	.146	b
45950298	400.1	.952	-.009	.030	.264	.976	c
45970273	391.4	-.818	.128	.192	.299	.002	a
46010573	388.6	-.582	-.110	.163	.548	.237	b
46281550	405.2	.343	-.058	.111	.945	.199	b
46410142	411.8	.809	.150	.081	.666	-.631	b
46440968	409.8	.748	.383	.596	.709	-.992	d
46530501	403.3	-.915	.071	.148	.073	.107	a

Table VI. (continued)

ID	K	$K^- \cdot \pi^-$	MMSQ	DMMSQ	P_Σ	cos θ	Comment
46711119	399.4	-.957	.097	.188	.080	-.824	a
46751008	418.2	.466	.112	.113	.969	-.257	b
46961555	389.1	.864	.225	.667	.226	-.568	e
47020435	394.0	-.513	.121	.180	.392	.809	a
47581302	432.6	.611	.134	.074	.956	-.382	b
47750018	429.9	-.078	-.080	.155	.556	.135	b
47880112	388.8	-.594	-.228	.272	.533	.663	a
48011519	398.8	-.730	-.010	.263	.180	-.850	a
48060146	401.4	-.960	.005	.196	.065	.415	a
48130377	408.9	-.902	-.289	.242	.036	.359	a

Comments

a. laboratory decay angle too large for $\Sigma^+ \to p\pi^0$

b. proton stops

c. Σ^+ stops, proton stops

d. proton scatters, proton length too great for $\Sigma^+ \to p\pi^0$

e. proton leaves, proton length too great for $\Sigma^+ \to p\pi^0$

f. proton scatters, proton length too great for $\Sigma^+ \to p\pi^0$, no missing mass fit because proton too short for measurement of the momentum

g. Σ^+ almost stops, proton stops, no missing mass fit

h. proton scatters, laboratory decay angle too large for $\Sigma^+ \to p\pi^0$

There are two experimental biases to the distribution in Eq. 6.1. It was generally difficult to separate events for which the proton decayed forward from the Σ^+ in the rest frame of the Σ^+. Also, events with large proton dip angles generally were not detectable. As was discussed in Sec. IIIH for Σ^- leptonic decays, biases such as these are even in $\cos\Theta$, and thus do not affect the determination of the asymmetry parameter by a maximum likelihood technique.

As was discussed above, the measured Σ^+ polarizations agreed with those obtained from the partial wave analysis, so that errors in our knowledge of the polarizations were quite small. Consequently, errors in the asymmetry parameter due to errors in the polarizations should be quite small in comparison with the statistical error.

E. $\Sigma^+ \to p\gamma$ Branching Ratio

1. Branching Ratio Criteria

A simple and straightforward determination of the $\Sigma^+ \to p\gamma$ branching ratio was made by applying cuts to all $\Sigma^+ \to p$ decays independent of the identity of the decay neutral. A well resolved sample was obtained with completely separated γ and π^o peaks in the MMSQ distribution for the missing mass fits. The criteria used in the branching ratio analysis were more restrictive than those for the asymmetry parameter determination. Additional events could be used for the asymmetry parameter because they had configurations which precluded their being $\Sigma^+ \to p\pi^o$ decays.

We used the same criteria as described in Sec. VIB in determining an event to be a $\Sigma^+ \rightarrow p\gamma$ decay; namely, that the event was resolved either by a range measurement of the proton or by the laboratory decay angle being too great for a $\Sigma^+ \rightarrow p\pi^o$ decay. We did not rely on the proton momentum determination from the curvature measurement in resolving the $\Sigma^+ \rightarrow p\gamma$ events. All of the 31 $\Sigma^+ \rightarrow p\gamma$ events used in the branching ratio measurement were included in the 61 events for the asymmetry parameter.

The analysis is discussed in terms of the variables MMSQ and DMMSQ, since DMMSQ is a measure of the resolution of the event. For the initial analysis and cuts, we were mainly concerned with eliminating a large fraction of the events with large DMMSQ in order to facilitate the later analysis and with eliminating events with lower scanning efficiency. DMMSQ was most sensitive to the measurement errors for the proton track, for leaving protons. Events with stopping protons were almost always resolvable, with small DMMSQ. As a working definition of resolvability of an event, we found that it was desirable to have at least a four standard deviation separation between the γ and π^o fits, or DMMSQ $< 0.25\ m_{\pi^o}^2$.

The procedure used in determining the cuts necessary to achieve the required resolution was to investigate the relation between DMMSQ and various variables such as position of the event in the chamber, decay angle, and Σ^+ momentum. Most of the variables involved were not relevant to the identity of the neutral, so that the branching ratio was nearly the ratio of γ events to π^o events which survived the cuts imposed.

A series of scatter plots was made of DMMSQ vs. another variable. An example is shown in Fig. 20 of DMMSQ vs. y, the position of the event in the bubble chamber along the entering beam direction. DMMSQ increases for events toward the back of the chamber, because a leaving proton traveled a shorter distance before leaving and consequently had a larger error in the measured momentum, and more events had leaving protons than in the center of the chamber. A cut on this variable was necessary in order to obtain a high enough potential proton length so that a large number of events would have had stopping protons regardless of whether the decay neutral was a γ or a π^o, and could thus be used in the branching ratio measurement. Such events were one class of events that we used in the branching ratio measurement, the other being events for which the γ events were resolvable because they were at large laboratory decay angles.

A first series of cuts was applied to the missing mass fits as a result of analyzing the scatter plots and noticing other features

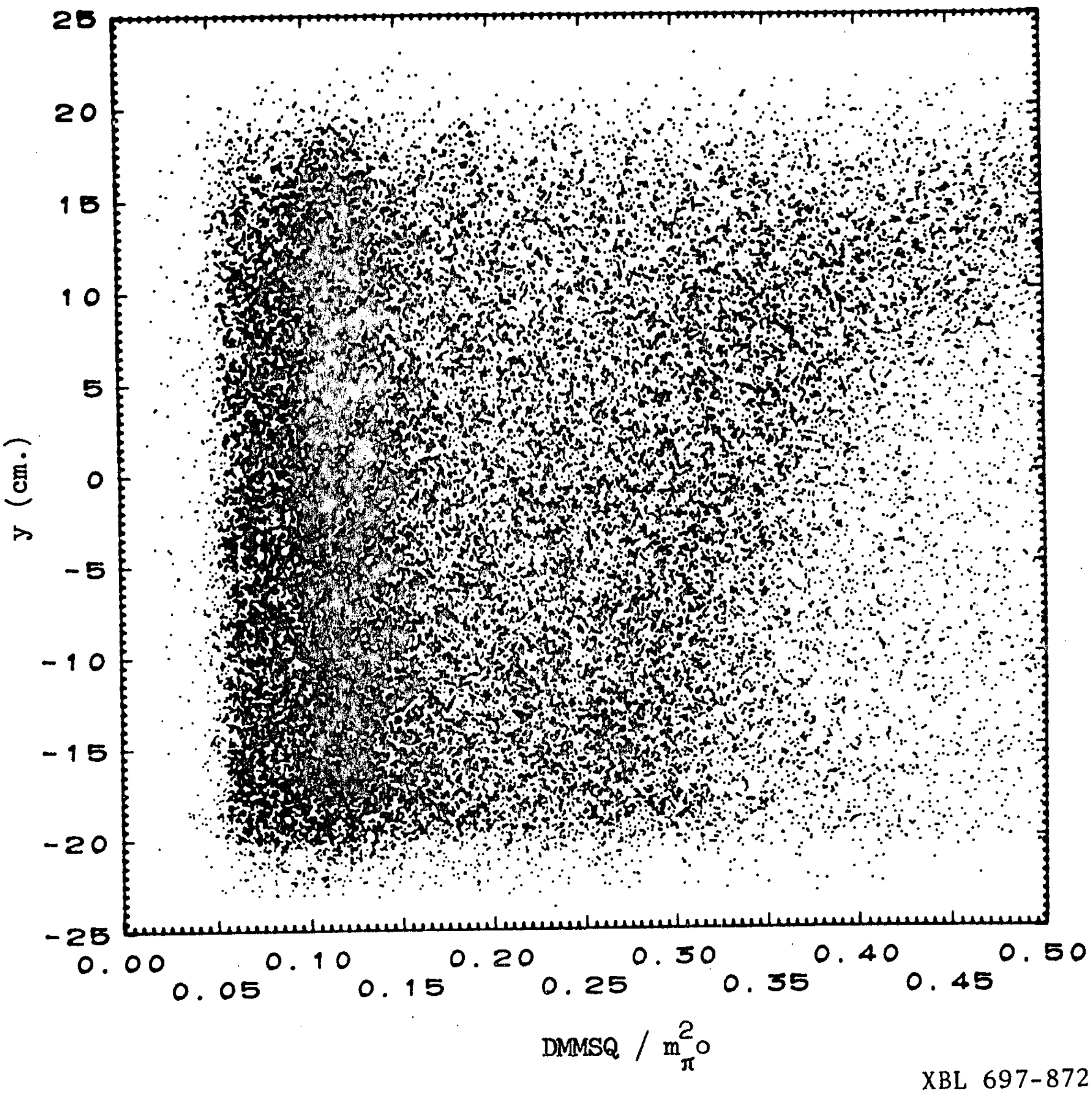

Fig. 20. DMMSQ, the missing mass squared error, in units of $m^2_{\pi^0}$, vs. y, the position in the chamber along the entering beam direction. The events with $y < -20$ and $y > 12$ were eliminated.

of the data:

1) A fiducial volume considerably stricter than the measuring volume was imposed to eliminate all events with $y > 12$ cm., approximately the last quarter of the bubble chamber, events at the front of the chamber with $y < -20$ cm., and events near the walls on the sides.

2) The length of the Σ^+ was required to be greater than 1 mm. in order to assure that the event was in fact a Σ^+ decay and that the scanning efficiency was reasonably high.

3) The confidence level for the missing mass fit was required to be greater than .01. This cut eliminated most of the poorly measured events and most of the K^-p elastic scatters.

4) The measured dip angle of the beam track, λ_K, was required to be $-.064$ rad. $< \lambda_K < .052$ rad. Some events with a large dip angle were bad measurements, where part of a different beam track was measured in one view. Others were non-beam events, as discussed before.

5) The measured laboratory dip angle of the proton was required to be less than 45°. The scanning efficiency for identifying protons as the decay product of the Σ^+ became increasingly poor as the proton dip angle increased. In addition, DMMSQ increased with larger dip angle because the proton length for protons leaving through the top or bottom of the chamber became correspondingly shorter. This cut affected γ and π^0 events differently, and it was corrected for, as will be discussed later.

After these cuts were imposed, 30,806 events remained. A histogram of MMSQ for these events is shown in Fig. 21. There is still no indication of a peak at MMSQ = 0, although the resolution has improved. A comparison with Fig. 17 shows that the proportion of events in the low MMSQ region has decreased by about a factor of two.

It was found that the appropriate variables to consider in achieving a separation of the γ and π^o peaks were p_Σ, the momentum of the Σ^+, and $(\vec{\Sigma}\cdot\vec{p})_{RF}$, the cosine of the angle between the laboratory Σ^+ direction and the direction of the proton in the rest frame of the Σ^+. Because the Σ^+ is polarized perpendicularly to its direction, the decay distribution is uncorrelated with the direction of the Σ^+. Consequently, apart from experimental biases, events should be uniformly distributed in $(\vec{\Sigma}\cdot\vec{p})_{RF}$.

A series of scatter plots was made of MMSQ and DMMSQ vs. $(\vec{\Sigma}\cdot\vec{p})_{RF}$ for several intervals of p_Σ. An example is shown in Fig. 22, where DMMSQ vs. $(\vec{\Sigma}\cdot\vec{p})_{RF}$ is shown for $400 < p_\Sigma < 500$ MeV/c. The plot contains about 6000 events. DMMSQ is well below 0.25 $m^2_{\pi^o}$ for almost all backward decays ($(\vec{\Sigma}\cdot\vec{p})_{RF} < 0$), while it increases and gets quite large for positive $(\vec{\Sigma}\cdot\vec{p})_{RF}$. This effect occurred because the laboratory angles for backward decays were larger and the laboratory momenta were lower. The effect of the Lorentz transformation, which tends to wash out the difference between the γ and π^o decays for events with small laboratory decay angles, has less effect for events with large laboratory decay angles. Since the laboratory momenta were lower, most of the events with stopping protons occurred for

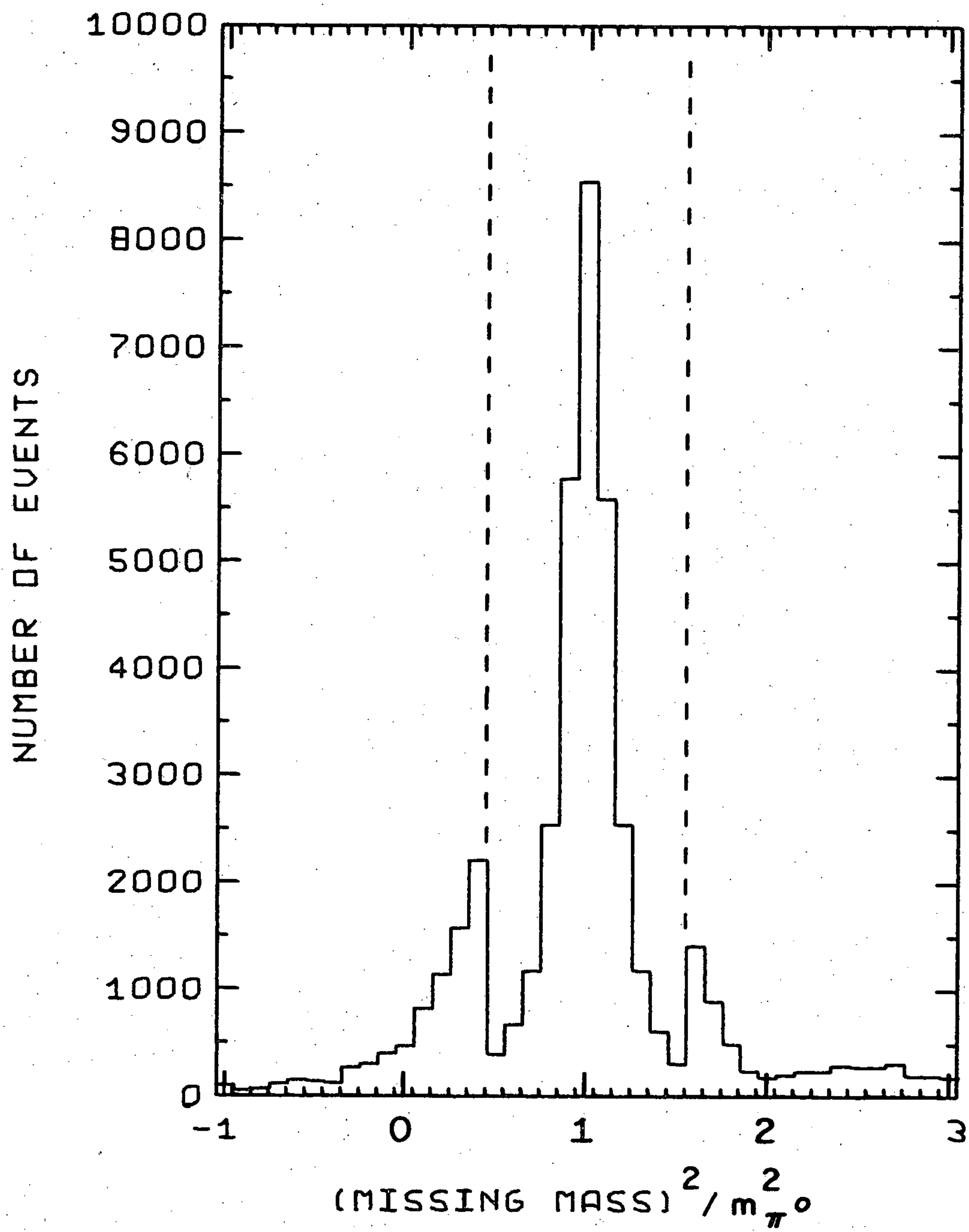

XBL 696-675

Fig. 21. The missing mass squared distribution for the 30,806 events satisfying the first set of selection criteria. The events in the tail regions indicated by the dashed lines have been multiplied by 10 in order to display them better.

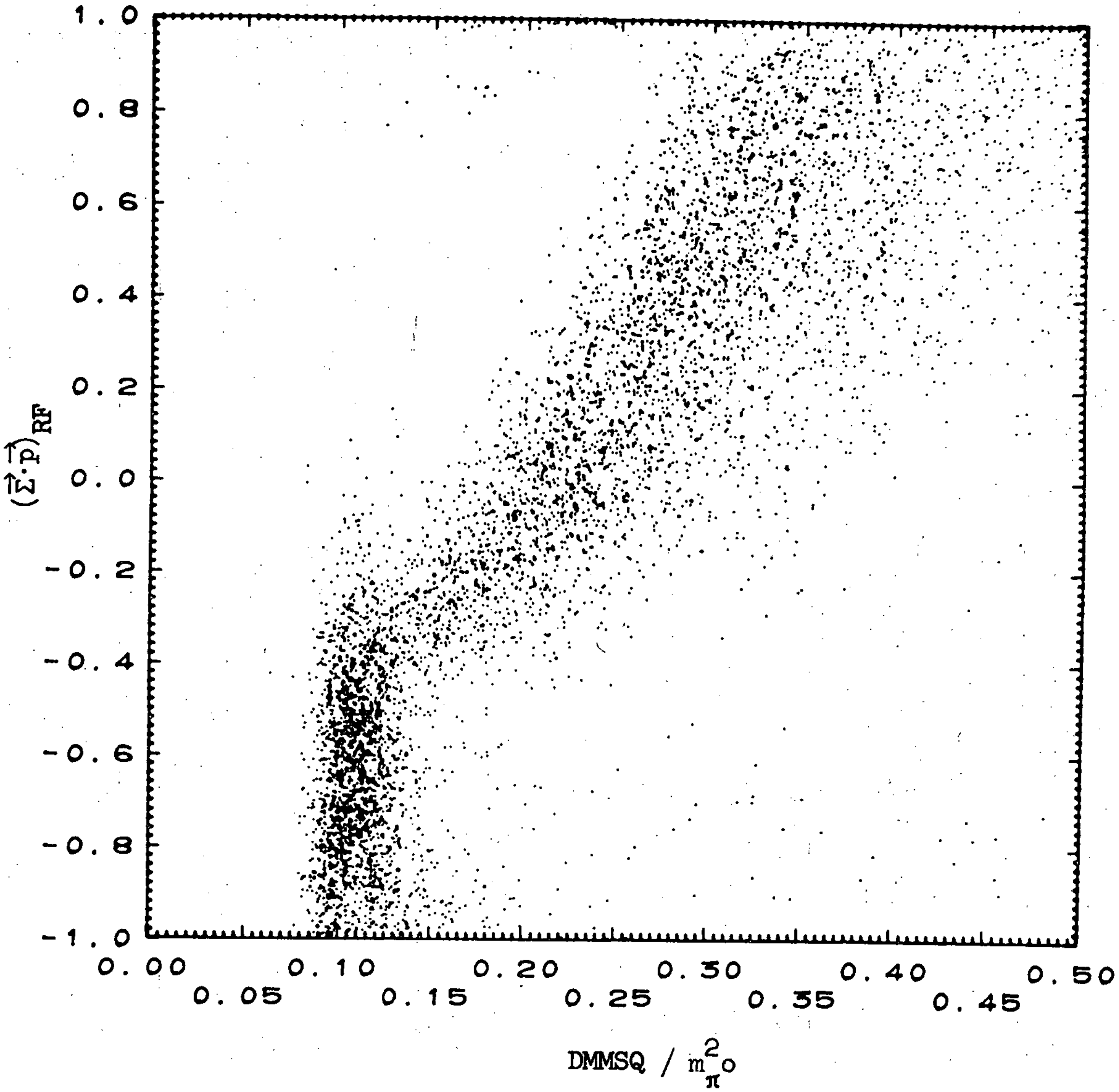

XBL 697-873

Fig. 22. DMMSQ, the missing mass squared error, in units of $m^2_{\pi^0}$, vs. $(\vec{\Sigma}\cdot\vec{p})_{RF}$, the cosine of the angle between the Σ^+ laboratory momentum and the proton momentum in the Σ^+ rest frame, for the 6000 missing mass events with $400 < p_\Sigma < 500$ MeV/c satisfying the first set of selection criteria. The vertical band consists of events with stopping protons, while the diagonal band consists of events with leaving protons.

negative decay cosines.

A scatter plot of $(\vec{\Sigma}\cdot\vec{p})_{RF}$ vs. p_Σ is shown in Fig. 23. The distribution of events in $(\vec{\Sigma}\cdot\vec{p})_{RF}$ is uniform, except for a depletion for forward angles because of poor scanning efficiency for small laboratory decay angles, and for backward angles at lower momenta because of poor scanning efficiency for short, low momentum protons.

A series of cuts was made in these two variables, based upon the information learned from the other scatter plots and after considerable experimentation. The cut was applied on the values of the variables for the appropriate fitted decay rather than for the missing mass fit. Thus, the variables were defined by the γ decay for events eventually judged to be γ decays, and by the π^0 decay for π^0 decays. The missing mass fit variables were used for the small number of events not fitting the π^0decay which were not γ decays either. The scatter plot in Fig. 24 shows the result of applying these cuts, with 11,775 events remaining after the cuts. The cuts are described below:

1) Events in region 1 were excluded because $p_\Sigma < 125$ MeV/c at decay. This was done in order to eliminate low momentum Σ's which either stopped or had a rather large uncertainty in momentum at decay because they were losing momentum rapidly.

2) Events in region 2 were excluded because the momentum of the proton from either a γ decay or a π^0 decay with the given p_Σ and RF decay angle would have been less than 150 MeV/c, corresponding to a range < 1.2 cm. The scanning efficiency was lower when the proton was short, although the efficiency was about uniform for

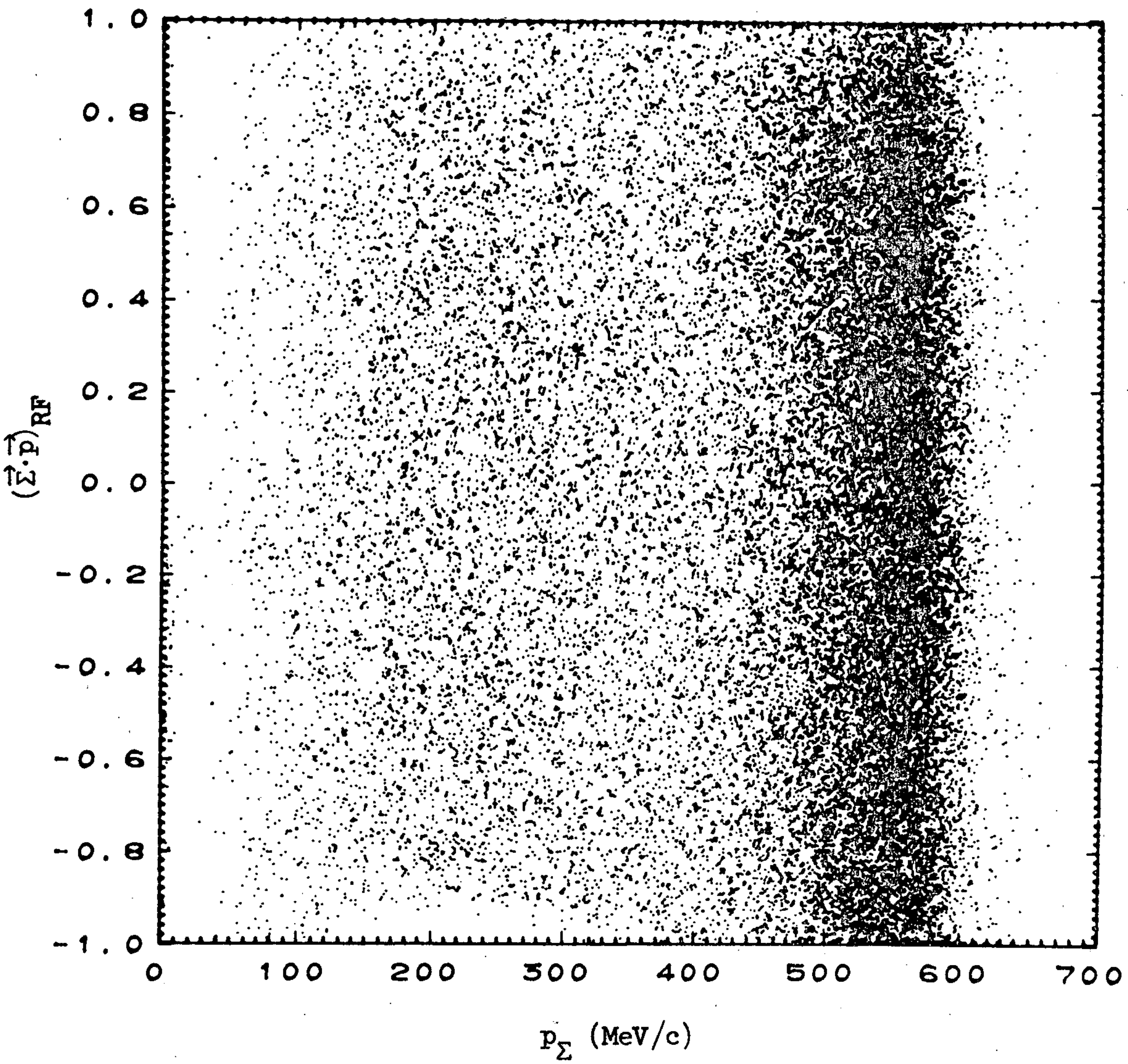

XBL 697-874

Fig. 23. p_Σ, the laboratory momentum of the Σ^+, vs. $(\vec{\Sigma}\cdot\vec{p})_{RF}$, for the 30,806 missing mass events satisfying the first set of selection criteria.

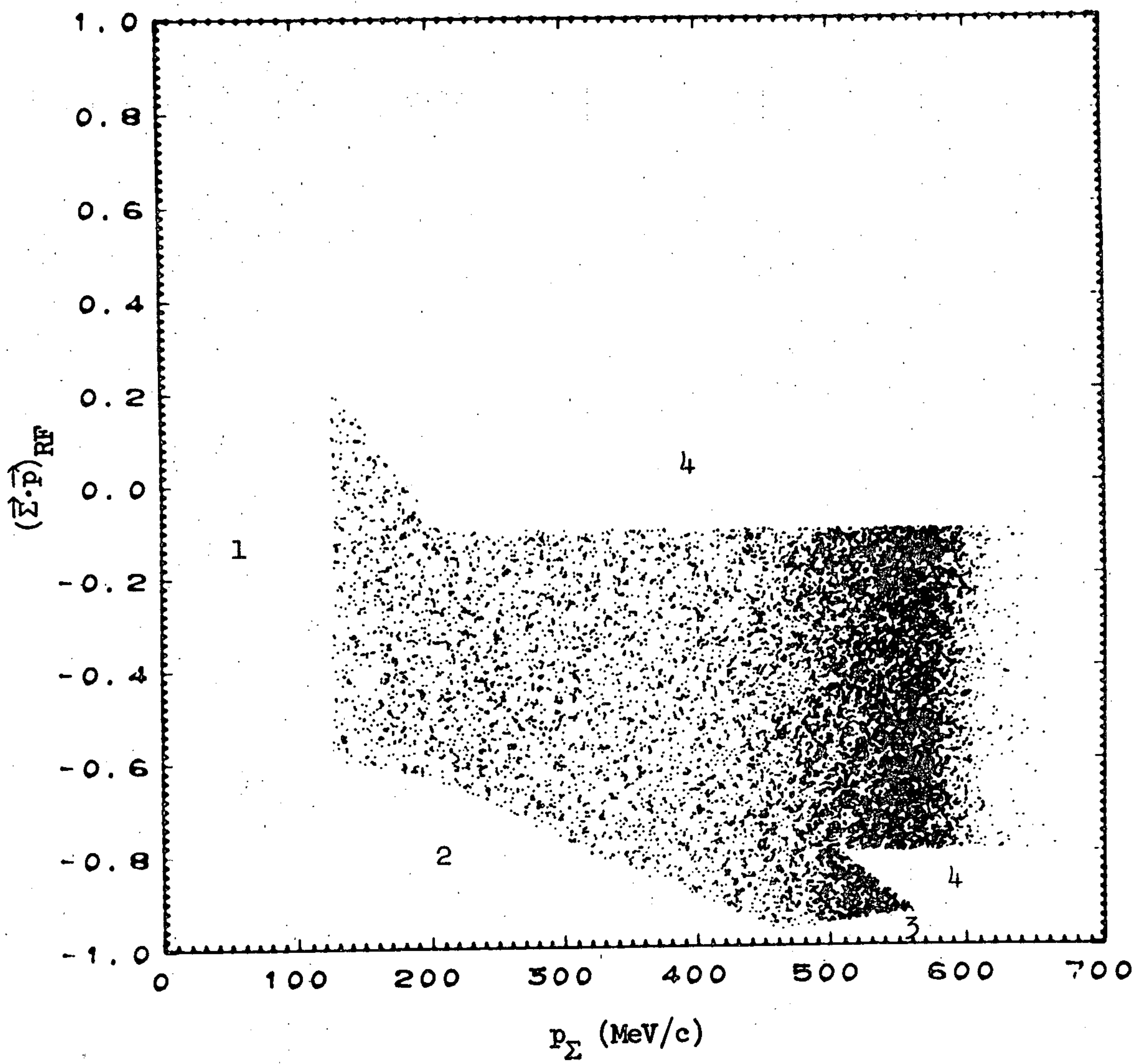

XBL 697-875

Fig. 24. p_Σ vs. $(\vec{\Sigma}\cdot\vec{p})_{RF}$ for the 11,775 events satisfying all the branching ratio criteria. The regions 1-4 that have been removed are explained in the text. A contour of a nearly straight line can be drawn from the region of accepted events at the upper left to the region at the lower right. Events to the left of the contour have protons which always stop for both γ and π^0 decays. Events to the right are resolvable because of the large decay angles for the γ decays, or, in a small region, because the γ events have a proton range too great for protons from a π^0 decay.

proton length $\geq$ 1 cm. In addition, DMMSQ increased considerably as the proton became very short because of the corresponding increase in uncertainty in the proton variables.

3) The scanning efficiency was lower for small laboratory angle between the Σ^+ and p. A minimum of 15° between the two tracks was required, corresponding to a laboratory cosine < 0.966. The events in region 3 were excluded because either the γ decay or the π^0 decay with the given p_Σ and RF decay angle would have resulted in a laboratory cosine > 0.966.

4) It was found that events were completely resolvable for the region $-0.8 < (\vec{\Sigma}\cdot\vec{p})_{RF} < -0.1$. In addition, the proton always stopped for both decay modes in the two small regions at the upper left and lower right of Fig. 24. The events in region 4 were not in any of these regions and were excluded.

a) Stopping proton regions. As a result of the fiducial volume defined, it was determined that all protons had a potential length of at least 10 cm. before leaving the stopping volume of the chamber. The two small regions in the figure outside the range -0.8 to -0.1 were included because the proton for both decay modes would have had a range < 10 cm. for the given p_Σ and RF decay angle, and thus would have stopped.

b) $-0.8 < (\vec{\Sigma}\cdot\vec{p})_{RF} < -0.1$ There are two kinds of events in this region. For higher p_Σ, this is the region of the Jacobian peak, where the maximum laboratory decay angle is achieved. The events in this region of the Jacobian peak have laboratory decay angles greater than those possible for any π^0 event at the same value of p_Σ, since the transverse momentum of the proton for the γ decay can be up to 35.6 MeV/c greater than that for the π^0 decay. (The proton RF momentum is 189 MeV/c for the π^0 decay and 224.6 MeV/c for the γ decay.) We have already discussed the resolution of such $\Sigma^+ \to p$ decays in Sec. VIB and in the analysis of the asymmetry parameter. The Jacobian peak for the π^0 decay occurs for laboratory angles which are possible for the γ decay to attain, when $(\vec{\Sigma}\cdot\vec{p})_{RF}$ is positive for the γ decay. The corresponding laboratory momenta differ greatly for the same laboratory angle, so that such π^0 events are highly resolvable. If any of these π^0 events were really γ events, they would be outside the region that we use for the branching ratio, since $(\vec{\Sigma}\cdot\vec{p})_{RF} > 0$ if they are considered as γ events, so that we are not missing γ events in the region that we are using because they appeared to be π^0 decays. For lower p_Σ, where the Jacobian peak is not present or where some of the γ events would occur at laboratory angles which are physical for the π^0 decay, the events are resolvable because the protons from the π^0 decay always stop, and the protons from the γ decay either always stop or have a length too great to be from the π^0 decay.

A histogram of MMSQ is shown in Fig. 25 for the 11,775 events lying within the region defined in Fig. 24. Here the events with low and high MMSQ are multiplied by 50 to show the structure. The γ events are discernible around MMSQ = 0, but the γ and π^0 peaks are not cleanly resolved. The asymmetry of the π^0 peak resulted from a shift in the π^0 peak of about 0.01 $m_{\pi^0}^2$ for events with stopping protons, probably from a small error in the range-momentum relation. The effect is more

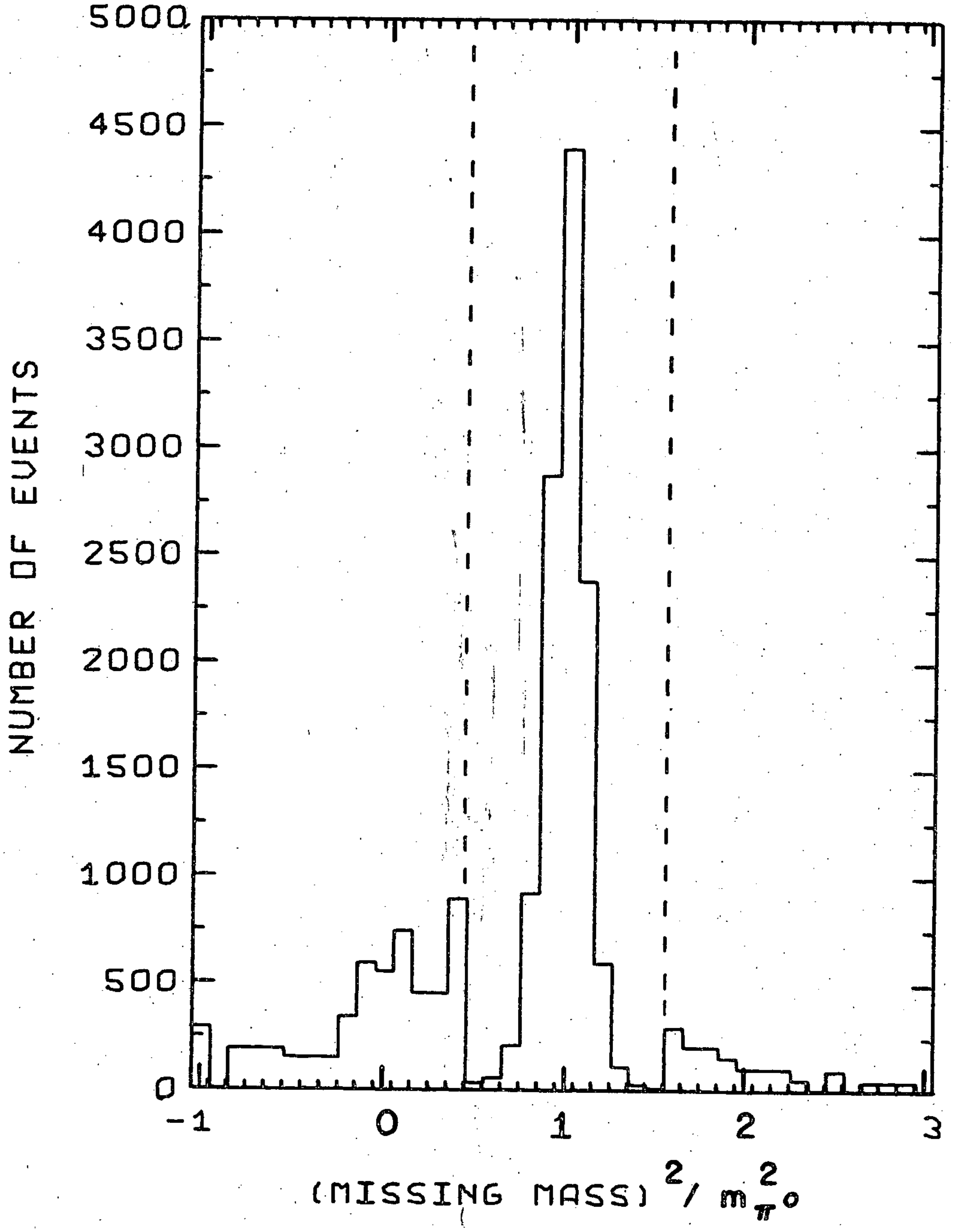

XBL 696-676

Fig. 25. The MMSQ distribution for the 11,775 events satisfying the criteria used to determine the $\Sigma^+ \to p\gamma$ branching ratio, before examination and remeasurement. The events in the tail regions indicated by the dashed lines have been multiplied by 50.

pronounced in Fig. 25 than in previous histograms because of the greater percentage of events with stopping protons in this histogram.

Careful examination and remeasurement of the events in the γ region allowed us to resolve the γ and π^0 peaks cleanly. The details are explained in the next section.

2. Evaluation of the Branching Ratio

The events in the low and high MMSQ regions of Fig. 25 indicated by the dashed lines were looked at in detail and were carefully remeasured. About 750 remeasurements were made in all, including those events remeasured for the asymmetry parameter determination.

It became clear that there were some events appearing in the low and high MMSQ regions because the proton scattered instead of stopping and was consequently measured for only a fraction of the length. Such events were not resolvable since the proton momentum was determined from curvature rather than range. In addition, there were events which had been badly measured, in that a small-angle proton scattering, visible as a small kink in the proton track, had been neglected by the measurer. All events where the proton scattered, resulting in either a visible proton recoil or a kink in the proton, and which lay in the low or high MMSQ regions, were removed from the MMSQ distribution. These events were almost all π^0 events, although conceivably a small number of γ events could have been removed in this way. An appropriate correction was made for the γ events in which the proton scattered, and is discussed below.

After remeasurement and careful examination of events on the scanning table, those events which were bad measurements, proton-scattering events, non-beam events, and non- $\Sigma^+ \to p$ events, were removed.

For the low MMSQ region, those events removed were distributed in the following way:

1) decay was $\Sigma^+ \to n\pi^+$ (31 events)

2) proton scattered, measured properly (26 events)

3) proton scattered, measured badly (7 events)

4) non-beam events (3 events)

5) other bad measurements, primarily events where the proton, although stopping in the chamber, had not been flagged as such by the measurer (7 events)

A histogram of the remaining events for the low and high MMSQ regions, and those in the π^0 peak, is shown in Fig. 26. The γ peak is cleanly separated from the π^0 peak, with no π^0 events below MMSQ = 0.35 $m^2_{\pi^0}$. The number of events below MMSQ = 0.25 $m^2_{\pi^0}$ is 31, all of which have only γ fits and are well resolved. The 3 events between 0.35 $m^2_{\pi^0}$ and 0.45 $m^2_{\pi^0}$ are all considered to be π^0 events. The event at -0.97 $m^2_{\pi^0}$ was badly measured and really lies in the γ peak. None of the events in the γ peak fit a π^0 decay when the fit without beam averaging was done. Two events which had had a good π^0 fit without beam averaging were considered non-beam events and were removed. We believe that both of these are π^0 events. The event with MMSQ = 2.83 $m^2_{\pi^0}$ is presumably an example of the decay $\Sigma^+ \to p\pi^0\gamma$, with a large γ energy. There was one event of the type $\Sigma^+ \to pe^+e^-$ at low MMSQ, but it did not survive the cuts imposed

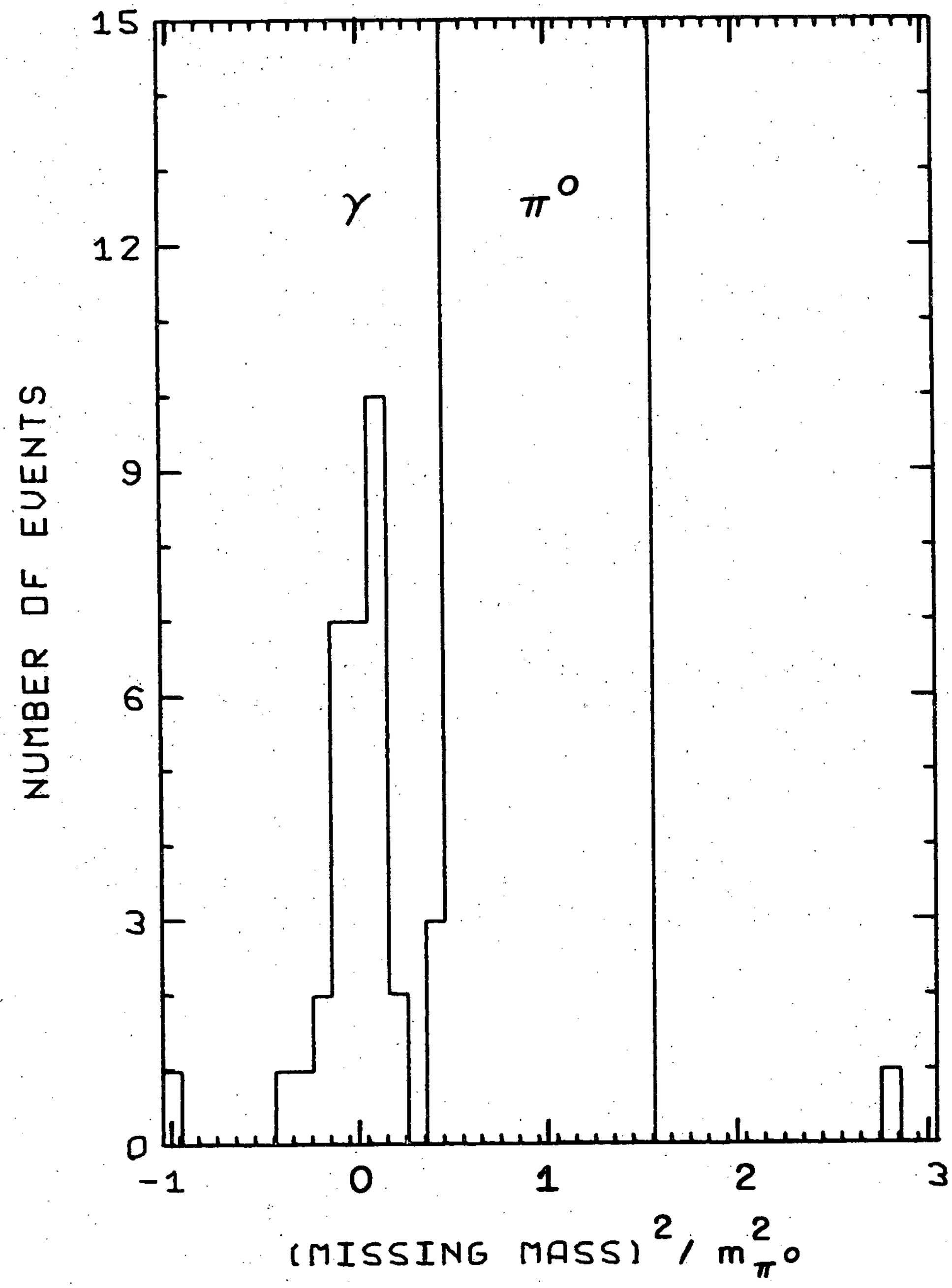

XBL 696-677

Fig. 26. The MMSQ distribution for the events used to determine the $\Sigma^+ \to p\gamma$ branching ratio, after examination and remeasurement of the events in the tail regions indicated by the dashed lines in Fig. 25. The 31 events below 0.25 are considered to be $\Sigma^+ \to p\gamma$ decays, the event at 2.83 is probably $\Sigma^+ \to p\pi^0\gamma$.

for the branching ratio. A scatter plot of p_Σ vs. $(\vec{\Sigma}\cdot\vec{p})_{RF}$ for the 31 $\Sigma^+ \rightarrow p\gamma$ events is shown in Fig. 27. The distribution of γ events seems to be in accord with that for π^0 events, as seen in Fig. 24, with most events occurring at high values of p_Σ.

The number of γ events for the branching ratio was 31 and the number of π^0 events was 11,670. Those events in the low and high MMSQ regions which were determined to be π^0 events were considered as such in evaluating the branching ratio. Two weights had to be applied to the events in order to evaluate the branching ratio. First, a weight was calculated for both the γ and π^0 events to account for those events lost by the restriction that the proton dip angle be less than 45°. This was done for each event by assuming an azimuthal distribution about the Σ^+ direction of $1 + \alpha P_\Sigma \cos\theta$ in the rest frame of the Σ^+, and, using the Σ^+ polarization for the event and the appropriate α, calculating the probability of the laboratory proton dip angle being less than 45°. The weight applied to the event was the inverse of this probability. The weight averaged 1.14 for both the γ and the π^0 events, so that there was no discernible difference in detection efficiency because of this cut. There were no weights larger than 2.25. The events removed from the γ region because of p-p scattering were accounted for by using the low-energy p-p scattering cross sections. The π^0 events were not weighted for scattering, because it was assumed that almost all of the π^0 events with a proton scatter were already included among the π^0 events. The average value of this weight for the γ events was 1.04.

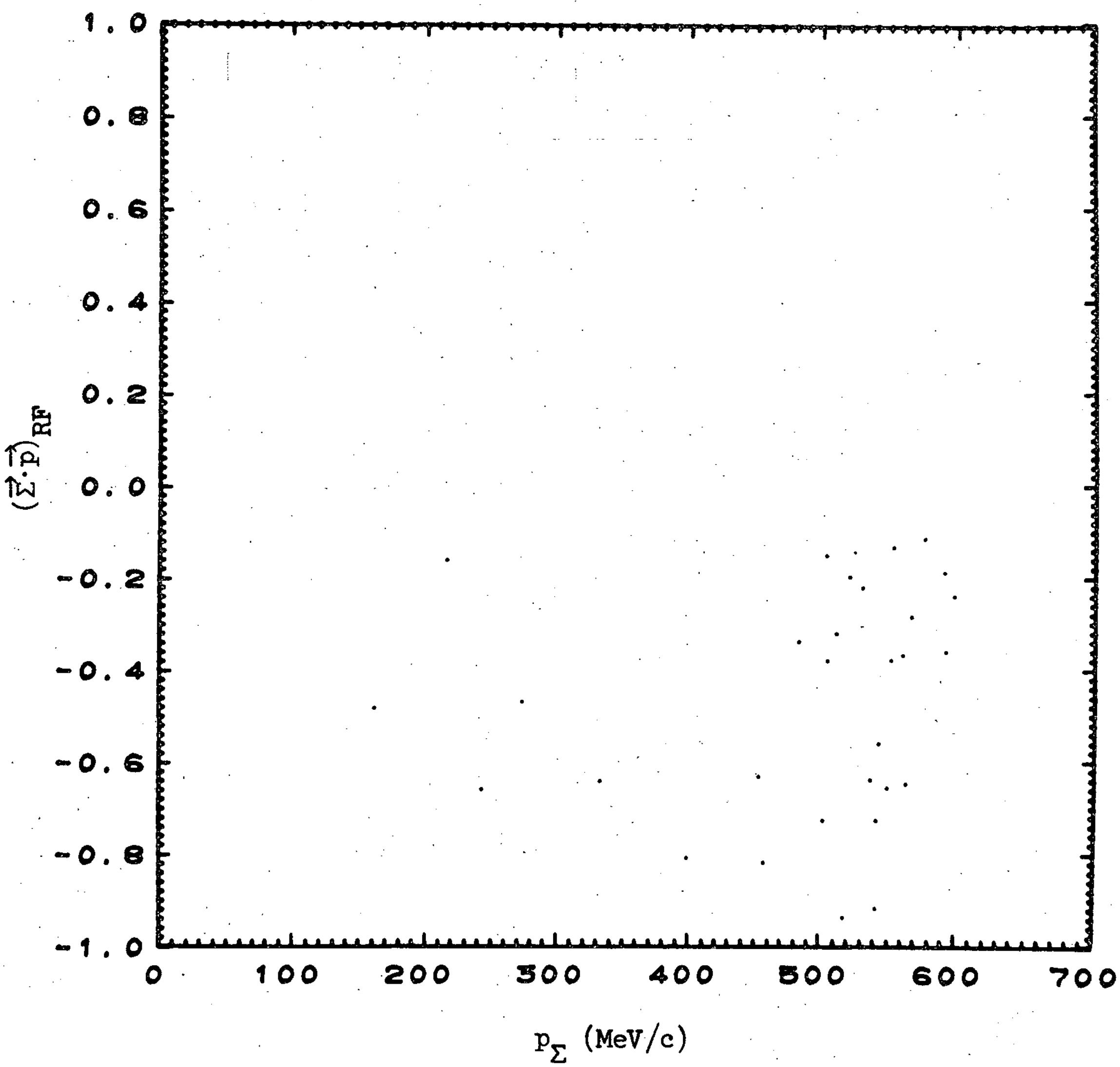

XBL 697-871

Fig. 27. p_Σ vs. $(\vec{\Sigma}\cdot\vec{p})_{RF}$ for the 31 $\Sigma^+ \to p\gamma$ events used in the measurement of the branching ratio. The scatter plot for the π^0 events is seen in Fig. 24, where the useable regions are defined.

The weighted number of γ events was 36.85, with a statistical error of 6.76, while the weighted number of π^0 events was 13,348. The branching ratio was

$$(\Sigma^+ \rightarrow p\gamma) \;/\; (\Sigma^+ \rightarrow p\pi^0) = (2.76 \pm 0.51) \times 10^{-3}.$$

We feel that we have considered all of the systematic errors in obtaining the branching ratio in this manner. We have chosen only regions of the variables p_Σ and $(\vec{\Sigma}\cdot\vec{p})_{RF}$ where both the γ and π^0 scanning and detection efficiencies are high. The relative efficiencies at any point of the scatter plot regions which we have used should not differ by more than a few percent in the worst cases, so that we have assumed them to be negligible. Because of the complete separation of the γ and π^0 peaks in Fig. 26, we have not had to subtract any background π^0 events from our γ events. A comparison with the high MMSQ region, where there is no decay comparable to $\Sigma^+ \rightarrow p\gamma$, is helpful in illustrating that a negligible number of π^0 events appear in the extreme tail regions of the π^0 peak.

The previous result of Bazin et al.[6] is about one standard deviation higher than our result, so that the experiments can be considered in agreement.

VII. THEORETICAL RESULTS FOR $\Sigma^+ \rightarrow p\gamma$

The theoretical analysis of weak electromagnetic decays such as $\Sigma^+ \rightarrow p\gamma$ was stimulated considerably by the measurement by Bazin et al. of the branching ratio for $\Sigma^+ \rightarrow p\gamma$, but the lack of experimental data for other decays has prevented experimental confirmation of any of the calculations. This experiment is able to comment on some of these calculations in light of our measurement of the asymmetry parameter and branching ratio for $\Sigma^+ \rightarrow p\gamma$.

Early work by Behrends[2] showed that the most general effective Lagrangian for $\Sigma^+ \rightarrow p\gamma$ is

$$\mathcal{L}_{eff} = \bar{p}\,(a + b\,\gamma_5)\,\sigma_{\mu\nu}\,q^\nu\,A^\mu\,\Sigma^+ + \\ + \text{Hermitian conjugate}\ , \tag{7.1}$$

where $\sigma_{\mu\nu} = i/2\ \left[\gamma_\mu, \gamma_\nu\right]$, A^μ is the electromagnetic field, q^ν is the proton four momentum, and a and b are parity-conserving (P.C.) and parity-violating (P.V.) amplitudes, respectively. We use the conventions for the γ matrices of Gasiorowicz[58], in which γ_4 is Hermitian, the γ_i are anti-Hermitian, and γ_5 is Hermitian. Other forms of coupling which one might consider on the basis of Lorentz invariance reduce to Eq. 7.1 when gauge invariance and momentum conservation are applied. From this effective Lagrangian it follows that the decay rate ω is given by

$$\omega = \frac{(|a|^2 + |b|^2)}{8\pi}\left(\frac{m_\Sigma^{\ 2} - m_p^{\ 2}}{m_\Sigma}\right)^3 \tag{7.2}$$

and the decay asymmetry of the proton is

$$I(\hat{q}) = 1 + \alpha \vec{P}_\Sigma \cdot \hat{q} \, , \tag{7.3}$$

where $\vec{P}_\Sigma$ is the Σ^+ polarization, $\hat{q}$ is the unit vector of the proton momentum in the rest frame of the Σ^+, and

$$\alpha = \frac{2 \, \mathrm{Re}(a^* b)}{|a|^2 + |b|^2} \; . \tag{7.4}$$

Several authors[59-61] have shown that CP invariance and SU(3) invariance of the amplitude implies that b = 0 for $\Sigma^+ \to p\gamma$, so that the asymmetry parameter $\alpha = 0$. We present here a calculation showing that with the assumption that the photon is a U-spin singlet, U-spin invariance of $\mathcal{L}_{eff}$ implies that $\alpha = 0$.

Assuming that the effective Lagrangian is given by Eq. 7.1, we write out the Hermitian conjugate term explicitly and find that

$$\begin{aligned} \mathcal{L}_{eff} &= \bar{p} \, (a + b \, \gamma_5) \, U^+ \, \sigma_{\mu\nu} \, q^\nu \, A^\mu \, \Sigma^+ + \\ &+ \bar{\Sigma}^+ \, (a^* - b^* \, \gamma_5) \, U^- \, \sigma_{\mu\nu} \, q^\nu \, A^\mu \, p \, . \end{aligned} \tag{7.5}$$

The operators U^+ and its Hermitian conjugate U^- are the U-spin raising and lowering operators, respectively, and have been inserted in anticipation of the U-spin properties of the weak interaction part of $\mathcal{L}_{eff}$. The negative sign for b^* comes from commuting the γ_4 from γ_4 p through the γ_5 to form $\bar{\Sigma}^+$.

We assume that $\mathcal{L}_{eff}$ is a U-spin scalar; this assumption is a special case of the assumption that $\mathcal{L}_{eff}$ is an SU(3) invariant, which is not necessary here. Σ^+ and p are assumed to be the members of a U-spin doublet, which is true in the case that they are members of the usual baryon octet, so that U = 1/2, and U_z = 1/2 for p, -1/2 for Σ^+. We assume that the photon is a U-spin singlet, which will be discussed below. Then the decay $\Sigma^+ \rightarrow p\gamma$ is a pure Δ U = 1 transition, with $\Delta U_z = +1$, so that the interaction Hamiltonian contains the U-spin raising operator, U^+.

Performing a 180° rotation in U-spin space, we obtain

$$\mathcal{L}^U_{eff} = \bar{\Sigma}^+ (a + b\,\gamma_5)\, U^-\, \sigma_{\mu\nu}\, q^\nu A^\mu\, p + + \bar{p}\, (a^* - b^*\,\gamma_5)\, U^+\, \sigma_{\mu\nu}\, q^\nu A^\mu\, \Sigma^+ \;, \tag{7.6}$$

since $\Sigma^+ \rightleftarrows p$, $U^- \rightleftarrows U^+$, and $A^\mu \rightarrow A^\mu$ under a U-spin rotation of 180°. For $\mathcal{L}_{eff}$ to be a U-spin invariant, $\mathcal{L}^U_{eff} = \mathcal{L}_{eff}$. Identifying terms, we find $a = a^*$ and $b = -b^*$, so that a is purely real and b is purely imaginary. From Eq. 7.4, we find that $\alpha = 0$. The assumption of CP-invariance requires a and b both to be real, so that combining U-spin and CP invariance, we would obtain b = 0. However, CP invariance is not necessary to obtain $\alpha = 0$. Our value $\alpha = -1.03\,^{+\,0.52}_{-\,0.42}$ is in two standard deviation disagreement with this result.

As is discussed by Gasiorowicz[58], the assumption that U = 0 for the photon is motivated by the Gell-Mann-Nishijima formula

$$Q = I_3 + Y/2 \;, \tag{7.7}$$

relating the electric charge to the third component of the isotopic spin and the hypercharge. The formula is valid for all known strongly interacting particles. Eq. 7.7 is the charge relation obtained from the relation for the current densities

$$J_\mu^{EM} = J_\mu^3 + 1/\sqrt{3}\ J_\mu^8 , \qquad (7.8)$$

where J_μ^3 and J_μ^8 are SU(3) generating currents. The particular combination of currents in Eq. 7.8 is a U-spin singlet, so that the photon has a U-spin singlet character. It is possible to have an additional current in Eq. 7.8 which is not a U-spin singlet, but this current, when integrated, would not contribute to Eq. 7.7 for any known particle. Such a current would thus not have any apparent physical manifestation, so that it is reasonable to assume that it is not present in Eq. 7.8. The SU(3) magnetic moment relations and electromagnetic mass differences, which are satisfied quite well, are consequences of the electromagnetic current having $U = 0$. Some relations among photoproduction amplitudes are obtained by Harari[62], using this assumption.

Several authors[60,61,63,64,65] have made dynamical calculations to obtain predictions for the branching ratio and asymmetry parameter, making use of CP invariance. Graham and Pakvasa[60] performed a pole-model calculation in which they used both baryon and meson poles to obtain relations among the P.C. and P.V. amplitudes for $B' \to B\pi$. The weak and strong vertices are described by effective Hamiltonians that are members of SU(3) octets. Data for the non-leptonic decays were used to obtain values for the parameters in the relations. They applied the pole model with only baryon poles to $B' \to B\gamma$, using the same weak vertex couplings and an SU(3) electromagnetic coupling at the second vertex. They assumed that the γ does not couple directly to the weak vertex. In this way, they obtained relations between the amplitudes for $B' \to B\gamma$ and $B' \to B\pi$. They found that the P.C. amplitudes dominate the γ decays, and assuming $\mu_{\Sigma^+} = \mu_p$, they obtained for R, the branching ratio $(\Sigma^+ \to p\gamma) / (\Sigma^+ \to p\pi^o)$, $R = 2.8 \times 10^{-3}$ and $\alpha = 0.061$, indicating a small SU(3) violation for the matrix element. Our measured value of R is in excellent agreement with the calculation, but our value of α is not.

Tanaka[61] assumed that the weak vertex in $B' \to B\gamma$ involves the $\Delta Q = 0$, $\Delta S = 1$ component of the weak hadronic current, $J^6 + i J^7$. He used SU(3) invariance to find the P.V. amplitudes for all decays to be 0. Using current commutation relations and the $\Sigma^+ \to p$ vertex calculated with a pole model, he calculated the P.C. amplitude for $\Sigma^+ \to p\gamma$ from the S-wave amplitude of $\Sigma^+ \to p\pi^o$. The branching ratio R came out too low by an order of magnitude, assuming that $\mu_{\Sigma^+} = \mu_p$ or using the present experimental values.

Mani <u>et al</u>.[63] used a model of Nishijima where the current is assumed to be part of the known weak hadronic current octet, as was done by Tanaka, but overall SU(3) invariance was not required. They used a pole model with the weak vertex described by the weak hadronic current and the electromagnetic vertex SU(3) invariant. Again, the γ was assumed not to couple directly to the weak vertex. They found that the P.C. amplitude vanished in the limit $\mu_{\Sigma^+} = \mu_p$, so that only the P.V. term survived. This result is in serious contradiction with the SU(3) result that the P.V. terms vanished when CP invariance was assumed. They obtain $R = 3.6 \times 10^{-3}$ and $\alpha = 0$, both of which are about two standard deviations from our measured values.

Papaioannou[64] used unsubtracted dispersion relations and related $\Sigma^+ \rightarrow p\gamma$ to ordinary Σ^+ decays and pion photoproduction. He obtained $R = 1.4 \times 10^{-3}$ and $\alpha = 0.2$, both of which are more than two standard deviations from our results.

Ahmed[65] related $B' \rightarrow B\gamma$ to $B' \rightarrow B\pi^o\gamma$ by current algebra techniques and expanded $B' \rightarrow B\pi^o\gamma$ in powers of photon momentum, obtaining a relation between $B' \rightarrow B\gamma$ and $B' \rightarrow B\pi^o$. The rate for $\Sigma^+ \rightarrow p\gamma$ depends sensitively on a parameter for the ordinary hyperon non-leptonic decays. Normalizing to the S-wave amplitude for $\Sigma^+ \rightarrow p\pi^o$, he found $R = 1.2 \times 10^{-3}$ and $\alpha = -0.6$, but the predicted P-wave amplitudes for the non-leptonic decays come out too small. Also, R is three standard deviations from our value, although α is in reasonable agreement. By changing the parameter to get reasonable agreement with both the S-wave and P-wave amplitudes for non-leptonic decays, he obtained $R = 2.3 \times 10^{-3}$ and $\alpha = -0.6$, both of which are in reasonable agreement with our values. The motivation for choosing the value of the non-leptonic parameter in the second case was to obtain closer agreement with the R of Bazin et al., but the theoretical justification is not clear. This model appears to incorporate a substantial violation of SU(3) because of the large asymmetry parameter obtained.

The possibility of a large CP violation for weak electromagnetic decays has been pursued by several authors.[66-68] Our measured values for R and α for $\Sigma^+ \rightarrow p\gamma$ do not rule out large CP violation. With SU(3) non-invariance also, it is possible to obtain a value of $\alpha = -0.4$.[67]

VIII. DISCUSSION

We have performed the first measurements of the asymmetry parameter α for the decays $\Sigma^- \to ne\bar{\nu}$ and $\Sigma^+ \to p\gamma$. Our result for $\Sigma^- \to ne\bar{\nu}$, $\alpha = -0.26 \pm 0.37$, is in accord with the prediction of a fit to Cabibbo's theory of semi-leptonic decays, when it is expressed in terms of the ratio g_A/g_V. We found for the combined electron-muon data a value $g_A/g_V = 0.19\,^{+\,0.20}_{-\,0.17}$. Our result for the decay $\Sigma^+ \to p\gamma$, $\alpha = -1.03\,^{+\,0.52}_{-\,0.42}$, disagrees by two standard deviations from the value of 0 predicted by SU(3) invariance of the matrix element. We have also measured the branching ratio $(\Sigma^+ \to p\gamma)\ /\ (\Sigma^+ \to p\pi^0) = (2.76 \pm 0.51) \times 10^{-3}$, which is in accord with the previous experimental result.

Further work on the asymmetry parameters for these decays, with considerable improvement in the statistics, should be done in the future, although the experimental techniques will be quite difficult, since the decays are so rare.

ACKNOWLEDGMENTS

I would like to thank my advisor, Professor Robert D. Tripp, for guiding me in my research and for helping to develop my experimental judgment. I would also like to thank Dr. Margaret Alston-Garnjost, Dr. Frank T. Solmitz, and Professor M. Lynn Stevenson for their help and guidance, and my fellow graduate students for many hours of enjoyable discussions.

Mr. Cadet Hand, III, Mr. James R. Smith, and Mr. Thomas Thomson supervised the scanning and measuring effort, and Mrs. Natalie Groteguth and Mr. Hand did outstanding work in managing the experiment library. I would also like to thank our scanners, with whom I spent a great deal of time, for their outstanding effort.

Finally I would like to acknowledge Professor Luis W. Alvarez, who has been a great inspiration to me in my development as an experimental physicist.

This work was performed under the auspices of the U. S. Atomic Energy Commission.

APPENDIX A. ASYMMETRY PARAMETER COEFFICIENTS FOR $\Sigma^- \to ne^-\bar{\nu}$

The expressions used in relating the asymmetry parameter to g_A/g_V for $\Sigma^- \to ne^-\bar{\nu}$ are tabulated below. The data were fitted to the distribution $1 + \alpha P_\Sigma \cos\theta$, where $\alpha = \beta\, b(x)/a(x)$, x is the ratio of the electron energy to its maximum value and β is the electron velocity. From the table below, one sees that $a(x) = f_1^2 \left[(2 - R_p - R)\, 1 + (-6 + 2R_p + 2/3\, R)\, Rx + 16/3\, R^2x^2 \right] + g_1^2 \ldots$ and that $b(x) = f_1^2 \left[(-1 + R_p + 1/3\, R)\, 1 + (8/3 - 2R_p + 2/3\, R)\, Rx - 8/3\, R^2x^2 \right] + g_1^2 \ldots$. The form factors f_i and g_i are defined in Sec. IVB, $R = E_e^{max}/m_\Sigma$, and $R_p = m_n/m_\Sigma$.

Term	1	Rx	R^2x^2	R^3x^3
		a(x)		
f_1^2	$2 - R_p - R$	$-6 + 2R_p + 2/3\, R$	16/3	
g_1^2	$2 + R_p - R$	$-6 - 2R_p + 2/3\, R$	16/3	
f_1g_1	$-2R$	$4 + 4/3\, R$	$-16/3$	
f_2^2	$2R^2$	$-4R(1 + 2/3\, R_p + R/3)$	$4 + 8/3\, R_p$	$-8/3$
f_1f_2	$2R(1 - R_p)$	$-4/3\, R(5 - R_p)$	$8/3\, (1 + R_p)$	
f_2g_1	$-2R(1 + R_p)$	$4(1 + R_p)(1 + R/3)$	$-16/3\, (1 + R_p)$	
		b(x)		
f_1^2	$-1 + R_p + R/3$	$8/3 - 2R_p + 2/3\, R$	$-8/3$	
g_1^2	$-1 - R_p + R/3$	$8/3 + 2R_p + 2/3\, R$	$-8/3$	
f_1g_1	$2 + 2/3\, R$	$-32/3 + 4/3\, R$	32/3	
f_2^2	$-2/3\, R^2$	$4/3\, R(1 + 2R_p - R)$	$8/3\, (-1 - R_p + 2R)$	
f_1f_2	$-2R + 2/3\, R_pR$	$4/3\, (R_p + 5R + R_pR)$	$-8/3\, (1 + 2R_p)$	
f_2g_1	$2/3\, R(3 + R_p)$	$-4/3\, (3 + 2R_p + R - R_pR)$	$8/3\, (2 + R_p)$	

APPENDIX B. SU(3) MATRICES

The 3x3 matrices $\overline{B}$, B, and J used in determining the SU(3) coefficients for baryon leptonic decays are shown below.

$$\overline{B} = \begin{vmatrix} \frac{\overline{\Sigma^o}}{\sqrt{2}} + \frac{\overline{\Lambda}}{\sqrt{6}} & \overline{\Sigma^-} & \overline{\Xi^-} \\ \overline{\Sigma^+} & \frac{-\overline{\Sigma^o}}{\sqrt{2}} + \frac{\overline{\Lambda}}{\sqrt{6}} & \overline{\Xi^o} \\ \overline{p} & \overline{n} & \frac{-2\ \overline{\Lambda}}{\sqrt{6}} \end{vmatrix}$$

$$B = \begin{vmatrix} \frac{\Sigma^o}{\sqrt{2}} + \frac{\Lambda}{\sqrt{6}} & \Sigma^+ & p \\ \Sigma^- & \frac{-\Sigma^o}{\sqrt{2}} + \frac{\Lambda}{\sqrt{6}} & n \\ \Xi^- & \Xi^o & \frac{-2\ \Lambda}{\sqrt{6}} \end{vmatrix}$$

$$J = \begin{vmatrix} \frac{\pi^o}{\sqrt{2}} + \frac{\eta}{\sqrt{6}} & \pi^+ & K^+ \\ \pi^- & \frac{-\pi^o}{\sqrt{2}} + \frac{\eta}{\sqrt{6}} & K^o \\ K^- & \overline{K^o} & \frac{-2\ \eta}{\sqrt{6}} \end{vmatrix}$$

REFERENCES

1. R. P. Feynman and M. Gell-Mann, Phys. Rev. 109, 193 (1958).
2. R. E. Behrends, Phys. Rev. 111, 1691 (1958).
3. W. Willis et al., Phys. Rev. Letters 13, 291 (1964) and H. Courant et al., Phys. Rev. 136, B1791 (1964).
4. C. T. Murphy, Phys. Rev. 134, B188 (1964).
5. U. Nauenberg, P. Schmidt, J. Steinberger, S. Marateck, R. J. Plano, H. Blumenfeld, and L. Seidlitz, Phys. Rev. Letters 12, 679 (1964).
6. M. Bazin, H. Blumenfeld, U. Nauenberg, L. Seidlitz, and C. Y. Chang, Phys. Rev. Letters 14, 154 (1965).
7. M. Watson, M. Ferro-Luzzi, and R. D. Tripp, Phys. Rev. 131, 2248 (1963).
8. N. Cabibbo, Phys. Rev. Letters 10, 531 (1963).
9. R. Bangerter, Alvarez Group Memo 574 and R. Bangerter, Ph. D. thesis, June, 1969, University of California, Lawrence Radiation Laboratory, Berkeley, California.
10. J. H. Burkhard, L. J. Lloyd, G. R. Lynch, F. L. Hodgson, G. T. Armstrong, and N. D. Travis, in Programming For Flying Spot Devices, New York, N. Y., 1965 (Columbia University, New York, 1966).
11. F. T. Solmitz, A. D. Johnson, and T. B. Day, Alvarez Group Programming Note P-117 (Lawrence Radiation Laboratory, Oct., 1965) unpublished.
12. O. I. Dahl, T. B. Day, F. T. Solmitz, and N. L. Gould, Alvarez Group Programming Note P-126 (Lawrence Radiation Laboratory,

July, 1968) unpublished.

13. Particle Data Group, Rev. Mod. Phys. 41, 109 (1969).

14. W. H. Barkas, Nuclear Research Emulsions, Vol. I (Academic Press, Inc., New York, N. Y., 1963); N. N. Biswas, I. Derado, K. Gottstein, V. P. Kenney, D. Lüers, G. Lütjens, and N. Schmitz, Nucl. Instr. Methods 20, 135 (1963).

15. G. Ang et al., Z. Physik 223, 103 (1969).

16. S. Barshay, U. Nauenberg, and J. Schultz, Phys. Rev. Letters 12, 76 (1964).

17. R. Bangerter, A. Barbaro-Galtieri, J. P. Berge, J. J. Murray, F. T. Solmitz, M. L. Stevenson, and R. D. Tripp, Phys. Rev. Letters 17, 495 (1966).

18. G. Källén, Elementary Particle Physics (Addison-Wesley Publishing Company, Inc., Reading, Mass., 1964), p. 361.

19. M. T. Burgy, V. E. Krohn, T. B. Novey, G. R. Ringo, and V. L. Telegdi, Phys. Rev. 120, 1829 (1960).

20. C. J. Christensen, A. Nielsen, A. Bahnsen, W. K. Brown, and B. M. Rustad, Phys. Letters 26B, 11 (1967).

21. F. S. Crawford, Jr., M. Cresti, M. L. Good, G. R. Kalbfleisch, M. L. Stevenson, and H. K. Ticho, Phys. Rev. Letters 1, 377 (1958); P. Nordin, J. Orear, L. Reed, A. H. Rosenfeld, F. T. Solmitz, H. D. Taft, and R. D. Tripp, Phys. Rev. Letters 1, 380 (1958).

22. P. Franzini and J. Steinberger, Phys. Rev. Letters 6, 281 (1961); W. E. Humphrey, J. Kirz, A. H. Rosenfeld, J. Leitner, and Y. I. Rhee, Phys. Rev. Letters 6, 478 (1961); B. Bhowmik, Nuovo Cimento 21, 567 (1961).

23. R. P. Ely et al., Phys. Rev. 131, 868 (1963).

24. V. G. Lind, T. O. Binford, M. L. Good, and D. Stern, Phys. Rev. 135, B1483 (1964).

25. C. Baglin et al., Nuovo Cimento 35, 977 (1965).

26. D. J. Miller, F. R. Stannard, A. Bezaguet, U. Nguyen-Khac, A. Haatuft, and A. Halsteinslid, Phys. Letters 11, 262 (1964).

27. R. P. Ely et al., Phys. Rev. 137, B1302 (1965).

28. J. Barlow et al., Phys. Letters 18, 64 (1965).

29. J. E. Maloney and B. Sechi-Zorn, Bull. Am. Phys. Soc. 14, 519 (1969).

30. E. Bierman, S. Kounosu, U. Nauenberg, L. Seidlitz, and A. P. Colleraine, Phys. Rev. Letters 20, 1459 (1968).

31. P. Franzini et al., in Proceedings of the 14th International Conference on High Energy Physics, Vienna, 1968 (CERN, Geneva, 1968), Abstract 262.

32. T. B. Day, R. G. Glasser, R. E. Knop, B. Sechi-Zorn, and G. A. Snow, in Proceedings of the 14th International Conference on High Energy Physics, Vienna, 1968 (CERN, Geneva, 1968), Abstract 375.

33. N. Barash, T. B. Day, R. G. Glasser, B. Kehoe, R. Knop, B. Sechi-Zorn, and G. A. Snow, Phys. Rev. Letters 19, 181 (1967).

34. C. Baltay et al., Phys. Rev. Letters 22, 615 (1969).

35. F. Eisele et al., Z. Physik 221, 1 (1969).

36. J. R. Hubbard, J. P. Berge, and P. M. Dauber, Phys. Rev. Letters 20, 465 (1968). The authors compile three experiments, including their own, to obtain this value. They feel that the

compiled value is probably too high, because of unreported experiments with no Ξ^- leptonic decays found. The preliminary results of the experiment in Ref. 37 indicate a somewhat lower branching ratio.

37. J. Duclos et al., in Proceedings of the 14th International Conference on High Energy Physics, Vienna, 1968 (CERN, Geneva, 1968), Abstract 253.

38. T. A. Romanowski et al., in Proceedings of the 14th International Conference on High Energy Physics, Vienna, 1968 (CERN, Geneva, 1968), post-deadline paper. This preliminary value is somewhat smaller than the other measured values of g_A/g_V.

39. L. K. Gershwin, M. Alston-Garnjost, R. O. Bangerter, A. Barbaro-Galtieri, F. T. Solmitz, and R. D. Tripp, Phys. Rev. Letters 20, 1270 (1968). In this paper we reported a value of $\alpha = -0.13 \pm 0.41$ for 49 $\Sigma^- \to ne^-\bar{\nu}$ events.

40. A. P. Colleraine et al., Bull. Am. Phys. Soc. 14, 519 (1969).

41. F. Eisele et al., in Proceedings of the Topical Conference on Weak Interactions, CERN, 1969 (CERN, Geneva, 1969), to be published in Z. Physik.

42. D. R. Harrington, Phys. Rev. 120, 1482 (1960) and Ph. D. Thesis, April, 1961, Carnegie Institute of Technology, Pittsburgh, Pennsylvania. Harrington's thesis contains the exact terms for both the spectrum and polarization terms, while his paper contains terms obtained after some approximations were made. In addition, there are several errors in the paper, although the thesis is correct.

43. I. Bender, V. Linke, and H. J. Rothe, Z. Physik 212, 190 (1968); V. Linke, University of Marburg preprint. Bender *et al.* contains the unpolarized spectrum terms, while Linke calculates the polarization correlation terms, although these polarization terms are not tabulated in an easily useable form. Both the spectrum and polarization terms (after integration of the neutron momentum) agree identically with Harrington's terms.

44. S. Weinberg, Phys. Rev. 115, 481 (1959).

45. N. Brene, L. Feje, M. Roos, and C. Cronström, Phys. Rev. 149, 1288 (1966).

46. H. T. Nieh and M. M. Nieto, Phys. Rev. 172, 1694 (1968).

47. C. Carlson, Phys. Rev. 152, 1433 (1966).

48. F. Eisele *et al.*, in *Proceedings of the Topical Conference on Weak Interactions, CERN, 1969* (CERN, Geneva, 1969), to be published in Z. Physik.

49. N. Cabibbo and R. Gatto, Nuovo Cimento 15, 159 (1960).

50. H. Whiteside and J. Gollub, Nuovo Cimento 54A, 537 (1968); H. Taft, Bull. Am. Phys. Soc. 14, 484 (1969); R. A. Burnstein, H. A. Rubin, and E. L. Erickson, Bull. Am. Phys. Soc. 14, 500 (1969).

51. Average of Refs. 23 and 25.

52. Average of Refs. 3, 4, 5, 15, 26, and 30.

53. Average of Refs. 3, 33, 34, and 35.

54. G. Conforto, Acta Phys. Acad. Sci. Hung. 22, 15 (1967). The value is obtained by compiling results from experiments involving various free-neutron decay correlations. The largest contribution is from Ref. 19.

55. G. Conforto, in Proceedings of the International School at Herceg-Novi, Yugoslavia, 1965, edited by M. Nikolić (Secretariat du Department de Physique Corpusculaire, Centre de Recherches Nucléaires, Strasbourg-Cronenbourg, France, 1965). Compiled from Refs. 24, 25, 27, and 28.

56. G. Quareni, A. Quareni-Vignudelli, G. Dascola, and S. Mora, Nuovo Cimento 14, 1179 (1959).

57. J. Schneps and Y. W. Kang, Nuovo Cimento 19, 1218 (1961); R. A. Burnstein, T. B. Day, F. Martin, M. Sakitt, R. G. Glasser, N. Seeman, and A. J. Herz, Phys. Rev. Letters 10, 307 (1963); R. Carrara et al., Phys. Letters 12, 72 (1964); and G. Quareni et al., Nuovo Cimento 40A, 928 (1965).

58. S. Gasiorowicz, Elementary Particle Physics (John Wiley and Sons, Inc., New York, N. Y., 1966).

59. Y. Hara, Phys. Rev. Letters 12, 378 (1964); M. Hirooka and M. Hosoda, Progr. Theoret. Phys. (Kyoto) 35, 648 (1966).

60. R. H. Graham and S. Pakvasa, Phys. Rev. 140, B1144 (1965).

61. K. Tanaka, Phys. Rev. 140, B463 (1965) and Phys. Rev. 151, 1203 (1966).

62. H. Harari, Phys. Rev. 155, 1565 (1967).

63. H. S. Mani, Y. Tomozawa, and Y. P. Yao, Phys. Rev. 158, 1577 (1967).

64. G. M. Papaioannou, Phys. Rev. 178, 2169 (1969).

65. M. A. Ahmed, Nuovo Cimento 58A, 728 (1968).

66. B. A. Arbuzov and A. T. Filippov, Phys. Letters 20, 537 (1966).

67. V. I. Zakharov and A. B. Kaidalov, J. Nucl. Phys. (U.S.S.R.) 5, 369 (1967), Soviet JNP 5, 259 (1967).

68. F. Salzman and G. Salzman, Nuovo Cimento 50A, 75 (1967).

TECHNICAL INFORMATION DIVISION
LAWRENCE RADIATION LABORATORY
UNIVERSITY OF CALIFORNIA
BERKELEY, CALIFORNIA 94720